Ontogenesis of the cornea and ciliary body: A morphological and molecular study

Hugh Robert Lennox Napier

Thesis presented for the degree of
DOCTOR OF PHILOSOPHY
In the Department of Human Biology
UNIVERSITY OF CAPE TOWN

August 2005

Declaration

I, Hugh Robert Lennox Napier, hereby declare that the work on which this thesis is based is my original work (except where acknowledgements indicate otherwise) and that neither the whole work nor any part of it has been, is being, or is to be submitted for another degree in this or any other university. I empower the University of Cape Town to reproduce for the purpose of research either the whole or any portion of the contents in any manner whatsoever.

Signed by candidate

Signature Removed

August 2005

Part of the work presented in this thesis has been published:

Napier HRL. and Kidson SH. 2005. Proliferation and cell shape changes during ciliary body morphogenesis in the mouse. Dev. Dyn. 233:213-223.

Acknowledgements

"What mad pursuit", indeed. It has been a pleasure though. I would sincerely like to thank my supervisor, Professor Susan Kidson for providing me with the opportunity to explore and discover. Her guidance, encouragement and enthusiasm have formed an integral part of this process.

Past and present members of the Kidson laboratory: Dr Paula Sommer, Dr Thandi Mgwebi, Dr Karen Pinder, Dr Lester Davids, Natalya Nikitina, Dr Purity Macheru, Dheshnie Govender and Robert Ndou, it has been a pleasure working with you, thank you.

I would like to extend a special thanks to Toni Wiggins, Barbara Möhr, Sharon Marshall, Melaney Peterson, Melanie Black, Miranda Waldron and Liz van der Merwe for the countless hours of their time that they have spent teaching me, and assisting with experiments.

I would also like to thank Professor Thomas Reh for his incredible hospitality and the wonderful opportunity he afforded me by allowing me to work in his laboratory. I worked hard, but had a lot of fun doing so, and that is mainly due to the welcoming members of his laboratory. A very special thanks to Chris McGuire, Melanie Roberts and Burak Gumuscu.

Finally, I would like to thank the South African Medical Research Council, National Research Foundation and University of Cape Town for scholarship and travel support.

Table of contents

List of Figures

List of Tables

Abstract

Ontogenesis of the cornea and ciliary body: A morphological and molecular study

The anterior segment of the eye includes the cornea, lens, iris, ciliary body and trabecular meshwork, with each of these elements playing a vital role in the maintenance of vision. The primary objective of this research is to contribute towards the understanding of how specific genes control tissue specification and structural morphogenesis of the developing anterior segment of the eye.

Despite its extensive use as a model organism, very little is known about the structure and development of the ciliary body in the mouse eye. Using scanning electron microscopy (SEM) the ciliary processes in the adult mouse were shown to form an irregular pattern, crossing over and interweaving, rather than lying parallel to one another, as observed in other mammals. Histological and SEM studies from E14.5 to P7 revealed that the first morphological sign of differentiation in the ciliary body is the appearance of an annular bulge around the optic cup margin; this is then gradually moulded to form discrete ciliary processes. A striking similarity between the developing capillary network and the adult ciliary folds was observed and suggests that the patterning template for the ciliary processes could be the underlying capillary network. Cell proliferation measurements and cell height assessments indicated that one of the first events occurring during the morphogenesis of ciliary processes is a proliferative surge occurring at about P0 in the outer ciliary epithelium. It is likely that this surge together with increasing cell heights leads to a bulging of this layer. After a slight delay, the inner ciliary epithelium responds by proliferating and extending inwards towards the lens. Final shaping of the ciliary processes is achieved through cell height reductions in the inner ciliary epithelium. Gene expression analyses revealed dynamic changes in *Bmp4* and *LEF1* expression patterns over the period of ciliary folding, while *Tgfβ1i4* expression in the ciliary body did not change during morphogenesis. These differences suggest that these genes play different roles in directing the specification and morphogenesis of the ciliary body. The temporal correlation between mitotic and cell height changes during ciliary body morphogenesis suggests that these processes play an integral role in the shaping of ciliary processes.

A complicated network of tight junctions within the corneal endothelium play an integral role in maintaining osmotic potentials within the cornea such that it remains transparent and functions normally. During development, early expression of the transcription factor, *Foxc1*, is essential for normal junction assembly and differentiation of the corneal endothelium. With a view to characterising and comparing junction assembly in $Foxc1^{+/+}$ and $Foxc1^{-/-}$ mice, immortal cell lines of the presumptive corneal stroma and endothelium were established. Microdissections of the periocular mesenchyme surrounding the optic cup margin at E12.5 were performed and the resulting primary cultures of these cells immortalised with the SV40 large T-antigen. Gene expression analyses showed that immortal $Foxc1^{+/+}$ cells continued to express *Foxc1*, while both $Foxc1^{+/+}$ and $Foxc1^{-/-}$ cells expressed *Foxc2*, *TGFβ1* and *Tgfβ1i4*. Comparative studies revealed that only $Foxc1^{+/+}$ cells formed adherens junctions (as marked by N-cadherin expression) in culture. When co-cultured with $Foxc1^{+/+}$ cells, $Foxc1^{-/-}$ cells still failed to form adherens junctions. It is likely that the observed low levels of cadherin expression in $Foxc1^{-/-}$ cells results in their inability to form primary associations with adjacent cells, which precedes normal junction formation. Despite the successful formation of adherens junctions in $Foxc1^{+/+}$ cells, no tight junctions formed in these cells. It is possible that the observed *in vivo* downregulation of *Foxc1* expression prior to tight junction assembly necessarily precedes tight junction formation. This may explain the lack of tight junction formation in $Foxc1^{+/+}$ cells, which were shown to maintain *Foxc1* expression. It is concluded that these cells could serve as an excellent tool in determining the role that lens derived signals play as potential regulators of *Foxc1* expression and tight junction assembly during corneal differentiation.

Chapter 1: Introduction

The eye is an exquisitely complex structure that functions to perceive the environment by collecting, focusing and processing light waves. Since humans are particularly visually oriented, understanding the factors that contribute to the onset of inherited and acquired eye diseases is of great relevance. A clear understanding of the basic anatomy of the eye and how it develops is integral in describing and ultimately treating eye diseases.

The primary objective of this research is to contribute towards the understanding of how specific genes control tissue specification and structural morphogenesis of the developing anterior segment of the eye. The anterior segment includes the cornea, which serves a protective function and is the primary structure through which light is focused; the lens, which further focuses light onto the retina and adjusts for near and distance vision; the iris which regulates the amount of light entering the eye; the ciliary body which produces aqueous humour and controls lens accommodation; and the trabecular meshwork which acts as a primary structure for the drainage of aqueous humour from the eye (Figure 1-1).

Glaucoma refers to a heterogeneous group of disorders that cause retinal ganglion cell death and optic nerve damage, ultimately leading to blindness. Many forms of glaucoma have a genetic basis, with a number of glaucoma-linked genes having been identified. However, the aetiology of the disease is often not clear. Patients with identical gene mutations can have greatly differing phenotypes. Accumulating evidence suggests that these differences could occur as a result of stochastic events during development or because of allelic differences in modifier genes between affected individuals (Anderson et al., 2001; Chang et al., 1999; Libby et al., 2003; Savinova et al., 2001).

During development, disruptions within the forming anterior segment (reviewed in Gould and John 2002; Gould et al., 2004) can lead to aberrations in aqueous humour production and flow dynamics. A clear understanding of how perturbations to the developing anterior segment result in increased intraocular pressure is thus crucial in characterising the onset of congenital eye diseases such as glaucoma.

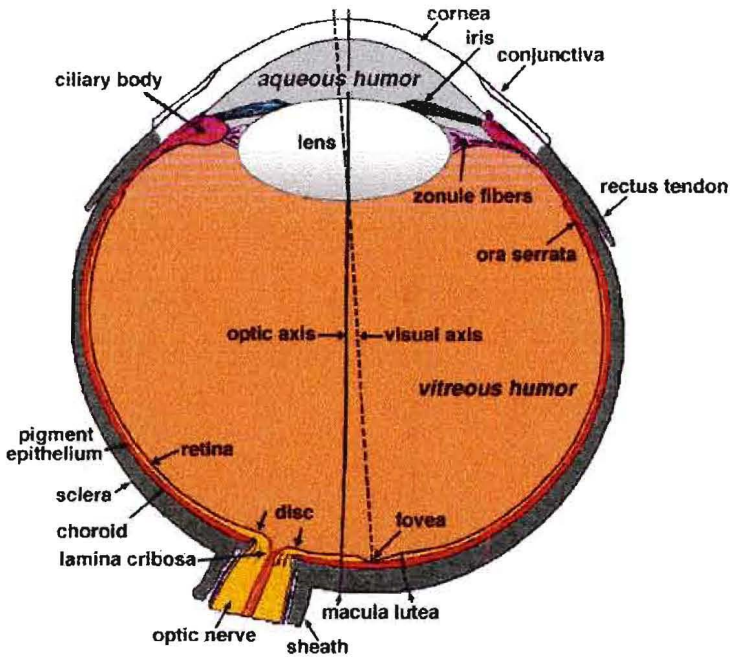

Figure 1-1: Anatomy of the human eye

http://webvision.med.utah.edu/imageswv/draweye.jpeg

1.1 The anterior segment of the eye

1.1.1 Structure of the ciliary body

The ciliary body of the eye is an intricate structure that fulfils several crucial roles essential for the maintenance of vision. A great deal is known about the structure and function of the ciliary body in humans. It extends from the iris root, anteriorly, to the ora serrata, posteriorly and consists of ciliary muscles (meridional, radial and circular fibres) and seventy to eighty ciliary processes (Davson, 1990). The ciliary processes synthesise aqueous humour, glycoproteins of the vitreous body, antioxidant enzymes and neuropeptides (Coca-Prados et al., 1999; Bishop et al., 2002). Zonular fibres connect the ciliary body to the lens (Hanssen et al., 2001) and together with the ciliary muscle they mediate lens accommodation and aqueous humour outflow through the trabecular meshwork.

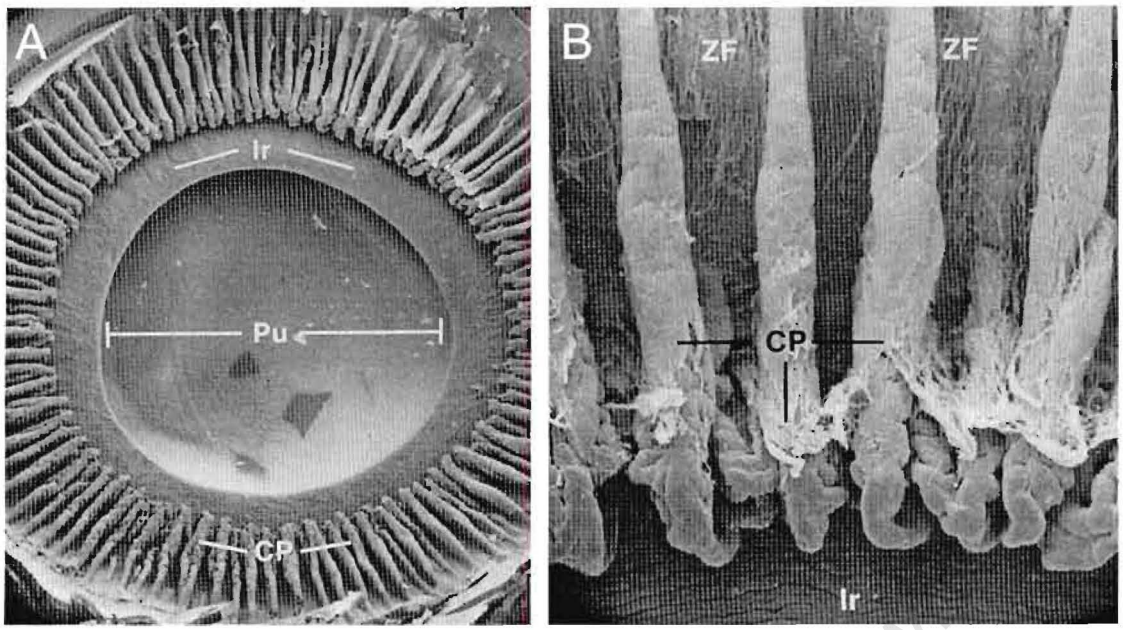

Figure 1-2: SEM of the guinea pig ciliary processes
A - SEM of an adult guinea pig eye, with the retina and lens removed revealing a parallel array of ciliary processes (cp). B - Higher magnification of the ciliary processes showing their regular parallel arrangement and the associated zonular fibres (zf). pu – pupil, Ir – iris. (Kessel and Kardon, 1979).

Scanning electron microscopic studies have shown that in many species, including guinea pig (Kessel and Kardon, 1979), chick (Bard and Ross, 1982a, 1982b) and humans (Davson, 1990; Ritch et al., 1996), ciliary processes form a remarkably regular arrangement of radial folds around the eye (Figure 1-2). However, in some animals such as the zebrafish (Soules and Link, 2005) and naked mole rat (Nikitina et al., 2004), the ciliary zone appears flattened. The impact that these structural differences have on normal ciliary body function is not clear. Furthermore, despite its common use in research as a model organism, the three dimensional structure of the adult mouse ciliary body has not been described. Nevertheless, ultrastructural studies have shown that in primates, rabbits and the mouse, each ciliary process (fold) is composed of an inner capillary core, surrounded by a loose stroma and covered with a double-layered epithelium, the inner ciliary epithelium (ice) and the outer ciliary epithelium (oce). The walls of the ciliary capillaries are extremely thin with fenestrations lining the entire circumference of the endothelium (Holmberg, 1959b; Smith, 1971). Plasma proteins are free to escape through these fenestrations into the surrounding stroma and in-between cells of the outer ciliary epithelium, with selective filtration of the blood plasma occurring in the inner ciliary epithelium (Smith, 1971; Smith et al., 1973; Raviola, 1977). Ultrastructural

studies of primate, rabbit and mouse eyes have revealed a complex network of intercellular junctions in the ciliary epithelia (Holmberg, 1959; Pappas et al., 1959; Raviola, 1971; Smith, 1971; Raviola and Raviola, 1978; Ober and Rohen, 1979). Gap junctions occur both between cells within a given epithelial layer as well as between cells of the two adjacent epithelial layers. This ensures that the ciliary epithelia serve as a functional syncytium. Cells of the outer, pigmented, ciliary epithelium are stabilised by adherens junctions, while the lateral walls of the inner, non-pigmented, ciliary epithelium have desmosomes basally and tight junctions apically. These differences indicate that maintenance of the blood aqueous barrier occurs at the level of the inner ciliary epithelium (reviewed in Raviola, 1977).

1.1.2 Structure of the cornea

The cornea not only serves as a physical barrier to the environment, but also is the primary structure through which light passes as it is focused onto the neural retina. This functionality obviously necessitates several structural refinements such as transparency and strength. The cornea comprises an outer epithelial layer, stroma and endothelium.

1.1.2.1 The corneal epithelium

The human corneal epithelium is a stratified, nonkeratinized, nonsecretory, squamous epithelium five to seven cells thick (Davson, 1990; Kaufman and Alm, 2003). Cells at the base of the epithelium are cuboidal, with more anterior cells flattening to form wing cells (1 – 3 cell layers) and the most superficial layer being squamous (3 – 4 cell layers). The basal cells are mitotically active and are the sole source of new cells in the corneal epithelium, with epithelial cells renewing approximately every seven days (Hanna et al., 1961). These basal cells are thought to originate from basal cells of the limbal epithelium with expression of the keratin pair K12 and K3 marking their differentiation (Chaloin-Dufau et al., 1993).

Newly synthesised cells differentiate and are pushed to the anterior surface of the corneal epithelium. Scanning electron microscopy of the epithelium reveals a surface in a constant state of flux, with older cells sloughing off the surface and newer cells replacing these cells. Despite this constant renewal of the corneal surface, all cells remain bound by tight junctions (McLaughlin et al., 1985) such that the epithelium still serves as an effective barrier to the environment.

Cells of the corneal epithelium rest on a basement membrane (40 – 60 nm thick) comprising type IV collagen, laminin and the proteoglycans perlecan, fibronectin and fibrin (Kaufman and Alm, 2003). Bowman's layer lies beneath the basement membrane and is 8 – 14 μm thick, consisting of randomly arranged collagen fibrils. It is acellular and is thought to be a modified superficial layer of the corneal stroma. In mice, Bowman's layer is far less robust and comprises a rudimentary layer of randomly distributed collagen fibrils (Haustein, 1983).

1.1.2.2 The corneal stroma

The corneal stoma accounts for approximately 90% of the cornea and thus the structure and composition of the stroma ultimately determines the optical properties of the cornea itself. The stroma consists of parallel arrays (200 – 250 lamellae) of collagen fibres and proteoglycans, which are synthesised, maintained and repaired by keratocyte cells (Kaufman and Alm, 2003). The keratocyte cells themselves are flattened and arranged parallel to the secreted matrix. The major structural component of the matrix consists of collagen type I fibres, with at least eighteen other collagen types occurring less abundantly (reviewed in Linsenmayer et al., 1998; Newsome et al., 1982). Of the proteoglycans, decorin, lumican, keratocan and mimican are each present in the cornea (Kaufman and Alm, 2003). Furthermore in the cornea, the proteoglycan sidechains are sulphated, which increases water retentive properties of the proteoglycans and promotes corneal transparency.

1.1.2.3 The corneal endothelium

The human corneal endothelium is a simple endothelium (5 μm high), consisting of flattened cells (±20 μm wide) arranged hexagonally (Davson, 1990; Kaufman and Alm, 2003). Cells of the corneal endothelium synthesise and rest on a basement membrane (Descemet's membrane), which is 5 – 10 μm thick.

Since the cornea is avascular the primary function of the corneal endothelium is to regulate the flow of ions and nutrients from the aqueous humour to nourish the stromal keratocyte cells. This function requires that the endothelial cells are metabolically active. Ultrastructural studies have confirmed this showing endothelial cells to have a prominent nucleus, numerous mitochondria, a prominent endoplasmic reticulum and Golgi apparatus (reviewed in Joyce, 2003; Kaufman and Alm, 2003). Of

crucial importance is that while nutrients and waste products are transported across the endothelium, the osmotic potential of the stroma must not change; thus, tight junctions surround the apical surface of the corneal endothelium and ensure that the passage of ions and water is tightly regulated across the endothelium (Hirsch et al., 1977; Kidson et al., 1999; Montcourrier and Hirsch, 1985; McLaughlin et al., 1985; Stiemke et al., 1991). Additionally, numerous gap junctions (Iwamoto and Smelser, 1965; Leuenberger, 1973; Kreutziger, 1976) occur on the lateral cell membranes and form an integral part of intercellular communication. Cell to cell associations within the corneal endothelium are strengthened by adhesion junctions with these cells expressing α-, β- and γ-catenin (plakoglobin) (Petroll et al., 1999) as well as N- and E-cadherin (Beebe and Coats, 2000; Ickes et al., 2002 in Joyce, 2003; Reneker et al., 2000). See Table 1.1 (Section 1.3.1) for a summary of cell junction components.

Unlike the basal cells of the corneal epithelium, cells of the human corneal endothelium are not mitotically active. Some mitoses can occur after injury (Joyce, 2003; Simonsen et al., 1981); however, in general the number of endothelial cells decreases with age and, in order to maintain a continuous endothelium, the average size of endothelial cells increases with age (Laing et al., 1976; Murphy et al., 1984).

Rabbit and bovine corneal endothelial cells divide more readily *in vivo* after wounding and even proliferate *in vitro* (Joyce et al., 1996). Nevertheless, analyses of cell cycle associated regulatory proteins suggests that both rabbit and human corneal endothelial cells are arrested in the G1-phase of the cell cycle; however, rabbit cells appear to break this arrest more readily (Joyce et al., 1996). Understanding the molecular basis for these subtle differences has important implications for corneal transplants. Culture of corneal endothelial cells also has important applications in studying the immunological features of graft rejection. The well-defined genetics of the mouse suggest it is an ideal candidate to model and characterise such events. Unfortunately primary cultures of adult mouse corneal endothelial cells have a limited proliferative potential (Joo et al., 1994). This necessitates the use of alternative model systems such as immortal cell lines to study corneal endothelial development and physiology.

1.2 Development of the vertebrate eye

The embryonic primordia that contribute to the developing eye include neuroepithelial tissues from the diencephalon (forebrain), the overlying surface ectoderm and immigrating neural crest and paraxial mesodermal cells (Noden 1975; Johnston, 1979; Barrio-Asensio et al., 1999; Barrio-Asensio et al., 2002; Osumi-Yamashita et al., 1994). The first stage of eye development involves the paired bulging of the lateral walls of the diencephalon that give rise to optic grooves (optic placodes) on either side of the forebrain (Figure 1-3A). These grooves enlarge and extend outwards to form the optic vesicles. Contact between the optic vesicle and overlying surface ectoderm results in a reciprocal induction between these tissues such that the surface ectoderm thickens in the region of contact forming the lens placode (Figure 1-3B). The closely apposed surface of the optic vesicle also thickens. Ultrastructural studies have shown that cytoplasmic processes and collagenous fibrils serve to connect the lens placode and optic vesicle (McAvoy, 1980) such that when the optic vesicle collapses to form the dorsal half of the two-layered optic cup, the lens placode is also drawn inwards and forms the lens pit (Figure 1-3C). As the optic cup deepens the lens pit forms a lens vesicle that separates from the surface ectoderm (reviewed in Pei and Rhodin, 1970; Ritch et al., 1996; Chow and Lang, 2001). The ventral half of the optic cup develops by the expansion of the dorsal layers ventrally (Figure 1-3D). As this occurs a branch of the internal carotid artery, the hyaloid artery, branches to form a network of capillaries in the optic cup. As the margins of the optic cup fuse along the choroid fissure this network of capillaries is separated from other vessels (Figure 1-3D, E). Blood supply to the eye is thus derived from the hyaloid artery and it exits the eye via the anterior annular vessel.

The lens vesicle consists of a single layer of cuboidal cells. As development proceeds, the posterior cells in the lens vesicle reduce their rate of DNA synthesis and elongate anteriorly forming primary lens fibres that eventually obliterate the cavity of the lens vesicle (Figure 1-3F). Cells of the lens then secrete a basement membrane that forms the hyaline capsule. Further differentiation of the primary lens fibres leads to the synthesis of crystallin proteins (Van Leen et al., 1987; Robinson and Overbeek, 1996), the degeneration of nuclei and extrusion of mitochondria and the endoplasmic reticulum from these cells (Chow and Lang, 2001). Cells at the anterior surface of the lens vesicle remain as non-mitotic epithelial cells, while cells on the periphery of the equatorial region form a germinative ring of mitotically active cells. Daughter cells from this region move into the equatorial region (bow of the lens) and start to elongate anteriorly and posteriorly. These cells form secondary

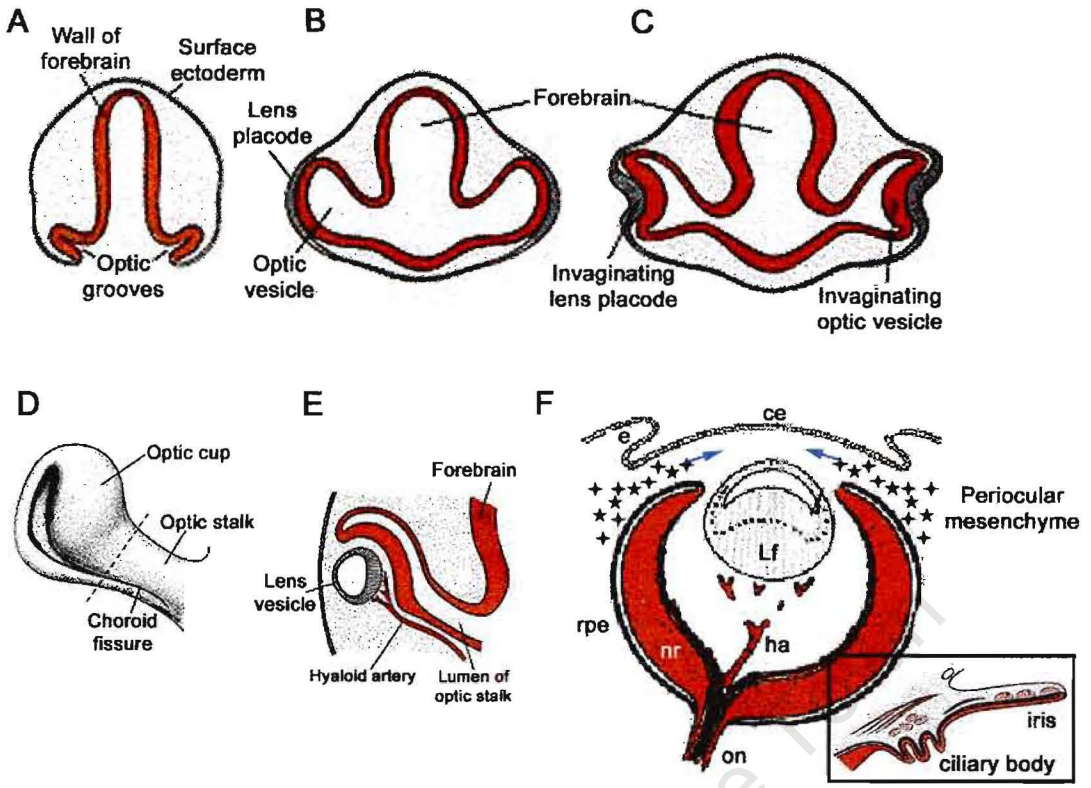

Figure 1-3: Development of the vertebrate eye

The first stage of vertebrate eye development involves the paired bulging of the lateral walls of the diencephalon, which forms the optic grooves on either side of the forebrain (A). These grooves enlarge and extend outwards, contacting the surface ectoderm (B). Reciprocal interactions between the neuroectoderm and surface ectoderm trigger the invagination of these apposed layers resulting in the formation of the optic cup and lens vesicle respectively (C). The ventral half of the eyecup develops by the expansion of the dorsal layers ventrally (D). E – cross section through D showing hyaloid artery. The inner layer of the optic cup forms the neural retina (nr), while the outer layer forms the retinal pigment epithelium (rpe) (F). The distal portion of the optic cup rim flattens and forms the iris, while the more proximal portion eventually forms a complex network of ciliary processes (F, insert). Ingressing periocular mesenchyme cells (F – blue arrows) contribute to the developing iris, ciliary body and cornea. ce – corneal epithelium, e – eyelid, ha, hyaloid artery, Lf – primary lens fibres, on – optic nerve. Figures modified from: http://www.vision.ca/eye/

lens fibres that form between the primary fibres and hyaline capsule in concentric layers. The generation of lens fibres continues in this way throughout life at a very slow rate (Ritch et al., 1996).

Concomitant to differentiation of the lens, the optic cup also differentiates with the inner layer of the optic cup forming the neural retina and the outer layer forming the retinal pigment epithelium.

The distal portion of the optic cup rim is further specified to form the iris, while the more proximal portion undergoes complex morphogenetic changes that result in radial folds, which eventually form a network of ciliary processes (Figure 1-3F, insert). While these epithelial modifications are occurring, neural crest and paraxial mesodermal cells invade the space between the optic cup margin, surface ectoderm (future corneal epithelium) and lens epithelium (Figure 1-3F, blue arrows). These cells contribute to the developing stromal and muscle tissues of the iris and ciliary body (Johnston et al., 1979; Barrio-Asensio et al., 1999; Barrio-Asensio et al., 2002) as well as the corneal endothelium and stroma (Kidson et al., 1999).

1.2.1 Development of the ciliary body

Despite a wealth of knowledge relating to the structure and function of the ciliary body, little is known about its ontogenesis. A central question that has not been fully addressed is how the two, initially parallel, epithelial layers of the presumptive ciliary body become folded. The majority of work in this area has been performed on developing chick embryos. Work has focused mainly on the role of intraocular pressure as the physical driving force of fold formation either acting directly (Coulombre and Coulombre, 1957; Bard and Ross, 1982b) or indirectly via its effect on cell proliferation (Stroeva, 1967; Reichman and Beebe, 1992).

The classical experiments performed by the Coulombres (Coulombre and Coulombre, 1957) involved experimental perturbation of ocular pressure by the insertion of micro-capillary tubes followed by histological analyses of the disrupted eyes. Chick eyes intubated with fine capillary tubes to drain accumulating vitreous failed to form ciliary processes (Coulombre and Coulombre, 1957). A model of ciliary folding was proposed suggesting that differential expansion between the globe of the eye and the anterior region of the eye in response to increasing IOP resulted in ciliary folding. In normal eyes, ciliary folding was shown to progress asymmetrically, initiating in the anterior ventral quadrant of the eye (Coulombre and Coulombre, 1957). Interestingly this asymmetric development correlates with the asymmetric development of the pericorneal cartilage. As the cartilage forms it may restrict the outward expansion of the subadjacent ciliary zone, leading to the ciliary region becoming folded.

Further support for this mechanical model of ciliary folding is derived from ultrastructural studies, which have shown that just prior to ciliary folding, cells of the inner ciliary epithelium detach from

one another (potentially imparting flexibility to these cells), while cells at the tip of the optic cup (future iris) cells remain firmly attached to one another and adhere to the lens through zonular fibres (Bard and Ross, 1982a). The flexibility and potential of the presumptive ciliary zone to fold was tested *in vitro* by immersing embryonic eyes in 50% ethanol, which led to a differential expansion between the retina and fixed pupillary margin and was sufficient to induce some ciliary folding (Bard and Ross, 1982b).

More recent structural studies have shown that changes in cell densities, heights and volumes are integral events occurring in normal ciliary folding in the developing chick (Reichman and Beebe, 1992). Analysis of cell proliferation within the ciliary epithelia in intubated and control sham-intubated eyes suggests that ciliary folding is triggered by a proliferative surge in the inner ciliary epithelium, which itself is prompted by a rise in intraocular pressure (Reichman and Beebe, 1992).

These findings clearly demonstrate that ciliary folding in the chick is a complex process integrating mechanical changes in cell structures and rates of proliferation. Superimposed on these changes are shifts in intraocular pressure. However, determining the subtleties of which events are necessary, sufficient or even independent of ciliary morphogenesis is very difficult. The main drawback of these experiments is that the perturbation itself is so severe that it is difficult to separate the direct mechanical effects from the secondary effects. For example it has been shown that the ciliary body assumes ultrastructural characteristics of ion-transporting epithelia prior to folding and is in fact capable of secreting aqueous humour as well as components of the vitreous prior to folding (Beebe et al., 1986; Porte et al., 1968 in Beebe, 1986; Bishop et al., 2002). This immediately poses questions of whether the lateral detachment of cells in the inner ciliary epithelium prior to ciliary folding relates to its function as a secretory epithelium or is an essential event preceding ciliary folding as proposed by Bard and Ross (1982a). Furthermore, changes in proliferation in intubated eyes (Reichman and Beebe, 1992) could result from essential morphogen signals draining from the eye rather than being a consequence of the lowered intraocular pressure.

1.2.1.1 Role of the lens in ciliary body development

In addition to characterising the changing cell dynamics within the ciliary epithelia, much work has centred on determining the source of molecular signals that control and direct ciliary body morphogenesis. Lens extirpation experiments result in micro-ophthalmic eyes, with the vitreous

failing to accumulate, suggesting that the lens is essential for producing vitreous or directing other tissues to synthesise vitreous (Coulombre and Coulombre, 1964). Control experiments in which the lens was replaced with a boiled lens have the same effect, with retinal growth and development proceeding normally, while the cornea, pigmented epithelium, choroid and sclera show a reduction in growth rate. Culture of embryonic optic cups, without the lens, in the anterior chamber of adult rat eyes results in no differentiation of the ciliary body or iris (Stroeva, 1967). Rotation of the lens within the optic cup or the addition of supernumerary lenses can induce corneal like differentiation of the retinal layers apposed to the anterior lens epithelium (Genis-Galvez, 1966; Genis-Galvez et al., 1967). A primitive, pigmented iridian border also forms adjacent to the rotated or ectopic lens, suggesting that the lens plays a role in differentiation of the ciliary body.

Recent co-culture experiments (Thut et al., 2001) support the above observations and demonstrate that the lens is capable of inducing the expression of early ciliary markers in the optic cup. In these experiments mouse eyes from E10.5 – E15.5 embryos were harvested and dissected such that the cornea and retinal pigment epithelium were removed. These optic cup rudiments were then co-cultured with mouse (E14.5) or chick (E3 – E8) lenses. Whole mount *in situ* hybridisation experiments showed that the lens induced expression of early markers of ciliary body differentiation (*Tgfβ1i4* and *Ptmb4*); however, later ciliary markers (*Tgfβ2*, *Sl00a6* and *Slc6a*) were not induced. These data suggest that the lens controls the initial specification of the ciliary body, while locally acting signals are likely to dictate subsequent ciliary body differentiation. For example, Link and Nishi (1998) suggest that differentiation of the avian iris and ciliary muscles is promoted by locally acting signals.

In mice expression of diphtheria toxin-A under the control of the αA-crystallin (Harrington et al., 1991; Key et al., 1992) or γF-crystallin (Klein et al., 1992) promoters severely abrogates normal lens development, which leads to microphthalmic eyes with multiple defects. Hemizygous mice develop relatively normal eyes pre- and postnatally. Eyes are reduced in size and do exhibit variable defects such as persistence of the hyaloid artery, thickening of the cornea and an expansion and folding of the retina. The retinal folding probably results from the overall reduction in eye size, through a failure to synthesise vitreous. In homozygous mice, eyes demonstrate severe microphthalmia and disorganisation of the anterior segment; however, the iris and ciliary epithelia, although reduced in size, do form. In these transgenic mice the lens disintegrates completely between P3 and P6 with the iris and ciliary epithelia remaining associated with the collapsed lens

structure. Thus no accurate assessment of postnatal iris and ciliary body morphogenesis is possible in these mice. A recent study has shown increased apoptosis in the ciliary zone of zαA-crystallin / diphtheria toxin-A zebrafish eyes (Kurita et al., 2003), which might explain the overall reduction in size of the iris and ciliary epithelia observed in mice.

Overall these findings suggest that ciliary body specification may occur independently of lens-derived signals. However, since the diphtheria toxin-A expressing lenses only degenerate during late embryonic development it is likely that lens-derived signals are present from E12.5 – E14.5 and may still contribute to the early specification of the ciliary zone in these transgenic animals. Expression analyses of early ciliary markers are essential for determining the precise role that the lens plays in ciliary body specification and morphogenesis in these animals.

1.2.1.2 Genes involved in ciliary body development

Presently the underlying molecular mechanisms responsible for the specification and coordinated morphogenesis of the ciliary body remain unclear. Despite recent studies identifying genes specifically expressed in the ciliary body (Thut et al., 2001; Kubota et al., 2004), little is known about genetic pathways or the specific role that individual genes play in ciliary body morphogenesis and/or function.

Bmp4 in the developing eye and ciliary body

Bone morphogenetic proteins (BMPs) belong to the transforming growth factor-β (TGF-β) superfamily of secreted polypeptide signalling molecules. The BMP family has over 30 members that have been shown to regulate diverse cellular processes such as cell proliferation, apoptosis, differentiation, cell fate determination and morphogenesis (Balemans and Van Hul, 2002; Hogan, 1996; Zhao, 2003). Bmp4 is essential for early embryogenesis with homozygous null mutant mice dying around the time of gastrulation (Fujiwara et al., 2001; Lawson et al., 1999; Winnier et al., 1995). In later embryonic development Bmp4 is essential for a host of inductive interactions between mesenchymal tissues and adjacent epithelial layers. *Bmp4* is expressed in many developing tissues that include the heart, lung, kidney, brain, limbs, hair, feathers, teeth, ear and eye (Hogan, 1996).

In the mouse eye, *Bmp4* is initially expressed in the distal optic vesicle (at 14-16 somites) and overlying surface ectoderm (Furuta and Hogan, 1998). A complex set of inductive interactions between the optic vesicle and ectoderm leads to a thickening of the surface ectoderm, which goes on to form the lens placode. The competence of the ectoderm to respond to these signals is dependent on *Bmp4* expression in the ectoderm, with the lens placode failing to form in *Bmp4* null mutants (Furuta and Hogan, 1998).

As the optic vesicle invaginates to form the optic cup, the lens placode is drawn inwards forming the lens vesicle. Although the lens does not express *Bmp4*, cells within the vesicle express Bmp receptors as well as phosphorylated forms of the Bmp responsive Smads, with Bmp signals playing an essential role in primary lens fibre cell differentiation and elongation in the mouse and chick eye (Belecky-Adams et al., 2002; Faber et al., 2002). In vitro cultures of lens vesicles with the known Bmp inhibitor noggin or transfection of noggin in developing chick eyes results in delayed primary lens fibre elongation (Belecky-Adams et al., 2002). Experiments in which a dominant negative form of the type 1 Bmp family receptor, *Alk6*, was expressed ectopically in the mouse lens under the control of the αA-crystallin promoter or the ectoderm enhancer of *Pax6* also led to inappropriate primary lens fibre cell differentiation and elongation (Faber et al., 2002). Interestingly, deficiencies in primary lens fibre elongation were most evident in the naso-ventral quadrant of the lens. This asymmetric phenotype may be explained by the known expression of *Bmp4* in the dorsal optic cup at this stage of development (Furuta and Hogan, 1998).

In the developing optic cup the Bmp receptor *Alk6* (*BmprIB*) is expressed in a region complementary to that of *Bmp4* in the ventral retina; with another receptor, *Alk3* (*BmprIA*), being expressed throughout the eye until E10.5 – E11.5 (Furuta and Hogan, 1998; Belecky-Adams and Adler, 2001). As suggested by the expression domain of these Bmp receptors, *Bmp4* is essential for the normal development of the ventral neural retina. Over-expression of noggin in the developing chick eye leads to micro-ophthalmic eyes with multiple defects affecting the neural retina, retinal pigment epithelium and lens (Adler and Belecky-Adams, 2002). In the retina the ganglion cell axons fail to enter optic nerve. Similarly overexpression of *Ventroptin*, another Bmp antagonist, which is normally expressed in the ventral retina, disrupts the normal retinotectal projection of axons (Sakuta *et al.*, 2001).

Expression of *Bmp4* during late embryonic and early postnatal development of the mouse is confined to the developing iris, ciliary body, and the retinal pigment epithelium (Chang et al., 2001). On the C57BL/6J background, *Bmp4* heterozygotes variably exhibit anterior segment abnormalities. The most striking features include a raised intraocular pressure, absent or blocked trabecular meshwork and Schlemm's canal and in some cases no ciliary body is formed (Chang et al., 2001). Subsequent research has demonstrated that expression of *Bmp4* in the ciliary body is essential for normal ciliary body development (Zhao et al., 2002): Exogenous expression of the Bmp inhibitor noggin, under the control of a αA-crystallin promoter, results in mice lacking a ciliary body. Although the ciliary epithelia are highly disorganised in these transgenic mice by P1, the adjacent retina and iris seem to develop normally. Expression analyses in wildtype mice show *Bmp4* transcripts are restricted to the inner ciliary epithelium at P1, which correlates with the localised phenotype (Zhao et al., 2002).

The muscle segment homeobox genes *Msx1* and *Msx2* (formerly *Hox7-1* and *Hox8-1*) play important roles in neural tube, neural crest and craniofacial development (Foerst-Potts and Sadler 1997). In the developing mouse eye, *Msx1* and *Msx2* demonstrate spatially restricted expression profiles that suggest a role in zoning and specifying regions of the optic cup (Monaghan et al., 1991). *Msx1* is first expressed in the inner layer of the optic cup at E12.5. Its expression is restricted to a band of cells below the apical portion of the optic cup that corresponds to the presumptive ciliary body. The domain of *Msx1* expression becomes more defined by E13.5 with expression levels peaking around E16.0. *Msx1* null mutants die in the immediate postnatal period and appear to have a normal ciliary body at this time (Satokata and Maas, 1994; Houzelstein et al., 1997). A functional redundancy for Msx1 and Msx2 has been proposed and it is thus possible that *Msx2* expression, normally restricted to the photosensitive neural retina, may compensate for the lack of *Msx1*.

Recent studies have shown that the effects of Bmp signalling are mediated by *Msx1*. Overexpression of *Msx1* or Bmps ventralises *Xenopus* embryos in a similar manner (Suzuki et al., 1997). Furthermore, *Msx1* expression in animal cap explants can be induced by RNA injections of Bmp2, -4, or –7 (Suzuki et al., 1997). Overexpression of *Msx2* in the developing mouse results in a downregulation of *Bmp4* in the dorsal optic cup at E10.5 and an upregulation of *Bmp7* (Wu et al., 2003), which further suggests a regulatory relationship between *Msx* and *Bmp* genes. Interestingly, in mice, Msx1 expression in the dorsal midline of the diencephalon is essential for the expression of

Wnt1 and *Pax6*, with ectopic expression of *Msx1* in the chick brain able to induce *Wnt1* expression (Bach et al., 2003). The tight coupling of *Wnt*, *Bmp* and *Msx* genes is further highlighted by studies showing that *Msx2* expression can be induced through either the canonical Wnt signalling pathway or through Bmp signalling pathways, with the co-smad, Smad4, acting as a necessary intermediate in both cases (Hussein et al., 2003). Together these findings suggest that Bmps directly regulate *Msx* expression, which serve to effect the normal downstream signalling events characteristic of Bmp signals.

Otx1 and *Otx2* are homeobox genes that play crucial roles in the normal organisation and differentiation of tissues within the head (Simeone et al., 1993; Acampora et al., 1996; Hide et al., 2002). *Otx1* and *Otx2* are both expressed within the developing eye. In the mouse, their initial expression domains overlap in the dorsal optic vesicle (9.5dpc). Subsequently, *Otx1* expression becomes restricted to the dorsal half of the optic nerve, retinal pigment epithelium and rim of the optic cup (presumptive ciliary body and iris). *Otx2* expression remains most notable in the retinal pigment epithelium (Martinez-Morales et al., 2001). *Otx1* null mutants demonstrate a broad range of phenotypes that include spontaneous epileptic behaviour as well as acoustic and visual defects (Acampora et al., 1996). Eyes of *Otx1* null mutants have reduced irises and lack ciliary processes and lachrymal glands. The precise role that *Otx1* plays in ciliary body morphogenesis has not been characterised. No data has been published as to whether the unfolded ciliary zone in these null mutants still functions as a secretory epithelium or not.

A final experiment performed by Zhao et al., (2002) was to analyse the expression domains of *Msx1* and *Otx1* in mice expressing noggin under the control of the αA-crystallin promoter. Wildtype mice at P1 and P7 express *Msx1* in the inner ciliary epithelium and ciliary muscle. In the transgenic mice, *Msx1* expression was completely abolished, confirming *Msx1* is a direct downstream target of Bmp signalling. At P1 in wildtype mice *Otx1* is expressed in the inner ciliary and iris epithelia as well as in the outer ciliary epithelium and iris stroma. By P7, *Otx1* expression predominates in the inner ciliary epithelium and iris epithelium. In transgenic mice, expressing noggin in the lens, *Otx1* expression is only downregulated in the ciliary zone, with expression in the iris epithelium persisting at P7. These observations suggest that the patterning of *Otx1* expression in wildtype mice is achieved independently of Bmp signals; however, maintenance of its expression in the ciliary zone is Bmp dependent, with maintenance of expression in the iris being independent of Bmp signals.

Genes with known expression in the ciliary body

At this stage the majority of gene expression data relating to the ciliary body is not correlated to morphogenetic events and most importantly no regulatory relationships have been elucidated. For example, the expression of several genes including, *Bmp7* (Zhao et al., 2002), collagen IX and XVIII (Dhawan and Beebe, 1994; Ylikärppä et al., 2003), *Cyp1b1* (Bejjani et al., 2002), LEF1 (Kubo et al., 2003), Notch 2 and Jagged (Bao and Cepko, 1997), PAI-1 (Masos et al., 2000), PEDF (Ortego et al., 1996), *Pdgfa* (Reneker and Overbeek, 1996), *TGFβ1* and *TGFβ2* (Gordon-Thomson et al., 1998) and *Tgfβ1i4* (Thut et al., 2001) have been mapped to the developing ciliary body, but their functions in ciliary body development are not known.

Lmx1b is a LIM homeodomain class transcription factor that is expressed in the mouse periocular mesenchyme from E10.5 (Pressman et al., 2000). Its expression persists in cells of the developing corneal stroma and by E14.5 expression extends to the forming extraocular muscles. At birth (P0), *Lmx1b* is expressed in the developing iris stroma, ciliary body, corneal endothelium and stroma and the presumptive trabecular meshwork. Although no ciliary processes are observed in *Lmx1b* null mutant mice, no characterisation of the role that *Lmx1b* plays in ciliary body morphogenesis has been made (Pressman et al., 2000).

Pax6 expression in the developing eye and ciliary body is well characterised (Graw, 1996; Grindley et al., 1995; Koroma et al., 1997; Macdonald and Wilson, 1996; Walther and Gruss 1991; Xu et al., 1999). *Pax6* is first expressed in the optic vesicle and surface ectoderm at E8.0. Later expression (E12.5) is restricted to the inner layer of the optic cup, the developing lens and surface ectoderm. By E17.5 expression persists in the corneal epithelium, lens epithelium and inner layer of the optic cup including the neural retina and presumptive iris and ciliary zones. Since mice with *Pax6* null alleles die neonatally with severe craniofacial defects (Hill et al., 1991), lacking eyes, nose and olfactory bulb, little can be deduced from these animals in terms of ciliary body morphogenesis. However, evidence does exist to suggest that *Pax6* gene dosage effects play an important role in the developing anterior segment (Baulmann et al., 2002; Collinson et al., 2001, 2003; Singh et al., 2002). In humans *PAX6* mutations have been linked to Aniridia (lack of the iris) and Peters' anomaly (congenital corneal opacity with defects in the corneal epithelium, Descemet's membrane and corneal stroma) (Graw, 1996). In mice, the conditional knockout of *Pax6* in the distal optic cup has demonstrated that *Pax6* plays a cell autonomous role in normal iris differentiation (Davis-Silberman et al., 2005). Additionally, over-expression of *Pax6* in mice results in a reduction in

corneal size, a flat iris with cyst like structures and no ciliary body development (Schedl et al., 1996).

1.2.2 Development of the cornea

Corneal morphogenesis is characterised by an elegant sequence of complex cellular rearrangements and differentiation events. Despite morphological similarities across species, the cellular events controlling corneal development in avians (Hay, 1979), humans (O'Rahilly, 1975), amphibians (Bard and Abbot, 1979) and rodents (Pei and Rhodin, 1970, 1971) differ.

The complexity of corneal morphogenesis is mainly a function of the different embryonic primordia that contribute to its development. The corneal epithelium differentiates from the overlying surface ectoderm. In the chick the corneal epithelium triggers a series of events leading to an influx of periocular mesenchyme cells, which differentiate into the corneal endothelium and stroma. Initially the corneal epithelium secretes an acellular primary stromal matrix of collagen fibrils and sulphated glycosaminoglycans, which forms a space between the corneal epithelium and lens epithelium (Hay, 1979). This facilitates a primary wave of cell migration at stage 22, resulting in the formation of the corneal endothelium by stage 25. As the corneal endothelium differentiates, cells become closely associated, form cell junctions (stage 27) and start to secrete hyaluronate into the primary stroma. Since hyaluronate is strongly hydrophilic, the corneal stroma swells enabling a second wave of cells to migrate between the corneal epithelium and endothelium and so form the cellular corneal stroma by stage 30. Corneal compaction and transparency occurs through the dehydration of the corneal stroma by the endothelial cells actively pumping water out of the stroma. This pumping is thought to be triggered by thyroxine secreted from the thyroid gland. Administration of thyroxine prior to stage 40 results in an increase in potassium levels, which presumably leads to increased pumping activity in the endothelium, so accelerating stromal dehydration (Masterson et al., 1975). Interestingly, the effects of thyroxine are also mimicked by members of the FGF and EGF families (Hay, 1979).

Structural and ultrastructural studies of the developing human cornea show that its development parallels that of the chick with waves of cell migration contributing to the formation of the corneal endothelium, the stroma and the primary pupillary membrane (reviewed in O'Rahilly, 1975). In the developing mouse, a single wave of cell migration occurs, with the corneal endothelium

differentiating at the same time as the corneal stroma (Pei and Rhodin, 1970, 1971; Kidson et al., 1999). Details of the morphological and molecular events that direct the differential specification of corneal endothelial and stromal cells in the mouse are limited. Interestingly, mutations in certain genes such as *Foxc1* in mice and its human homologue FKHL7 have similar effects on corneal development. It is unclear how these conserved molecular signals direct structural morphogenesis in a similar way, despite acting in different cellular environments, as formed by single or multiple waves of cell migration. Morphological descriptions of the developing chick eye demonstrate that appropriate formation of the corneal endothelium precedes stromal differentiation and is essential for corneal compaction and transparency. Similarly, in the developing mouse, appropriate formation of the corneal endothelium is essential for normal formation of the anterior chamber (Kidson et al., 1999). Characterising the cascade of molecular and cellular events that occurs during differentiation of the corneal endothelium is thus essential in describing and understanding congenital diseases.

1.2.2.1 Genes involved in corneal development

In the developing chick, classic induction experiments suggest that the lens plays a crucial role in specifying cells of the corneal endothelium (Genis-Galvez, 1966; Genis-Galvez et al., 1967). Lens extirpations and rotations suggest that signals derived from the lens epithelium are integral in triggering differentiation of the corneal endothelium. These findings are borne out by recent experiments, which show that factors secreted specifically by the lens epithelium regulates the expression of endothelial specific genes (N-cadherin) in presumptive corneal mesenchyme cells (Beebe and Coats, 2000).

Recent work has centred more specifically on characterising the role that specific genes play in the patterning and differentiation of presumptive corneal mesenchyme cells. Information on candidates such as TGFβ2, TGFα, EGF and EGF receptor, *Pitx2*, *Lmx1b*, *Six3*, *Pdgfra*, *Pax6*, *Foxc1* and *Foxc2* has been primarily derived from gene expression analyses or through the generation of null mutant mice.

Some spontaneous mutations that affect normal corneal differentiation have also been identified. For example, homozygous mice for mutations in the *corn1* gene are normal at birth; however, by P12 the cells of the corneal epithelium start to proliferate causing a dramatic thickening of the epithelial layer (Smith et al., 1996). Although keratin 14 is normally expressed in the epithelial

basal cells, its expression is expanded throughout the hyperplastic epithelium in *corn1* mice (Wang et al., 2000). By P14 the corneal stroma becomes highly vascularised (Smith et al., 1996) and expression of keratocan and lumican are upregulated (Wang et al., 2000).

TGFβ1*, *TGFβ2* and *TGFβ3

The transforming growth factors are a group of polypeptide signalling molecules that play crucial roles in regulating cell proliferation, differentiation, survival, extracellular matrix formation, bone and cartilage development, immune and inflammatory responses, wound healing, haematopoiesis and nervous system development (reviewed in Dünker and Krieglstein, 2000). Three β-type transforming growth factors are found in mammals. Their expression patterns are distinct, but often overlap. Furthermore, since they are secreted signalling molecules, significant differences in mRNA expression levels and protein expression often exist (Pelton et al., 1991).

TGFβ1, *TGFβ2* and *TGFβ3* and their receptors are all expressed in the developing and postnatal eye (Gordon-Thomson et al., 1998; Joyce and Zieske, 1997; Li et al., 1999; Pelton et al., 1991). Low levels of mRNA of *TGFβ1* and *TGFβ2* are observed in the cornea, with strong immunoreactivity to the proteins of all three (*TGFβ1*, *TGFβ2* and *TGFβ3*) occurring in the corneal epithelium. In the lens mRNA and protein expression is strongest in the germinative zone for all three forms. Only mRNA of *TGFβ2* is observed in the anterior lens epithelium, although low levels of protein expression for all three forms occur in the lens epithelium (Gordon-Thomson et al., 1998).

Targeted deletions for *TGFβ1* (Shull et al., 1992; Kulkarni et al., 1993), *TGFβ2* (Sanford et al., 1997) and *TGFβ3* (Proetzel et al., 1995; Kaartinen et al., 1995) have been generated with only *TGFβ2* null mutant mice having an eye phenotype. *TGFβ2* null mice are characterised by a hypercellular infusion of partially differentiated cell types in the posterior chamber of the eye, no lamination of the neural retina and a corneal stroma that is about one-third of its normal thickness at E18.5 (Sanford et al., 1997). Further analyses of *TGFβ2* null mice eyes suggest that the thinning of the corneal stroma results from a decrease in the synthesis of extracellular matrix components such as lumican, keratocan and collagen I, rather than a decrease in rates of cell accumulation and proliferation in the stroma (Joyce et al., 2002; Saika et al., 2001). Furthermore, in *TGFβ2* null mice

no corneal endothelium forms, with the corneal stroma remaining closely associated with the lens epithelium, so preventing normal anterior chamber formation (Saika et al., 2001).

TGFα, EGF and EGF receptor

Homozygous mutant *TGFα*$^{-/-}$ mice are viable, but exhibit a pronounced derangement and waviness of the fur and whiskers as well as having variable degrees of anterior segment dysgenesis including corneal inflammation and scarring (Luetteke et al., 1993; Mann et al., 1993). In order to further characterise the role *TGFα* plays in the developing anterior segment, transgenic mice expressing *TGFα* and EGF under the control of the αA-crystallin promoter have been generated (Reneker et al., 1995; Reneker et al., 2000). Interestingly these mice both present almost identical phenotypes, with an uncontrolled migration of periocular mesenchyme cells occurring around the entire lens to form a greatly enlarged and abnormal cornea with no corneal endothelium, as well as filling the posterior chamber of the eye and optic nerve. Since both *TGFα* and EGF bind to the EGF receptor (EGFR), and this receptor is expressed in the migrating periocular mesenchyme (Reneker et al., 1995), it was postulated that endogenous *TGFα* expression in the developing corneal and conjunctival epithelia (Reneker et al., 2000) act as chemo-attractants for the mesenchyme cells. This is supported by crossing αA-crystallin / *TGFα* mice with waved-2 mice (mice carrying a point mutation in the EGFR kinase domain (Luetteke et al., 1994)). Eye defects in these *TGFα* / wa-2 mice were significantly reduced, with the anterior segment still failing to form; however, the accumulation of mesenchyme cells around the lens was significantly diminished (Reneker et al., 1995). The lack of a normal anterior segment is most likely due to the corneal endothelium not forming, as determined through N-cadherin expression analyses (Reneker et al., 2000).

Pitx2, *Lmx1b*, *Six3*, *Pdgfra* and *Pax6*

Gene expression analyses have shown *Pitx2* (Kitamura et al., 1999), *Lmx1b* (Pressman et al., 2000), *Six3* (Hsieh et al., 2002) and *Pdgfra* (Schatteman et al., 1992) are expressed in the periocular mesenchyme, which ultimately differentiates to form the corneal stroma and endothelium. Baulmann et al. (2002) show weak expression of *Pax6* in the differentiating corneal stroma and endothelium, with strong expression in the corneal epithelium.

Mice with null mutations in *Pitx2* (Gage et al., 1999; Lin et al., 1999; Lu et al., 1999; Kitamura et al., 1999) or *Lmx1b* (Pressman et al., 2000) and chick embryos over-expressing *Six3* (Hsieh et al.,

2002) show similar corneal phenotypes. *Pitx2*$^{-/-}$ mice show an exaggerated migration of periocular mesenchyme cells into the anterior region of the eye, forming an abnormally thick mesothelial layer, which is invaded by lens epithelial cells at E12.5 (Gage et al., 1999; Kitamura et al., 1999). In *Lmx1b*$^{-/-}$ mice the anterior chamber is reduced in depth, with the corneal stroma not compacting by birth and containing ectopic blood vessels. Defects in the corneal stroma are attributed to poor construction of the extracellular matrix with collagen fibres having large diameters and showing an irregular non-orthogonal arrangement. Furthermore expression of keratocan (a proteoglycan essential for collagen fibrillogenesis and corneal transparency) was not evident at E13.5 or E15.5 (Pressman et al., 2000). Reciprocal gene expression analyses on the two null mutant backgrounds suggest that *Pitx2* and *Lmx1b* do not fall in a linear hierarchy of gene regulation (Lu et al., 1999; Pressman et al., 2000).

Knock-down experiments in zebrafish have shown *Six3* is essential for normal development of the forebrain and eye (Carl et al., 2002). Misexpression of *Six3* in the developing chick eye results in an abnormal eye morphology that includes a protrusion of the cornea (Hsieh et al., 2002). Although comprising all three layers, the cornea was significantly thicker, with the corneal stroma appearing uncondensed. The structure of the corneal endothelium was also compromised. Interestingly cells of the corneal stroma appear to have elevated levels of extracellular matrix components as assayed by collagen IX and *Keratocan* expression. Expression levels of *Pitx2* and *Lmx1b* were determined to be similar and unaffected in this system; however, the number of periocular mesenchyme cells was reduced. This reduction in cell number was attributed to reduced rates of cell proliferation in mesenchyme cells over-expressing *Six3* (Hsieh et al., 2002).

The platelet-derived growth factor A-chain (*Pdgfa*) and its receptor (*Pdgfra*) are predominantly expressed in non neuronal, neural crest derived tissues. In the developing eye they play an important role in lens differentiation as well as that of the cornea (Schatteman et al., 1992; Reneker and Overbeek, 1996). Mice harbouring mutations in the *Pdgfra* gene (*Patch* mutants) exhibit similar phenotypes to mice with null mutations (Morrison-Graham et al., 1992; Soriano, 1997). The population of periocular mesenchyme cells is greatly reduced in *Patch* mutant mice with a very thin cornea (approximately half the width of wildtype controls) forming (as examined at E13.5 and E16.5; Morrison-Graham et al., 1992). Over-expression of *Pdgfa* under the control of the αA-crystallin promoter primarily results in defects in lens differentiation; however, corneal

morphogenesis is also affected with the corneal stroma appearing thicker and expanded (Reneker and Overbeek, 1996).

The effect of *Pax6* gene dosage on eye development is well characterised and has been briefly described in Section 1.2.1.2 (Genes involved in ciliary body development). With particular reference to corneal development 53 % of $Pax6^{+/-}$ mice show mild to severe corneal phenotypes (Baulmann et al., 2002). Consistently one-third of all $Pax6^{+/-}$ mice have an opaque cornea (leucoma), with a central cleft (lens-corneal bridge) lined with epithelial cells and iridocorneal adhesions (synechiae) extending from the central iris to the cornea. Interestingly these phenotypes are partially rescued in $Pax6^{+/+} \leftrightarrow Pax6^{-/-}$ or $Pax6^{+/+} \leftrightarrow Pax6^{+/-}$ chimeric mice (Collinson et al., 2000, 2001, 2003). In these mice the primary factor controlling anterior segment development is normal formation of the lens. In $Pax6^{+/+} \leftrightarrow Pax6^{-/-}$ mice, $Pax6^{+/+}$ cells are preferentially included in the forming lens, which seems to abrogate further dysgenesis (Collinson et al., 2000). Further analyses have revealed that $Pax6^{-/-}$ cells are also preferentially excluded from all layers of the forming cornea, particularly those of the corneal epithelium where *Pax6* is most strongly expressed (Collinson et al., 2003).

Foxc1* and *Foxc2

Foxc1 and *Foxc2* belong to the forkhead / winged helix family of transcription factors, which are characterised by a forkhead DNA binding domain comprising three alpha helices, flanked by two loops, or "wings" (Clark et al., 1993). Members of this family of transcription factors have only been found in opisthokont organisms (animals and fungi) where they play fundamental roles in regulating both embryonic development and metabolism in the adult (reviewed in Carlsson and Mahlapuu, 2002; Kaufmann and Knöchel, 1996).

In humans mutations in forkhead genes have been implicated in various congenital defects that include disruptions to the anterior segment of the eye. Humans with gene mutations or chromosomal duplications of the region containing *FOXC1* exhibit various defects in the anterior segment and can develop congenital glaucoma or present with Axenfeld-Rieger anomaly (characterised by a prominent, anteriorly displaced Schwalbe's line, iris strands adherent to Schwalbe's line, hypoplasia of the iris stroma and focal iris atrophy) (Honkanen et al., 2003; Lehmann et al., 2000; Mears et al., 1998; Mirzayans et al., 2000; Nishimura et al., 1998, 2001; Panicker et al., 2002). In the eye, mutations in *FOXC2* cause distichiasis (additional diminutive

eyelashes) and ptosis (drooping of the upper eyelid) (Fang et al., 2000; Traboulsi et al., 2002). *FOXL2* mutations are associated with blepharophismosis-epicanthus inversus syndrome (BPES), which is characterised by narrowed palpebral apertures (blepharophismosis), drooping of the upper eyelid (ptosis) and an inversion of one of the lid folds (epicanthus inversus) (De Baere et al., 1999; reviewed in Lehmann et al., 2003). Finally, mutations in *FOXE3* are associated with the onset of Peters' anomaly (characterised by persistent corneolenticular adhesions), cataracts and a high incidence of glaucoma (Ormestad et al., 2002; Semina et al., 2001).

Mice homozygous for null mutations in the *Foxc1* gene die at birth with multiple abnormalities that include hydrocephalus, skeletal, ocular, renal and cardiovascular defects (Hong et al., 1999; Kidson et al., 1999; Kume et al., 1998, 2000, 2001; Rice et al., 2003, 2005; Smith et al., 2000; Winnier et al., 1999). Mice with a spontaneous mutation (*ch/ch*), which have similar defects, have been previously described (Gruneberg, 1943). Kume et al. (1998) have shown these mice contain a nonsense mutation at nucleotide 366 (C to T transition) of the coding region. This mutation results in a protein truncation in the third helix of the DNA binding domain, presumably rendering it inactive.

Foxc1$^{-/-}$ mice are born with their eyes open and the lens attached to the cornea, preventing the formation of an anterior chamber. Ultrastructural studies have shown that corneal differentiation is severely affected in these mice (Kidson et al., 1999). Firstly the corneal epithelium, which usually comprises 2 – 3 cell layers at E18.5, thickens in *Foxc1*$^{-/-}$ mice to include 5 – 7 cell layers. The corneal stroma is also thickened with disorganised irregularly arranged stellate cells that are loosely packed. No corneal endothelium forms (Kidson et al., 1999).

Gene expression analyses reveal that *Foxc1* is expressed in the periocular mesenchyme cells that surround the eye at E11.5 (Kidson et al., 1999). This expression is maintained as the cells migrate between the corneal epithelium and lens epithelium. By E12.5 *Foxc1* expression in the corneal stroma is greatly diminished, but it persists in the periocular mesenchyme cells (Hiemisch et al., 1998; Kidson et al., 1999). By E13.5 no *Foxc1* expression is evident in the differentiating cornea. The initial expression of *Foxc1* in the migrating periocular mesenchyme cells at E11.5 is likely to serve as a competence factor for the interpretation of other signals that drive corneal differentiation. Evidence does exist to suggest that the downregulation of *Foxc1* in the differentiating corneal stroma and endothelium is essential for normal morphogenesis. In *Lmx1b* null mutants, corneal

differentiation is disrupted with gene expression analyses showing that *Foxc1* expression persists in the differentiating corneal mesenchyme at E13.5 and E15.5 (Pressman et al., 2000). No gene expression differences between wildtype and *Foxc1*$^{-/-}$ mice for *Pitx2*, *Lmx1b*, *Pdgfa* or *Pdgfra* have been reported (Kidson et al., 1999; Smith et al., 2000).

Foxc2$^{-/-}$ null mutants die pre- or perinatally with skeletal and cardiovascular defects (Iida et al., 1997; Winnier et al., 1997, 1999). Although no detailed analysis of the developing eye in *Foxc2*$^{-/-}$ mice has been made, anterior segment defects in *Foxc2*$^{+/-}$ mice have been reported (Smith et al., 2000). *Foxc2*$^{+/-}$ mice variably exhibit defects in Schlemm's canal, the trabecular meshwork, ciliary body and iris, with the iris pigment epithelium appearing flattened and the iris stroma much reduced.

Double heterozygote mice (*Foxc1*$^{+/-}$ / *Foxc2*$^{+/-}$) have similar phenotypes to those of single heterozygotes; however, in some animals more exaggerated phenotypes are observed, including: malformations to the ciliary body, long connections between the iris and cornea, corneal vascularisation and mice being born with open eyelids (Smith et al., 2000). Based on these findings and data showing *Foxc1* and *Foxc2* are expressed in similar domains, it seems reasonable to suggest that these genes fulfil similar functions in the developing eye. Nevertheless, despite the overlapping expression domains, complementary expression analyses in *Foxc1*$^{-/-}$ and *Foxc2*$^{-/-}$ mice (Winnier et al., 1999) suggest that these genes are expressed independently of one another.

1.3 *In vitro* models of corneal differentiation

Although corneal transplants have a high success rate, graft rejection remains a problem (Joyce, 2003). Furthermore, full-thickness corneal transplants are often unnecessary, since often only the corneal endothelium is dysfunctional. In these cases partial transplants of the posterior stroma, Descemet's membrane and endothelium are preferable. The success of this technique is obviously dependent on the donor age, which is linked to the number of endothelial cells (Laing et al., 1976; Murphy et al., 1984). Several strategies have been employed to increase cell numbers in the corneal endothelium, the most obvious being the culture and expansion of untransformed endothelial cells, which are then seeded onto the transplant tissue. However this technique requires that the corneal endothelial cells be coaxed from their arrest in G1-phase of the cell cycle (Joyce et al., 1996). Other strategies have used endothelial cells transformed with SV40 T-antigen to drive proliferation in

cultured endothelial cells (Aboalchamat et al., 1999; Wilson et al., 1993). This is obviously not ideal in a clinical context, with cells retaining the potential to proliferate independently of normal cell cycle controls.

Thus refinement of present approaches to corneal transplants is essential. Ideally endothelial cells within donor tissues could be stimulated to proliferate and expand *in vivo* through administration of appropriate growth factors. In order to achieve this a clear understanding of the cellular events controlling corneal differentiation is first necessary. Since the corneal endothelium differentiates from a small population of migrating mesenchyme cells, it is not easy to map these cellular events *in vivo*. Thus development of *in vitro* models that mimic normal corneal differentiation is crucial.

Establishing cell lines of immortalised presumptive corneal mesenchyme cells could serve as a suitable model system. The SV40 large T-antigen is a well characterised oncoprotein, which interacts primarily with the retinoblastoma and p53 tumour suppressor genes so disrupting the G1/S and G2/M checkpoints of the cell cycle (Ali and DeCaprio 2001; Pipas and Levine, 2001, Uramoto et al., 2004). Thus small populations of cells from embryonic tissues can be immortalised with this oncoprotein and expanded. These expanded cell populations allow precise descriptions of molecular or morphological changes that occur during differentiation to be made. One drawback of immortal cell lines is that their molecular characteristics can change with time. Ultimately they may no longer serve as appropriate models for the tissues from which they were derived.

In any model system it is first necessary to confirm that the system does in fact accurately (or reasonably) reflect and model the tissues and cellular processes of interest. Within the developing cornea, the formation of adherens and tight junctions serve as key events marking the endothelium's ability to function as an "ionic pump". In the developing mouse adherens (as marked by N-cadherin expression) and tight junctions (as marked by the expression of Z0-1) form early during differentiation of the corneal endothelium (Beebe and Coats, 2000; Ickes et al., 2002 in Joyce, 2003; Kidson et al., 1999; Mgwebi, PhD thesis, 2004; Reneker et al., 2000; Xu et al, 2002). Thus with a view to establishing an *in vitro* model of the developing corneal endothelium, accurate characterisation of cell junction formation is essential.

1.3.1 Cell junctions

Cell junctions serve as crucial points of contact between cells and with the extracellular matrix. Most cell junctions are anchored to the cytoskeleton and so impart mechanical strength to tissues, which is particularly important in epithelia. Cell junctions are easily classified according to their functions: i) occluding junctions serve to regulate the paracellular passage of ions and solutes as well as functionally compartmentalising the apical cell membrane; ii) anchoring or adhesion junctions mechanically attach cells to neighbouring cells or the extracellular matrix; iii) communicating junctions mediate the passage of chemical or electrical signals between adjacent cells (Alberts et al., 1994). Table 1-1 summarises the different types of cell junctions, their associated cytosolic proteins and attachment to the cytoskeleton.

Table 1-1: Summary of cell junction components

Junction	Transmembrane linker proteins	Extracellular ligand	Intracellular attachment proteins	Intracellular cytoskeletal attachment
Occluding junctions				
Tight junctions	occludin, claudins, JAM	occludin, claudins, JAM	ZO-1, -2, -3, aPKC cingulin, spectrin, AF-6, PAR3, 6, MAGI-1, -2, -3	actin filaments
Adhesion to other cells				
Adherens	cadherin (e.g. E-, N-, P-cadherin)	homotypic binding to cadherin in adjacent cell	α-, β-, γ-catenins, vinculin, α-actinin	actin filaments
Desmosome	cadherin (desmogleins, desmocollins)	heterotypic binding to cadherin in adjacent cell	desmoplakins, plakoglobin	intermediate filaments
Adhesion to the extracellular matrix				
Adherens	integrin	extracellular matrix proteins	talin, vinculin, α-actinin	actin filaments
Hemidesmosome	integrin	extracellular matrix (basal lamina) proteins	desmoplakinlike protein	intermediate filaments
Communicating junctions				
Gap junctions	connexins	connexins		none

Data summarised from Alberts et al., 1994; Balda and Matter, 2000; Goodenough, 1999; Jamora and Fuchs, 2002; Matter and Balda, 2003.

1.3.1.1 Adherens junctions

Cell-cell adherens junctions are essential elements in both epithelial and non-epithelial tissues. In both cases members of the cadherin superfamily of intercellular adhesion proteins serve to connect cells via their actin filaments (Alberts et al., 1994). The ability of cells to form and disassemble cell junctions is essential in both embryonic development and for the maintenance of adult tissues. A complex series of events leads to cell junction formation.

Briefly, in a calcium dependent process, multiple adhesive interactions between the extracellular cadherin domains (EC1 –5) of cadherin proteins in adjacent cells establish homophilic bonds (Chappuis-Flament et al., 2001). Clusters of cadherin contacts stimulate cytoskeletal rearrangements such that the carboxyl terminus of the cadherin protein becomes stably bound to the cortical actin filaments (reviewed in Braga, 2002; Jamora and Fuchs, 2002). For example, in E-cadherin based junctions, this binding is achieved through an initial binding of β-catenin to the carboxyl terminus of E-cadherin. Once a cadherin-cadherin homotypic complex has formed α-catenin binds to β-catenin and either binds directly to actin filaments, or indirectly via the linker protein vinculin (Jamora and Fuchs, 2002). Regulation of the complex cytoskeletal rearrangements that occur during junction formation are regulated by the Rho family of small GTPases (reviewed in Braga, 2002; Jamora and Fuchs, 2002). Rho subfamily members contribute to stress fibre elongation, Rac mediates lamellipodia and ruffle formation and Cdc42 is involved in the formation of filopodia.

Disruptions to cadherin (Larue et al., 1994; Radice et al., 1997a, 1997b; Riethmacher et al., 1995) or catenin (Torres et al., 1997; Haegel et al., 1995) proteins often result in embryonic lethality. Furthermore, appropriate assembly of adherens junctions is essential for establishing cellular polarity through the subsequent formation of tight junctions. It is thought that adherens based junctions promote this by: i) physically bringing cell membranes in close apposition, ii) providing spatial cues for the delivery of junctional components to the membrane and iii) triggering signalling pathways that initiate desmosome or tight junction assembly (Braga, 2002).

1.3.1.2 Tight junctions

Tight junctions are essential functional elements of epithelial sheets serving to regulate the paracellular passage of solutes and ions as well as forming epithelial compartments by preventing the mixing of apical and basolateral membrane components (Braga, 2002). Structurally, tight junctions are composed of an anastomosing network of strands, which form a seal around the cell apex. These strands consist of occludin and claudin proteins, which both have four extracellular loops that bind to occludin and claudin proteins of adjacent cells. It has been suggested that the ratio and distribution of occludin and claudin proteins within the strands determines the permeability properties of a given tight junction (Balda and Matter, 2000). The tight junction associated proteins zonula occludens (ZO)-1, ZO-2, ZO-3 all associate with each other around tight junctions and form a bridge between occludin and claudin proteins in the membrane and actin filaments of the cytoskeleton (Balda and Matter, 2000; Goodenough, 1999).

1.4 Specific aims

Anterior segment dysgenesis refers to a heterogeneous group of disorders whose onset has a strong genetic component (Gould and John, 2002; Gould et al., 2004). Often there is a great deal of phenotypic variance within groups of people sharing the same genetic defect, which clearly points to the multifactorial nature of this group of disorders. The mouse represents an important experimental model of multifactorial diseases. The large number of inbred mice strains are invaluable in identifying modifier genes, which variably affect expressivity of a given gene defect. However, its effective use as a model system requires a detailed understanding of its anatomy and development.

Although a great deal is known about early eye development and the role that various genes play, little is known about the late embryonic and early postnatal stages of mouse eye development. Importantly, it is at these stages that several structures within the anterior segment develop. With particular reference to the developing ciliary body no assessment of its postnatal development has been made. Little is known of how cell dynamics such as cell heights or mitotic rates change as ciliary processes form in the mouse. Furthermore, the structure of the adult ciliary body has not been described.

In addition to describing structural changes that occur during development of the anterior segment, it is crucial to understand the underlying genetics that direct and effect these changes. Mice with null alleles have served an invaluable role in identifying genetic factors necessary for normal eye development. Although genes such *Foxc1* are known to direct differentiation of the corneal tissues, it is difficult to accurately provide a detailed characterisation of the morphological and genetic changes that occur within the presumptive corneal stroma and endothelial cells as they differentiate *in vivo*. Establishing *in vitro* cultures of these cell populations can serve as important models of such events.

The specific aims of this study are thus:

- To determine whether the structure of the adult mouse ciliary body is similar to other vertebrates.
- To determine the molecular and morphological sequence of events that leads to ciliary body specification, differentiation and morphogenesis by:
    - Providing a detailed structural description of the developing ciliary body and exploring how the ciliary epithelia fold to form ciliary processes from two initially parallel cell layers.
    - Potential models for ciliary folding will be explored. For example, whether a simple flexure of the epithelia leads to their folding or if more complicated changes in cell dynamics such as cell height changes and differential rates of proliferation between the ciliary epithelia contribute to its morphogenesis.
    - Finally the temporal relationship between the formation of ciliary processes and the expression of *Bmp4*, *Tgfβ1i4* and LEF1 will be examined.

- To determine whether immortal cell lines of presumptive corneal mesenchyme cells, dissected from E12.5 *Foxc1*$^{+/+}$, *Foxc1*$^{+/-}$ and *Foxc1*$^{-/-}$ eyes can be successfully used to model corneal differentiation events *in vitro*.
    - To determine whether wildtype immortal cell lines retain molecular characteristics of normal periocular mesenchyme cells by mapping the expression profiles of *Foxc1*, *Foxc2*, *TGFβ1* and *Tgfβ1i4* in *Foxc1*$^{+/+}$ cells. Potential differences in expression between *Foxc1*$^{+/+}$ and *Foxc1*$^{-/-}$ cells will also be assessed.

- The suitability of this culture system to model normal corneal differentiation events occurring during early specification of the corneal endothelium will be tested by assessing the ability of wildtype cells to form adherens and tight junctions in culture.
- Comparative studies of junction formation in *Foxc1*$^{+/+}$ and *Foxc1*$^{-/-}$ cells will be used to test the hypothesis that early *Foxc1* expression in corneal mesenchyme cells is necessary for junction assembly in the corneal endothelium. Additionally these experiments will indirectly test the role that lens derived signals play in determining the assembly of cell junctions in the corneal endothelium.

Chapter 2: Materials and Methods

2.1 Animals and genotyping

All experimental procedures performed on animals were approved by the UCT animal ethics committee (Licence number 01/11). The Bmp4^{lacZ} (Lawson et al., 1999) and Foxc1^{lacZ} (Kume et al., 1998) transgenic mice were generously provided by Brigid Hogan (Duke University). The Bmp4^{lacZ} mice were maintained on an ICR background, while the Foxc1^{lacZ} mice were maintained on a mixed C57BL6J / 129 background. Experiments performed on wildtype mice made use of ICR, C57BL6/J and C57BL6J / 129 mice strains.

2.1.1 DNA extraction

Genomic DNA from embryonic tissues and adult tail cuts was extracted using a conventional enzyme lysis and phenol-chloroform protocol (Sambrook et al., 1989). Briefly, tissues were digested overnight at 56°C with proteinase K (300 µg / ml) (Roche) in lysis buffer (100 mM Tris·HCl pH8.0, 5 mM EDTA pH8.0, 200 mM NaCl and 0.2 % SDS). An equal volume of 0.5 M Tris saturated phenol (pH 8.0) was added and samples were left rotating at room temperature for 1 h. Following a 10 min centrifugation at 10 000 g at room temperature, the upper aqueous was removed and an equal volume of chloroform added. Samples were then centrifuged for 5 min at 10 000 g at room temperature. The resulting aqueous phase was removed and DNA precipitated overnight at -20°C, in two volumes of absolute ethanol. Following a 10 min centrifugation at 10 000 g at 4°C, DNA pellets were washed in 70% ethanol, recentrifuged, air-dried for 10 min and resuspended in 20 µl distilled water (dH_2O).

2.1.2 Bmp4^{lacZ} genotyping

The *Bmp4* gene consists of five exons with two transcription start sites in exons 1a and 1b respectively and the protein coding region spanning exons 3 and 4 (Kurihara et al., 1993). Homologous recombination with a *lacZ* targeting vector resulted in most of exon three being replaced by the coding region of the β-galactosidase gene, while retaining the normal regulatory elements of the *Bmp4* gene (Figure 2-1) (Lawson et al., 1999).

Based on this Bmp4^{lacZ} construct, two PCR based genotyping strategies were followed. Firstly, primers specific to the *lacZ* gene itself were used (Appendix Table A-1, Figure 2-1 and Figure 3-1A). These primers specifically amplify a 279 bp product in DNA extracted from *Bmp4*$^{+/-}$ and *Bmp4*$^{-/-}$ mice. In this study it was not necessary to distinguish between *Bmp4*$^{+/-}$ and *Bmp4*$^{-/-}$ mice since only developmental events occurring perinatally were of interest and *Bmp4*$^{-/-}$ mice die during early embryonic development (Winnier et al., 1995).

A second set of primers, also specific to the *lacZ* cassette, was designed; however, the 5' primer was designed to fall upstream of the *lacZ* insertion site in the targeted allele (Appendix Table A-1, Figure 2-1 and Figure 3-1A). These primers were primarily designed for genotyping *Foxc1* x *Bmp4* double heterozygote animals, but were also used for genotyping the Bmp4^{lacZ} mouse strain. All repeat elements within the targeted allele were masked using RepeatMasker (http://www.repeatmasker.org/) and the primers were then designed to flank the *lacZ* insertion site using Primer3 (http://frodo.wi.mit.edu/cgi-bin/primer3/primer3_www.cgi). A 497 bp product is amplified in DNA extracted from *Bmp4*$^{+/-}$ and *Bmp4*$^{-/-}$ mice. Restriction enzyme digests with AvaI and SmaI were used to confirm the specificity of the PCR product.

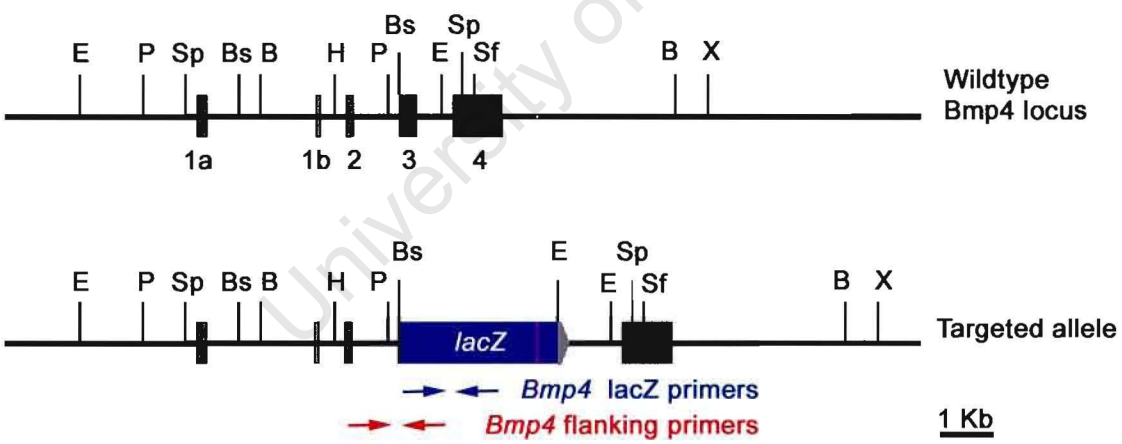

Figure 2-1: Targeted disruption of the *Bmp4* gene

(Adapted from Lawson et al. 1999)

The wildtype *Bmp4* allele contains five exons, with two transcription start sites in exons 1a and 1b and the protein coding region spanning exons 3 and 4 (black box). In the targeted allele most of exon 3 is replaced with the β-galactosidase gene (blue box) in frame with the translational start sites. The *lacZ* specific primers used for genotyping are shown in blue, while the flanking primers are shown in red. B, BamHI; Bs, BsmI; E, EcoRI; H, HindIII; N, NotI; P, PstI; Sf, SfiI; Sp, SpeI; X, XbaI.

2.1.3 Foxc1^{lacZ} genotyping

The *Foxc1* gene contains a single protein coding exon flanked by 5' and 3' untranslated regions (Hiemisch et al., 1998). Homologous recombination with a *lacZ/PGKneo*^{r} cassette resulted in most of this coding exon and 3' untranslated region being replaced with the β-galactosidase gene, which remained under the control of the *Foxc1* promoter (Figure 2-2) (Kume et al., 1998).

A multiplex PCR reaction was used to distinguish wildtype, heterozygote and mutant genotypes. A single forward primer, 5' to the site of homologous recombination, was used together with two reverse primers; one reverse primer being specific to the normal non-targeted *Foxc1* allele, and the other specific to the β-galactosidase gene (Figure 2-2). Thus *Foxc1*$^{+/+}$ DNA amplifies a 124 bp product, *Foxc1*$^{+/-}$ DNA amplifies both a 124 bp and a 370 bp product and *Foxc1*$^{-/-}$ DNA amplifies a 370 bp product.

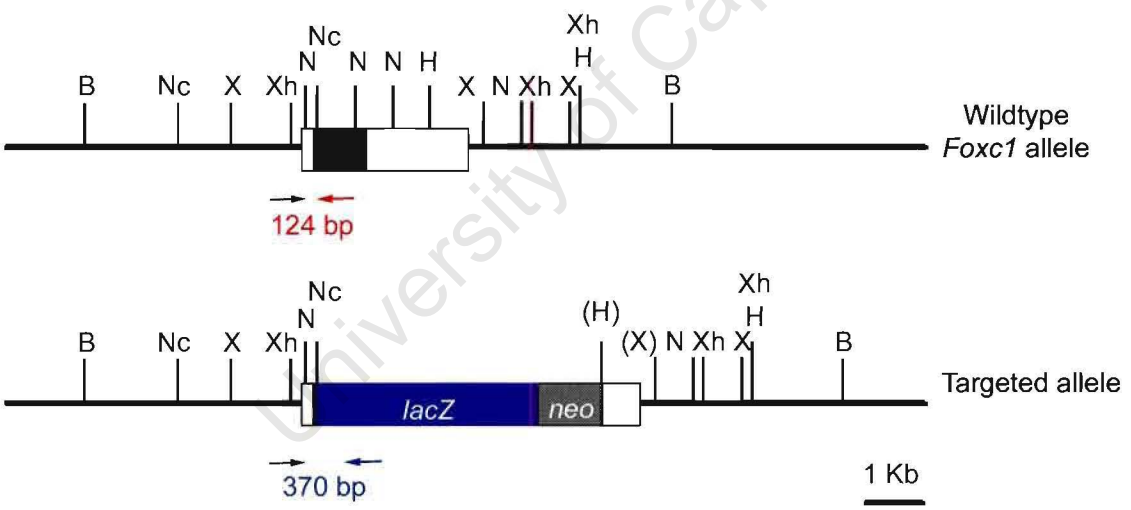

Figure 2-2: Targeted disruption of the *Foxc1* gene

(Adapted from Kume et al., 1998)

The wildtype *Foxc1* allele contains a single protein coding exon (black box), flanked by 5' and 3' untranslated regions (open boxes). The targeted allele comprises both the β-galactosidase (blue box) and neomycin resistance (grey box) genes in frame with the translational start site. The common forward primer used for genotyping is shown in black, with the reverse primer for the wildtype allele in red and the *lacZ* reverse primer shown in blue. B, BamHI; H, HindIII; N, NotI; Nc, NcoI; X, XbaI; Xh, XhoI. Parentheses indicate the loss of a restriction site.

2.2 Scanning electron microscopy

Eyes from embryonic days E17.5 and E18.5, postnatal stages P0 – P7 and from adult ICR mice were dissected and processed for scanning electron microscopy. Following dissection, the eyes were placed in Karnovsky's fixative (1.5% paraformaldehyde (Merck), 0.5% glutaraldehyde (Agar Scientific) in 0.1M Sorenson's phosphate buffer (SPB), pH 7.4, and while in fixative, the posterior globes of the eyes were pierced with a tungsten needle. The whole eyes were left in fixative at 4°C. After 24 – 48 h of fixation, eyes were cut equatorially, the lens carefully removed and the anterior half of the eye placed in Karnovsky's fixative overnight. For some adult eyes the anterior half of the eye was inverted after removing the lens. Tissues were then washed in SPB and post-fixed in 2% OsO_4 in phosphate buffer at room temperature for 2 h. All samples were then dehydrated through a standard ethanol series after being washed in SPB and then distilled water. Samples were critical point dried (CPD 020, Balzers), mounted on stubs, sputter coated with gold palladium for 20 min (Balzers sputter coater) and viewed using a S440 scanning electron microscope (Leo, Leica).

2.3 Histology

Embryonic and postnatal development of the ciliary body was examined in ICR mice. Whole embryonic heads, half heads or eyes from E14.5 to P7 were fixed in 4% paraformaldehyde (Merck) at 4°C overnight. After 1 hour of fixation the posterior globes of dissected eyes were pierced twice with a tungsten needle to ensure penetration of the fixative. All tissue was washed in phosphate buffered solution (PBS) (pH 7.4) after fixation and dehydrated through an ethanol series at 4°C. Tissues were cleared in xylol (3 x 20 min exchanges) at room temperature, left overnight in wax at 60°C and embedded the following morning. During fixation and processing samples were agitated using a rotating mixer. Tissue was sectioned at 5 μm or 6 μm and stained using haematoxylin and eosin.

2.3.1 Cell heights

Cell heights were measured as follows: For each developmental stage, five sections from mice from two different litters were analysed. Photographs of the cross sections from P0 and P7 were analysed using Adobe Photoshop 5.5. Cell heights were measured in three regions: at the neural retina –

ciliary body boundary, at the tips of ciliary processes and at the ciliary body – iris boundary (Figure 3-9). Heights were calculated by drawing lines across the epithelia at these points and then measuring and converting them to micrometers using a scale bar. Paired t-tests were used for all comparisons (Statistica version 6).

2.4 Gene expression analyses

2.4.1 LacZ staining

Timed matings between *Bmp4*$^{+/-}$ adult mice were set up, and embryos from E17.5 and E18.5 pregnant females were harvested. Eyes from these embryonic mice as well as a postnatal series (two separate litters) from P0 – P7 were dissected. Whole eyes were fixed for 30 min in 4% paraformaldehyde (Merck) at 4°C on a rotating mixer. The posterior globe of the eye was then sliced transversely using a razor blade and tissues were fixed for a further hour. Tissues were washed extensively, 4 –5 exchanges of 1 x PBS for 15 – 30 min each, at room temperature. Tissues were then incubated in Xgal staining solution (Appendix Table A-2) overnight, in the dark, at 37°C. The following day, tissues were washed in 1 x PBS, whole eyes were photographed and then processed to wax as for histology. Times for tissue clearing in xylol were reduced to 3 x 15 min exchanges. Tissue was sectioned at 6 µm and either mounted unstained, or counterstained briefly (30 – 60 s) with eosin before being mounted.

2.4.2 *In situ* hybridisation

Standard techniques were used for *in situ* hybridisation, with some modification (Braisant and Wahli, 1998). Tissues were dissected and processed for histology using RNAse free solutions (solutions were treated with 0.01% DEPC (Sigma)). Tissue sections, 6 – 7 µm, were transferred onto SuperFrost plus (Menzel-Glázer) slides, and affixed by baking for 2 h at 60°C.

2.4.2.1 Riboprobe synthesis

For riboprobe synthesis, *Tgfβ1i4* (IMAGE clone AW240300.1) or LEF1 (Reh laboratory) plasmid DNA was purified (Nucleobond® AX, Macherey-Nagel) and linearised with SalI (for antisense

probe) or NotI (for sense probe). Sense (SP6) and antisense (T7) probes were generated by transcribing 1 μg of linearised template DNA in the presence of digoxigenin (DIG) labelled UTP (Roche) using SP6 or T7 RNA polymerases respectively (Gibco or Roche). Reactions were allowed to proceed overnight in the presence on RNAsin (Promega). Transcription reactions were performed at 40°C for SP6 RNA polymerase and 37°C for T7 RNA polymerase. After the in vitro transcription reaction, samples were treated with DNaseI (Promega) (15 – 30 min at 37°C) to remove the template DNA. Following this, the riboprobe was precipitated with 0.1M lithium chloride and 2½ volumes ethanol overnight at -20°C. RNA pellets were resuspended in 20 μl of DEPC treated dH_2O. Once in solution, 20 μl of hybridisation buffer (Appendix Table A-3) was then added. Aliquots were stored at -80°C.

2.4.2.2 Hybridisation

Tissues were dewaxed in xylol and hydrated through an ethanol series to water, then transferred to 1 x PBS and finally 2 x SSC. For prehybridisation, sections were incubated at 60°C (*Tgfβ1i4*) or 65°C (LEF1) in hybridisation buffer (Table 2-2) for two hours. Following this 1 μg/ml riboprobe in hybridisation buffer was added to the tissue sections and hybridised overnight under a coverslip in a humidity chamber (with 50% formamide and 2 x SSC).

2.4.2.3 Washes and immunocytochemistry

After hybridisation, tissue sections were washed twice (1 x 15 min, 1 x 30 min in 50% formamide, 1 x SSC and 0.1% Tween-20) at the hybridisation temperature. Following two washes in MABT (Appendix Table A-3) at room temperature sections were blocked with 2% Boehringer blocking reagent and 20% goat serum in MABT for 1.5 h at room temperature. Tissue was incubated overnight at room temperature with a 1:2000 dilution of an anti-DIG-alkaline phosphatase conjugate (Roche) in blocking solution.

2.4.2.4 Colour detection

Tissue sections were washed five times in MABT, with agitation, and then twice in NTMT (Appendix Table A-3). For colour detection, slides were allowed to react with nitroblue tetrazolium

(NBT)/5-bromo-4-chloro-3-indolyl phosphate(BCIP) (330 μg/ml NBT and 165 μg/ml BCIP (Roche and Sigma)) in NTMT. The reaction was stopped with PBS and tissues were post fixed in 4% paraformaldehyde (Merck) for 30 min and then mounted.

2.5 Immunocytochemistry

2.5.1 von Willebrand factor (Factor VIII) staining

Eyes from E18.5 ICR mice were dissected and processed through to wax as for histology. Sections cut at 6 μm were transferred onto SuperFrost plus (Menzel-Glázer) slides and used for immunocytochemistry. Sections were first hydrated and then treated for 20 min with Pro Enzyme (DAKO) at 37°C. von Willebrand factor expression was detected using a rabbit polyclonal anti-human factor VIII antibody (DAKO) (1:500 dilution in 1% bovine serum albumin (BSA) in PBS, for 1 h at room temperature). Sections were then washed in PBS and incubated with EnVision dual link secondary antibody (DAKO). Colour detection was carried out using standard procedures with 3,3-diaminobenzidine terahydrochloride (DAB) (Sigma) as a substrate. Sections were then counterstained with haematoxylin for 30 s, dehydrated and mounted using Entellan (Merck).

2.5.2 BrdU labelling

In two separate experiments embryonic and neonatal ICR mice from E18.5 to P7 were labelled with bromo-deoxy-uridine (BrdU) (Sigma). Pregnant females were injected intraperitonealy with BrdU (120 μg per gram body mass) for 2 h prior to being sacrificed. Neonates were injected subcutaneously in the dorsal neck region with BrdU at a concentration of 100 μg per gram body mass. P0 mice were labelled for 2½ h, while all other neonates were labelled for 24 h before being sacrificed. All mice were sacrificed at the same time on successive days. Eyes and gut tissue were dissected and processed through to wax as described for histology. For each developmental stage ten 6 μm sections from each eye were transferred onto 3-(triethoxysilyl)-propylamin (Aptes) (Merck) coated slides and used for immunocytochemistry. Sections from the gut were used as a positive control tissue. BrdU incorporation was detected using a mouse monoclonal anti-BrdU antibody (Roche) (1:20 dilution in 0.5% bovine serum albumin (BSA) in Tris buffered saline TBS, overnight at 4°C). Sections were then washed in TBS and incubated with biotinylated sheep anti-

mouse immunoglobulins for 1 h at room temperature (1:1000 dilution in 0.5% BSA in TBS). Colour detection was carried out using standard procedures for the streptABComplex/HRP kit (DAKO) and 3,3-diaminobenzidine terahydrochloride (DAB) (Sigma) as a substrate. Sections were then counterstained with haematoxylin for 30 s, dehydrated and mounted using Entellan (Merck).

2.5.2.1 Cell counts and statistics

For each of the two independent experiments, ten sections at each developmental stage at the level of the optic nerve were photographed and analysed. For each eye section, both ciliary zones of the eye (i.e. both the left and right side of the section) were analysed. Thus for each stage a total of 20 counts was obtained. For all samples, BrdU positive and negative nuclei in the ciliary epithelia were counted. The prospective ciliary zone in the inner ciliary epithelium was delineated using the histologically obvious neural retina and iris boundaries (Figure 3-9). These delineated borders were extended to the outer ciliary epithelium. Ciliary muscle cells adjacent to the outer ciliary epithelium were excluded from the counts. For each cross section the number of BrdU positive cells was expressed as a percentage of the total number of cells to normalise for differences in size between cross sections. A mean percentage for the number of dividing cells in each layer was then calculated. Initially results from the two independent experiments were compared. Independent t-tests (Statistica version 6.1) were used to compare the number of dividing cells within each epithelial layer at each developmental stage. No significant difference between the two experiments was found. Consequently, data from the two experiments were pooled and used as such for all subsequent analyses.

2.5.3 Neurofilament and Collagen IX

Neurofilament and Collagen IX immunostaining was performed on tissues processed for *in situ* hybridisation. Once the colour reaction was complete, tissue sections were washed in 1 x PBS (phosphate buffered saline, pH 7.4) and then processed as follows. Tissue was blocked and permeabilised using 1% Triton X-100 and 5 – 10% goat serum in 1 x PBS for 30 min at 4°C. Primary antibodies were diluted in 1 x PBS containing 0.15% Triton X-100 and 5% goat serum (Neurofilament M 1:1000; Collagen IX 1:100) and left overnight at room temperature. Sections were washed three times in 1 x PBS for 5 – 10 min each at room temperature. Secondary antibodies (Alexa, goat anti-rabbit, 488 for Neurofilament and goat anti mouse, 568 for Collagen IX) were

diluted 1:500 in 1 x PBS containing 0.3% Triton X and 1% goat serum and incubated for 1 – 2 h in the dark at 4°C. After washing three times in 1 x PBS slides were mounted with Fluoromount-G (Southern Biotechnology Associates, Inc.).

2.5.4 SV40 large T-antigen

Cells, cultured on 12 mm coverslips were washed in 1 x PBS and then fixed for 15 min in 2% paraformaldehyde (Merck) at room temperature. Cells were then washed three times in 1 x PBS and permeabilised with 100% methanol for 15 min at -20°C. Cells were then incubated with a 1:1 dilution of the mouse monoclonal anti-SV40 large T antigen clone Pab101 in 0.1% BSA in 1 x PBS) for 2 h at room temperature and then transferred to 4°C and incubated overnight. Cells were then washed three times with cold 1 x PBS and incubated with a donkey-anti-mouse-cy3 secondary antibody (1:1000 dilution in 0.1% BSA in 1 x PBS) for 1 h at room temperature. Cells were washed three times in 1 x PBS and incubated with a 1:50 dilution of DAPI (50 µg/ml) in 1 x PBS for 10 min at room temperature. Cells were washed once in 1 x PBS and mounted in mowiol with n-propyl galate (3,4,5-Trihydroxybenzoic acid n-propyl ester, Sigma).

2.5.5 β-galactosidase, Foxc2, N-cadherin and ZO-1

2.5.5.1 Cells in culture

Cells, cultured on 12 mm coverslips, were washed in 1 x PBS and then fixed for 10 – 15 min in 4% paraformaldehyde (Merck) with 0.15% Triton X-100 at room temperature. Cells were then washed three times in 1 x PBS and blocked in 0.5% BSA in 1 x PBS for 1 h at room temperature. Primary antibodies (β-galactosidase: (polyclonal antibody, Invitrogen) 1:250; Foxc2: (polyclonal antibody, Research genetics, gift from Dr Brigid Hogan) 1:200; N-cadherin: (polyclonal antibody, Santa Cruz Biotechnology) 1:300 and ZO-1: (monoclonal antibody, gift from Dr Brigid Hogan) 1:250) were all diluted in 0.5% BSA in 1 x PBS and incubated overnight at 4°C. Cells were then washed three times with cold 1 x PBS and incubated with secondary antibodies (donkey anti-rabbit-cy3 or goat anti-rabbit-alexafluor for polyclonals and donkey anti-mouse-alexafluor for monoclonals) diluted 1:1000 in 0.5% BSA in 1 x PBS for 1 h at room temperature. Cells were washed three times in 1 x PBS and incubated with a 1:50 dilution of DAPI (50 µg/ml) in 1 x PBS for 10 min at room

temperature. Cells were washed once in 1 x PBS and mounted in mowiol with n-propyl galate (Sigma).

2.5.5.2 Hanging drop cultures and N-cadherin immunofluorescence staining

Confluent 10 cm plates of wildtype and *Foxc1*$^{-/-}$ cells were trypsinised, pelleted and then resuspended in 1 ml of culture medium. For each hanging drop, 30 µl of the resuspended cells was pipetted onto the lid of a 35 mm culture dish, which was then placed on the dish itself and left for 48 – 72 h at 39°C. Cell aggregates were then processed for immuoncytochemistry as described for cells in culture. Modifications to the protocol included more extensive washes being performed after incubation with the primary antibody. Cells were washed three times in 1 x PBS and then left in 0.5% BSA in 1 x PBS for 2 h at 4°C. The secondary antibody (Donkey anti-rabbit-cy3) was diluted 1:1000 in 0.1% BSA in 1 x PBS and incubated for 1 h at room temperature. Following this the cell aggregates were washed twice in 0.5% BSA in 1 x PBS and a third wash was left for a further hour at room temperature. Finally the cells were washed three times, for 5 min each, in 1 x PBS before being mounted with Fluoromount (DAKO).

2.6 Microdissections and cell cultures

2.6.1 Immortalising primary cell cultures

Primary cultures of periocular mesenchyme from the anterior region of E12.5 mouse eyes were established and immortalised as follows. Small wedges (±0.05 mm^3) of cells from this region were teased away using tungsten needles and placed in 24 well plates. For each embryo 4 – 5 wedges were cultured in the same plate for 48 – 72 h at 37°C (in DMEM (Sigma) containing 20% foetal calf serum (FCS)). Following this initial expansion, the primary cultures were then immortalised by infection with a retrovirus encoding a temperature-sensitive mutant SV40 large T-antigen as well as a gene conferring neomycin resistance (Frederiksen *at al.*, 1988; Jat and Sharp, 1989). The ψ_2 producer cell line packages the mutant SV40 T-antigen in an attenuated retrovirus, which is secreted from the cells. Thus viral containing supernatant was harvested from the producer cell line by harvesting culture medium from confluent cultures dishes (after 4 – 5 h), briefly centrifuging the medium at 2000 rpm and filtering the medium through 0.45 µm filters. This filtered medium was

used immediately to infect the primary cultures. Polybrene (8 μg / ml medium, Sigma) was used as a carrier molecule to facilitate infection. Cells were incubated at 37°C for 2 h, after which the medium was replaced with DMEM containing 20% FCS. Cells were left at 37°C overnight and then transferred to 33°C. After 48 h they were expanded in selective media containing 400 μg / ml geneticin (G418, Sigma) for 10 – 14 days. Untransformed mouse embryonic fibroblasts were used as control cultures during selection. All control cells died by the end of the first week.

2.6.2 Cell cultures

All cells were cultured using standard vented tissue culture plates (Greiner Bio-one).

2.6.2.1 Primary cell cultures and immortal cell lines

Primary cultures of periocular mesenchyme cells were grown in DMEM (Sigma) containing 20% foetal calf serum (FCS) (Highveld Biological (Pty) Ltd.) and 100 I.U. penicillin and streptomycin at 37°C with 5% CO_2. After immortalisation cells were cultured at 33°C with 5% CO_2. Cells were initially cultured with DMEM containing 20% FCS and later this was reduced to 10% FCS.

2.6.2.2 Mouse embryonic fibroblast cells

Frozen stocks of mouse embryonic fibroblasts (passage 2) were thawed and cultured at 37°C with 5% CO_2 in DMEM containing 10% FCS, sodium pyruvate (1 mM), L-glutamine (2 mM), β-mercaptoethanol (0.001%) non essential amino acids and 100 I.U. penicillin and streptomycin.

2.6.2.3 ψ_2 producer cell line

Frozen stocks of the ψ_2 producer cell line were thawed and cultured at 37°C with 5% CO_2 in DMEM containing 5% FCS and 100 I.U. penicillin and streptomycin. When harvesting viral containing supernatant from confluent plates, medium was containing 10% FCS was used.

2.7 Western blotting

2.7.1 Protein extraction and quantitation

Protein was extracted from ICR adult mouse kidneys and cells in culture. Adult tissues were dissected, weighed, homogenized in complete extraction buffer (Table 2-3) (volume (ml) = 19 x the weight in grams) and left overnight at 4°C. Cultured cells were treated similarly. Cells from a confluent 10 cm plate were washed three times in cold 1 x PBS, then lifted with a rubber-policeman in 150 µl complete extraction buffer and left overnight at 4°C. Cell lysates from tissues and cells were centrifuged at 10 000 g for 15 min at 4°C and the supernatant was then divided into aliquots and stored at -80°C.

Protein quantitation was performed using a Bio-Rad assay (Bio-Rad). Briefly, the Biorad dye was filtered through Whatman number 1 paper and BSA was used to make a standard curve with protein concentrations ranging from 0.2 – 1.4 mg/ml. Protein from tissues and cells were diluted 1:5 in 1 x PBS and protein absorbance measured at 595 nm.

2.7.2 Gel electrophoresis, transfer and immunodetection

Thirty micrograms of protein was denatured by boiling for 2 min in sample buffer (Appendix Table A-4) and run on a polyacrylamide gel (5% stacking gel and 12% separating gel) at 150 V at room temperature. Protein was transferred to a Hybond ECL nitrocellulose membrane (Amersham) membrane at 8 V, overnight at 4°C. Blots were washed in TBS-T (Appendix Table A-4) after transfer and then blocked in 5% low fat milk powder in TBS-T for 4 h at room temperature. The primary antibody (Foxc1: polyclonal antibody, Research genetics, gift from Dr Brigid Hogan) was diluted 1:1000 in block and incubated overnight at 4°C. Blots were washed extensively in TBS-T and the secondary antibody (goat anti-rabbit tagged to HRP, 1:1500 in TBS-T) was incubated for 1 h at room temperature. Following extensive washes in TBS-T, an enhanced chemiluminescence kit (Amersham Biosciences) was used to detect proteins.

2.8 RT-PCR

2.8.1 RNA extraction and quantitation

Confluent 10 cm plates of wildtype and *Foxc1*$^{-/-}$ cells were trypsinised, pelleted and then resuspended in 1 ml of cold TriPure Isolation Reagent (Roche). Cells were lysed by repeated trituration. Two hundred micro litres of chloroform (with iso-amyl-alcohol (49:1)) was added, cell lysates were vortexed briefly, left to stand at room temperature for 10 min and then centrifuged at 12 000 g for 15 min at 4°C. The upper aqueous layer (±400 µl) was removed and the RNA precipitated at -20°C overnight. RNA was pelleted by centrifugation (12 000 g for 10 min at 4°C), pellets were washed in 75% ethanol and then resuspended in 50 µl DEPC treated dH_2O. RNA was quantitated using a Nanodrop (Nanodrop Technologies).

2.8.2 cDNA synthesis and RT-PCR

One microgram of RNA was used to for each cDNA synthesis reaction. Briefly, oligo-dT primers were prebound to a reaction mix of RNA, oligo-dT primers (2.5 mM) and dH_2O by heating at 70°C for 5 min and cooling on slushy ice for 5 min. Following this dNTPs (3 mM), $MgCl_2$ (4 mM), transcription buffer and RNasin (1u / µl) (Promega) were added to the reaction mix. Any contaminating DNA was removed by DNAse-I (1u / µg RNA) (Promega) digestion for 90 min at 37°C. The DNAse-I was then heat denatured at 75°C for 5 min and 1 µl of M-MLV reverse transcriptase (Promega) was added to all positive control experiments and incubated at 42°C for 60 min.

Standard PCR using primers for *RiboS12*, *TGFβ1*, *Tgfβ1i4*, and a multiplex reaction for *Foxc1* and β-galactosidase was performed using cDNA synthesised from each *Foxc1*$^{+/+}$ and *Foxc1*$^{-/-}$ cell line (Appendix Table A-5).

Chapter 3: Results

3.1 Genotyping

Genomic DNA extracted from mouse embryos or adult tail cuts was used to identify wildtype, heterozygote and mutant animals. In this study two transgenic mice strains were used.

Firstly animals in which the main coding exon (exon 3) of the *Bmp4* gene was replaced with the β–galactosidase gene, $Bmp4^{lacZ}$, (Lawson et al., 1999) (Figure 2-1) were used to map the expression patterns of *Bmp4* during late embryonic and early postnatal development. Since homozygous mutant animals die during early embryonic development (Winnier et al., 1995), the primers used for genotyping in this study were only required to distinguish between wildtype and heterozygote animals. To this end two primer sets were designed and used interchangeably. Primers specific to the lacZ gene, (Figure 2-1 and Figure 3-1A, shown in red) amplify a PCR product of 279 bp in DNA extracted from heterozygote mice (Figure 3-1B). The second primer set was designed to include part of the third intron, 5' to the site of homologous recombination as well as part of the β–galactosidase gene (Figure 2-1 and Figure 3-1A, shown in magenta). Only DNA extracted from heterozygote animals amplified a PCR product (497 bp) (Figure 3-1C). Specificity of this product was confirmed using restriction enzyme digests. Both *AvaI* and *SmaI* restriction digests (restriction site shown in green, Figure 3-1A) produced the expected products (328 bp and 169 bp for *AvaI*; 330 bp and 167 bp for *SmaI*) (Figure 3-1C).

Transgenic mice in which the single coding exon of the *Foxc1* gene was replaced with β–galactosidase gene, $Foxc1^{lacZ}$, (Kume et al., 1998) were genotyped using a single forward primer 5' of the site of homologous recombination and two reverse primers, one specific to the normal *Foxc1* gene transcript and the other specific to the β–galactosidase gene (Figure 2-2). DNA extracted from wildtype mice thus gives rise to a single PCR product of 126 bp, DNA from heterozygotes gives both a 126 bp and a 370 bp product, and DNA from mutant animals gives rise to a single 370 bp product (Figure 3-1D).

Figure 3-1: Mouse genotyping

(A) Part of intron 3 of the *Bmp4* gene (in black text) near the site of homologous recombination, with the 5' region of the β–galactosidase gene shown in blue. Mice were genotyped using *lacZ* specific primers (A, shown in red) or primers flanking the site of homologous recombination (A, shown in magenta). Primers specific to the *lacZ* gene amplify a 279 bp product in DNA extracted from $Bmp4^{+/-}$ mice (B). The primers flanking the site of homologous recombination amplify a 497 bp product in DNA extracted from $Bmp4^{+/-}$ mice (C). Restriction enzyme digests confirmed the specificity of the product generated using the flanking primers. Restriction digests with *AvaI* and *SmaI* (A, restriction site shown in green) produced the expected products of 328 bp and 169 bp, and 330 bp and 167 bp respectively (C). Foxc1 mice genotypes were determined using a multiplex reaction with three primers (Table 2-1). DNA extracted from $Foxc1^{+/-}$ mice amplifies two products (370 bp and 126 bp), $Foxc1^{-/-}$ DNA amplifies a 370 bp product, while $Foxc1^{+/+}$ DNA amplifies a 126 bp product (D).

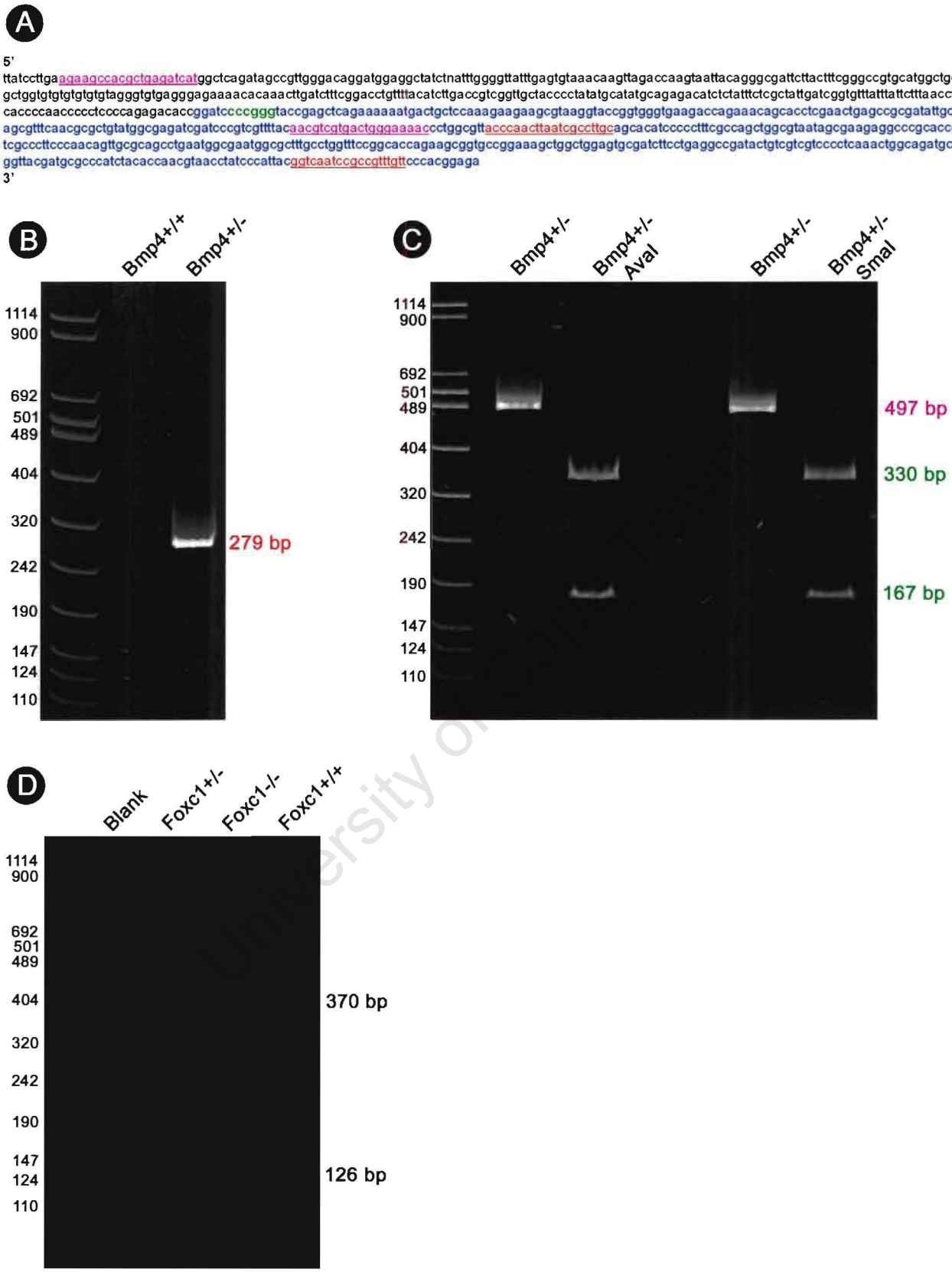

Figure 3-1: Mouse genotyping

3.2 Ciliary body morphogenesis

3.2.1 Structure of the adult mouse ciliary body

Studies on mouse ciliary body have largely been confined to examinations of histological sections and *in situ* analysis. It is difficult to make deductions about the three dimensional structure from this type of information alone. The first part of this study therefore aimed to provide a detailed morphological description of the adult mouse ciliary body using scanning electron microscopy. Since the mouse eyecup is deeply concave, obtaining a complete view of the ciliary body was difficult. Thus both inverted and non-inverted half eyecups were examined. In all, ten eyes were analysed. Figure 3-2A shows an inverted adult eye with the cornea, iris, pupillary margin and band of ciliary processes clearly visible. A non-inverted eyecup is shown in Figure 3-2C, with the iris and part of the ciliary region visible. The most striking feature of the ciliary processes is their irregular arrangement (Figure 3-2B). In other vertebrates, such as the chick, guinea pig, and in humans the ciliary processes form regular, parallel radial folds (Figure 3-2B, insert (Kessel and Kardon, 1979)). In the mouse the ciliary processes overlap and even intersect each other. Zonular fibres are most prominent in the valleys between ciliary processes (Figure 3-2D). The narrow pars plana (approximately 45 μm in width) is found posterior to the ciliary processes (Figure 3-2F). (This was only visible sometimes and when the tilt of the specimen was appropriate). Viewing down onto the ciliary zone near the iris root reveals that the ciliary processes are raised and project upwards from the iris with a gully-like space between the iris and the ciliary folds (Figure 3-2D, 3-2E - arrow). The ciliary processes appear to form regular bridges than span this gully (Figure 3-2E). Anteriorly, at the iris root, there appears to be a smooth zone of transition between the iris and ciliary processes (Figure 3-2E, 3-2G and 3-2H). Examination of both inverted and non-inverted eyes (Figure 3-2G and 3-2H respectively) revealed a smooth region, suggesting that the smoothness is not an artefact arising from stretching during inversion. The smooth zone merges into the epithelium that covers the iris, where a rougher surface is evident (Figure 3-2H).

Figure 3-2: Structure of the adult mouse ciliary body

Inverted and non-inverted views of bisected half eyecups are shown in A and C respectively. Ciliary processes (cp) in the mouse form an irregular interwoven network (B), whereas in other vertebrates such as the guinea pig the ciliary processes form a regular, parallel network (B - insert; (Kessel and Kardon, 1979)). Zonular fibres (zf) are most prominent in the valleys between ciliary processes (D). Viewing down onto the ciliary zone at the iris margin in D and E shows that the ciliary processes are raised, projecting upwards from the iris (i). In E (arrow) gully-like spaces between the ciliary processes are evident. The narrow pars plana (pp) (±45 μm) is found posterior to the ciliary processes (F). Anteriorly, at the iris root, there appears to be a smooth zone of transition between the iris and ciliary processes (G, H - braces). This smooth zone was observed in both inverted (G) and non-inverted (H) eyes. c – cornea, nr – neural retina, scale bar = 200 μm in A, C; 50 μm in B, D – H.

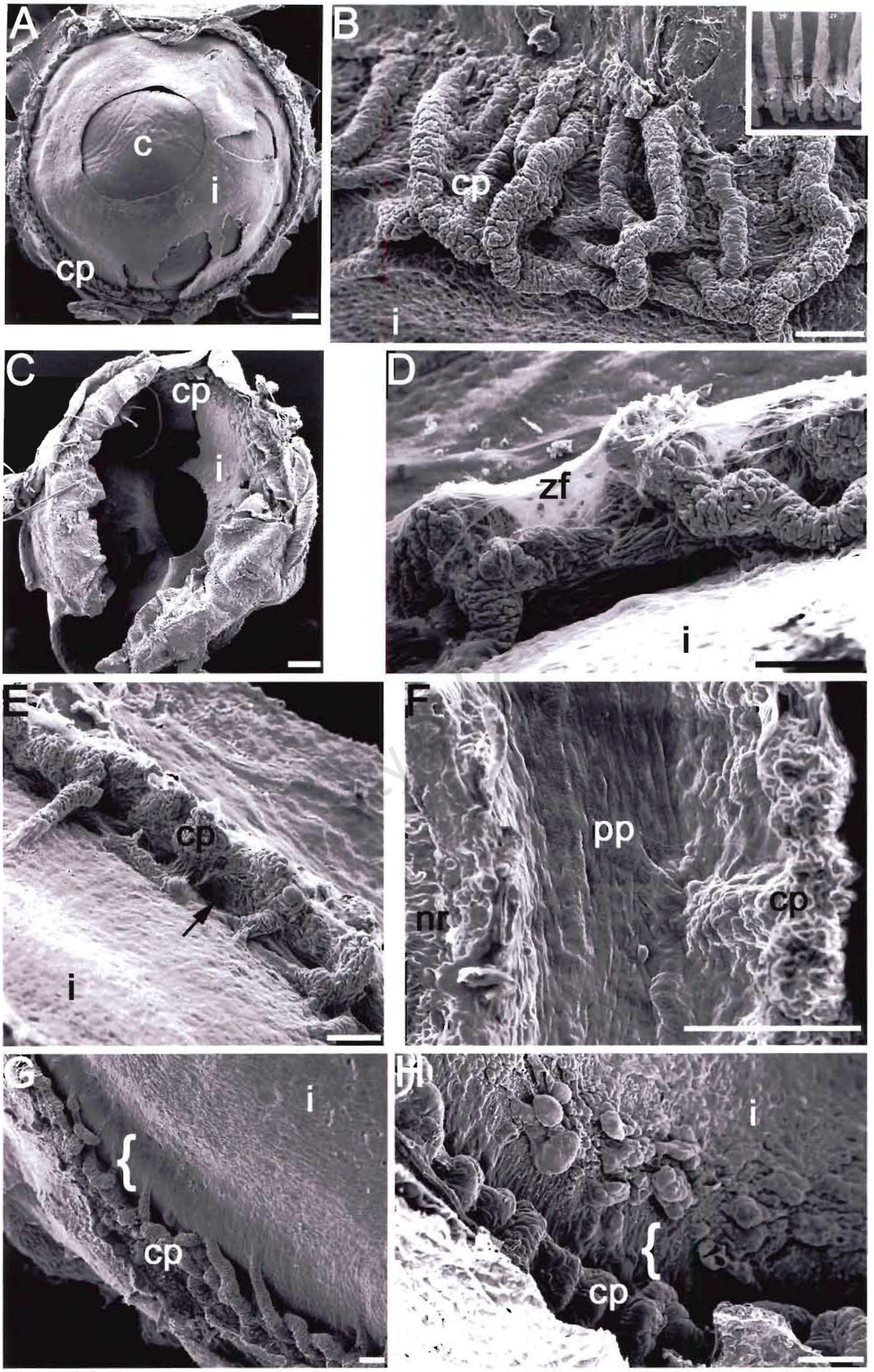

Figure 3-2

3.2.2 Differentiation and zoning of the presumptive ciliary body

In order to establish the sequence of events that occur during ciliary body morphogenesis, a detailed study of the histiogenesis of the ciliary body was performed. In the mouse the developing optic vesicle is formed by E8.5 and invaginates to form a bilayered optic cup by E10.5 – E11.5 (Pei and Rhodin, 1970). It was found that the rim of the optic cup begins to differentiate into the prospective iris and ciliary body between E14.5 and E15.5 with an anterior tapering of cells in the prospective iris-ciliary body zone (Figure 3-3A and 3-3B). By E15.5 a distinct boundary between cells of the neural retina and the prospective ciliary body is evident (Figure 3-3B). The differentiating neural retina is thicker and has densely packed stratified layers of cells, whereas the presumptive ciliary zone is comprised of pseudostratified columnar cells. By E16.5 the separate prospective iris and ciliary body zones can be distinguished. Iris epithelial cells form a simple, low columnar layer, with the adjacent inner epithelium of the ciliary body being thicker and pseudostratified. As development proceeds cell heights in the iris epithelium continue to decline. In the prospective ciliary zone, the inner ciliary epithelium (closest to the lens) forms a pseudostratified columnar layer, while cells of the outer ciliary epithelium (continuous with the retinal pigment epithelium) form a low columnar epithelium (Figure 3-3C). By E17.5 the slightly more columnar cells of the outer ciliary epithelium are distinct from the cuboidal cells of the retinal pigment epithelium (Figure 3-3D). The forming processes appear to elaborate from an initial bulging of the outer ciliary epithelium inwards towards the inner ciliary epithelium at P0 (Figure 3-3F and Figure 3-9A). Ciliary folding initiates around E18.5, with each ciliary process forming around a capillary (Figure 3-3E, arrowhead). High power light microscopy revealed the presence of squamous endothelial cells, pericytes and luminal red blood cells, confirming the identity of these capillaries (Figure 3-3E insert). In order to further confirm their identity, E18.5 eyes were stained for von Willebrand factor (Factor VIII) (Figure 3-4), which is expressed in vascular endothelial cells (McComb et al., 1982; Hyldahl, 1985). A well-established network of capillaries adjacent to the basement membrane of the outer ciliary epithelium is apparent (Figure 3-4, arrowheads).

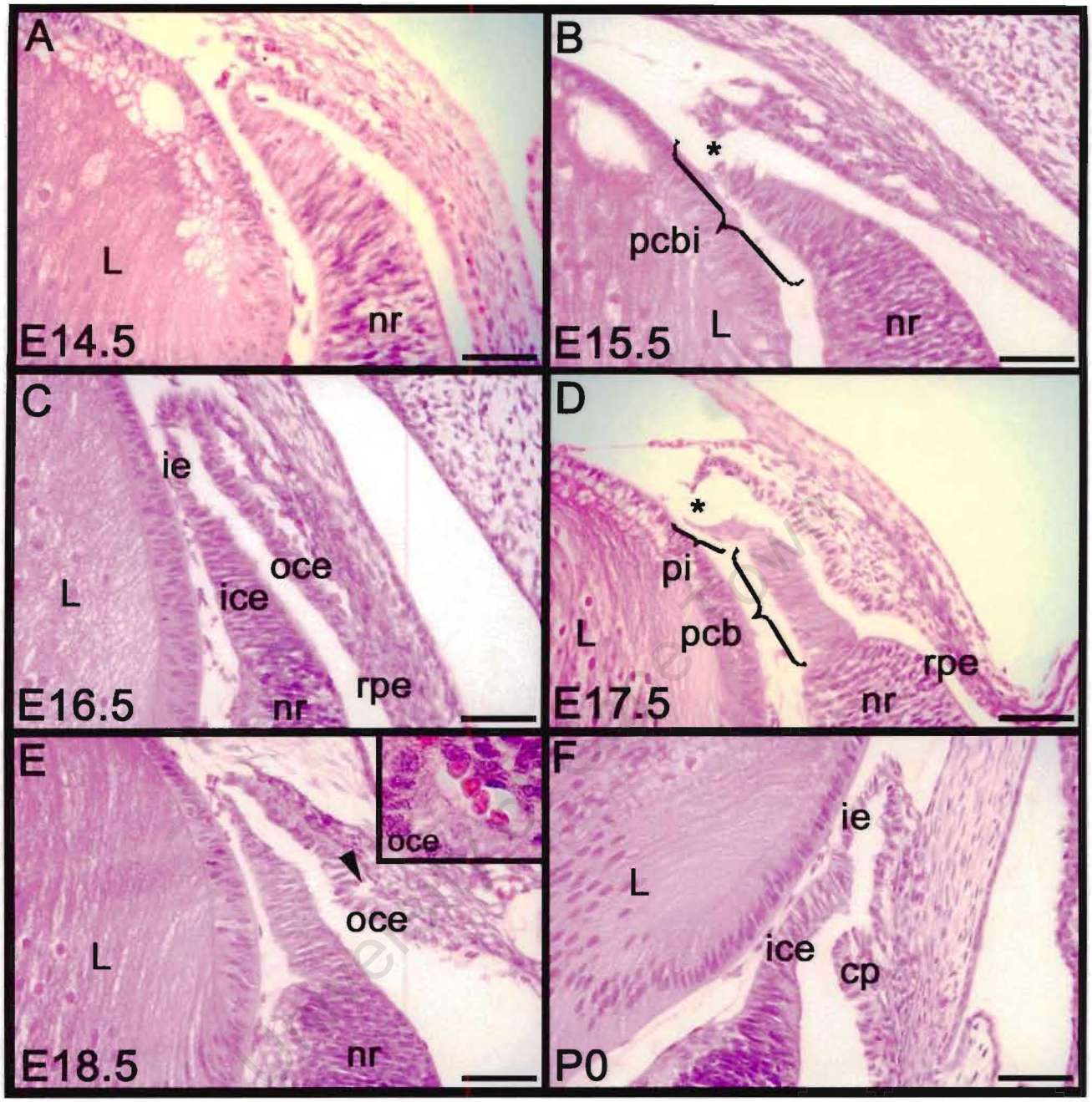

Figure 3-3: Histological series of the developing ciliary body from E14.5 to PO

At E14.5 (A) the tip of the optic cup is slightly tapered. The zone between the neural retina (nr) and the prospective ciliary body and iris (pcbi) becomes distinct at E15.5 (B). By E16.5 (C) the tip of the optic cup elongates further and cells of the anterior neural retina (nr), inner ciliary epithelium (ice) and iris epithelium (ie) can be distinguished. At this stage the outer ciliary epithelium (oce) also becomes distinct from the retinal pigment epithelium (rpe). At E17.5 (D) the prospective iris (pi), prospective ciliary body (pcb) and neural retina zones are clearly established. At E18.5 (E) the outer ciliary epithelium starts to bulge. Note the capillary in the cleft of the forming ciliary process (arrowhead). Insert is a high power view of a capillary at E18.5. By P0 (F) the first ciliary processes (cp) have started to form. * artefact of processing, L – lens, scale bar = 50 μm.

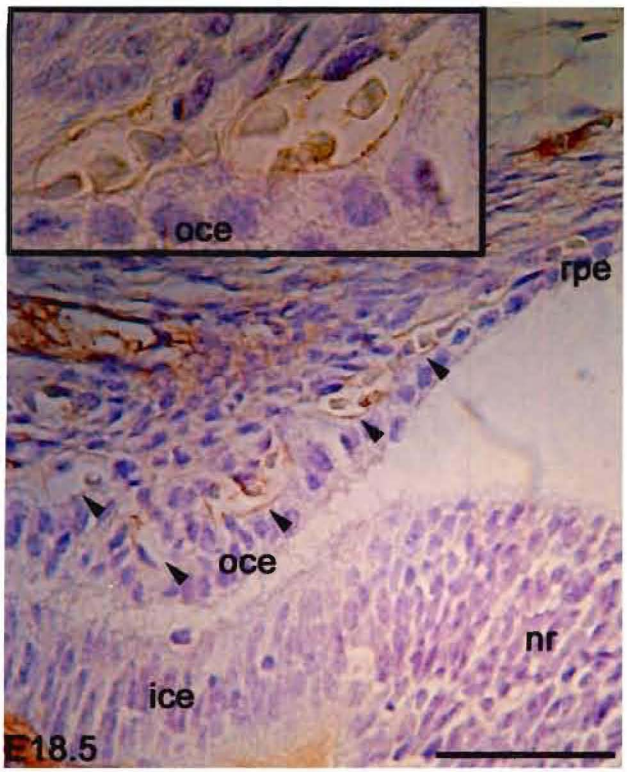

Figure 3-4: Blood capillaries immunostained for von Willebrand factor

At E18.5 the presence of underlying capillaries adjacent to the outer ciliary epithelium was confirmed by the expression of von Willebrand factor (arrowheads). At high power magnification, staining (brown) is clearly restricted to the endothelium of the capillaries (insert). ice – inner ciliary epithelium, nr – neural retina, oce – outer ciliary epithelium, rpe – retinal pigment epithelium, scale bar = 50 μm.

3.2.3 Postnatal development and gene expression patterns in the developing ciliary processes

In the mouse, *Bmp4* (Chang et al., 2001), *Msx1* (Monaghan et al., 1991), *Otx1* (Martinez-Morales et al., 2001) and *Tgfβ1i4* (Thut et al., 2001) are first expressed around the rim of the optic cup from E12.5 – E14.5. This expression correlates temporally with morphological differentiation of the ciliary body from the neural retina, suggesting that these factors may play a role in patterning and specifying the ciliary body. Similarly, in the chick, early expression of LEF1 in the ciliary marginal zone (Kubo et al., 2003), suggests a role for this transcription factor in zoning the ciliary body during morphogenesis. Although *Otx1* knockout mice fail to form ciliary processes (Acampora et

al., 1996) and knockdown of Bmp4 by exogenous noggin expression causes severe disruptions to the ciliary epithelium (Zhao et al., 2002), no study has mapped or correlated the postnatal expression of any of these genes to normal ciliary body morphogenesis. Thus the expression patterns of *Bmp4*, *Tgfβ1i4* and LEF1 during development of the ciliary body were examined. X-gal staining of $Bmp4^{lacZ}$ mice (Lawson *et al.*, 1999) was used to map *Bmp4* expression domains, while *in situ* hybridisation was used to map *Tgfβ1i4* and LEF1 expression.

Bmp4 is first expressed in the presumptive ciliary zone at E14.5 (Chang et al., 2001), with transcription restricted to the inner ciliary epithelium and iris epithelium. This pattern of expression persists through late embryonic and early postnatal development (Figures 3-5A and 3-5C). At P0 expression also starts to extend into the iris stroma (Figures 3-5C). Ciliary processes are evident by P4 and appear to result from an expansion of the outer ciliary epithelium. Interestingly, as the ciliary processes form and bulge into the inner ciliary epithelium, *Bmp4* is expressed at the tips of the extending ciliary processes (Figure 3-5E). By P6, morphogenesis of the ciliary body and iris appears complete, and *Bmp4* is expressed in both ciliary epithelia and the entire iris (Figure 3-5G). The apparent expression in the corneal endothelium and lens circumference at P6 is likely to be the result of artefactual trapping of the Xgal stain. In the adult, *Bmp4* continues to be expressed in the iris epithelium, but not the stroma (Figure 3-6A). Expression in both ciliary epithelial layers is also maintained in the adult (Figure 3-6A), with expression appearing more intense in the inner ciliary epithelium (Figure 3-6C). *Bmp4* expression has also been reported in the retinal pigment epithelium and optic nerve at E14.5 (Chang et al., 2001). This expression pattern was observed throughout late embryonic and early postnatal development as well as in the adult (Figure 3-6E and 3-6G).

Expression of *Tgfβ1i4* around the margin of the optic cup is first evident at E12.5 – E13.5 (Thut et al., 2001; Figure 3-16A). This pattern of expression persists during the course of development; however, as the iris starts to differentiate from the presumptive ciliary body at E18.5, expression of *Tgfβ1i4* becomes restricted to the presumptive inner ciliary epithelium and is not expressed in the iris (Figure 3-5B). The lens epithelium, retinal ganglion cells and inner nuclear layer of the neural retina also express *Tgfβ1i4*. By P0, expression intensifies in the inner ciliary epithelium, while no *Tgfβ1i4* expression is observed in the iris epithelium (Figure 3-5D, iris epithelium demarcated by arrowheads). During the course of ciliary folding, the pattern of *Tgfβ1i4* expression in the ciliary body remains unchanged and is restricted to the inner ciliary epithelium (Figure 3-5F and 3-5H). However, in the developing iris, expression seems to extend from the inner ciliary epithelium along

the forming iris epithelium at P4 (Figure 3-5F, red arrowhead). By P6, *Tgfβ1i4* is expressed along the entire iris epithelium, but not in the iris stroma (Figure 3-5H). In the adult, the inner ciliary epithelium and lens epithelium continue to express *Tgfβ1i4* (Figure 3-6B). Distinct expression of *Tgfβ1i4* in the retinal ganglion cells and inner nuclear layer of the neural retina were clearly evident by P0 (Figure 3-6D), with these cell layers continuing to express *Tgfβ1i4* in the adult eye (Figure 3-6F). At all stages examined from E18.5 – P6, the optic nerve expressed *Tgfβ1i4* (Figure 5H). Unfortunately, the tissue sections of the adult eyes used for *in situ* analysis did not include the optic nerve.

Figure 3-5: *Bmp4* and *Tgfβ1i4* expression in the developing mouse ciliary body and iris

During late embryonic (E17.5, A) and early postnatal development (P0 – P2, C) *Bmp4* expression is restricted to the inner ciliary epithelium (ice) and iris epithelium (i). By P4 (E), *Bmp4* expression is evident at the tips of the forming ciliary processes in the outer ciliary epithelium (oce) (E, arrow) and starts to extend into the iris stroma. By P6, both ciliary epithelial layers and the entire iris express *Bmp4*. At E18.5 (B), *Tgfβ1i4* expression is restricted to the inner ciliary epithelium, lens epithelium (le), retinal ganglion cells (rgc) and inner nuclear layer (inl) of the neural retina. *Tgfβ1i4* is not expressed in the presumptive iris epithelium at this stage (B, arrowheads). This expression pattern persists through early postnatal development (P0, D). By P4 (F), *Tgfβ1i4* expression is maintained in the inner ciliary epithelium, lens epithelium and layers of the neural retina. However, *Tgfβ1i4* expression also starts to extend along the iris epithelium (ie) (F, red arrowhead). By P6 (H), the entire iris epithelium expresses *Tgfβ1i4*, together with the inner ciliary epithelium, lens epithelium, retinal ganglion cells and inner nuclear layer of the neural retina. nr – neural retina, L-lens. Scale bar = 50 μm.

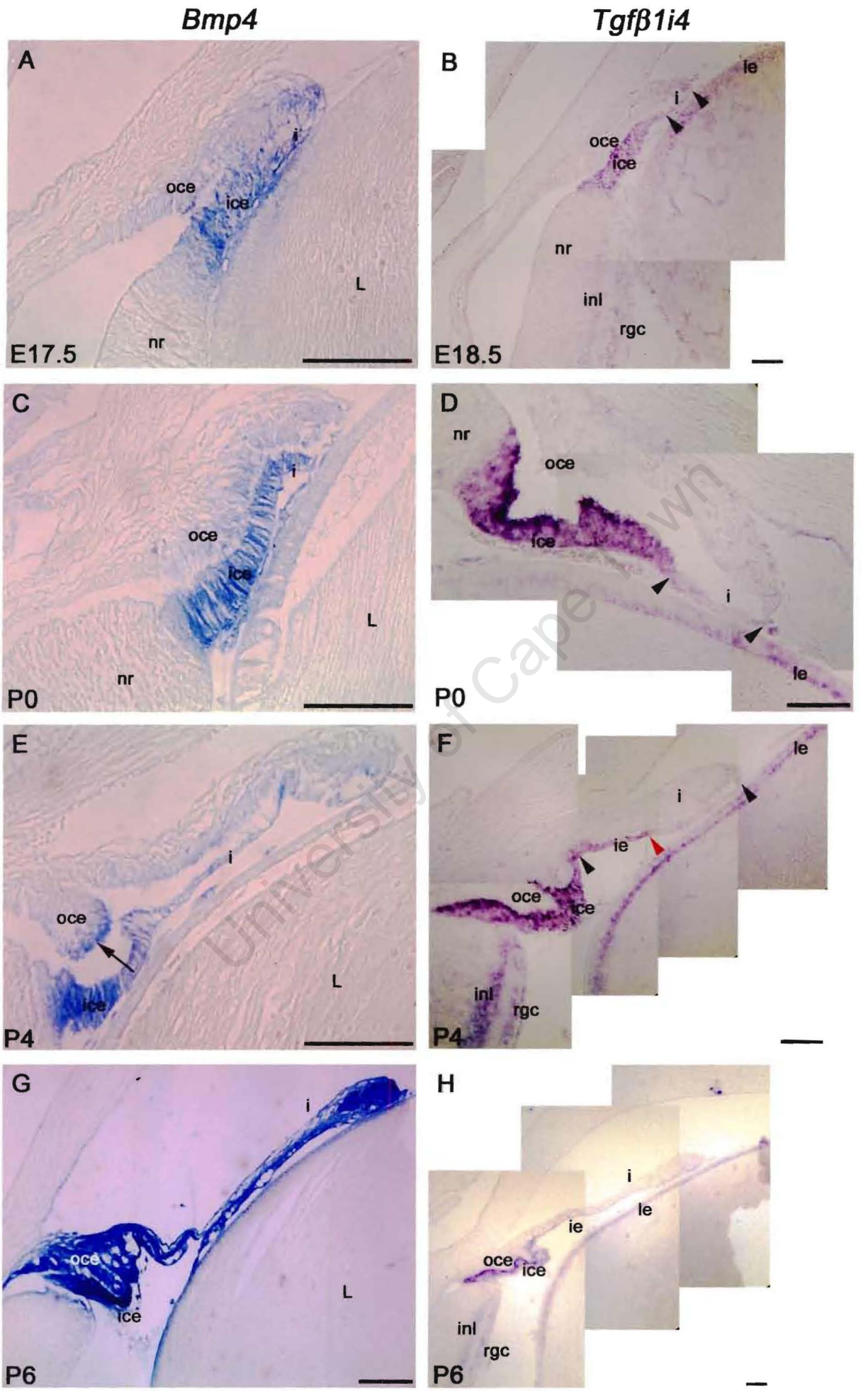

Figure 3-5

Figure 3-6: *Bmp4* and *Tgfβ1i4* expression in the adult eye

In the adult, *Bmp4*, continues to be expressed in both ciliary epithelial layers and the iris epithelium (ie), but not the iris stroma (A). In the ciliary epithelia, expression appears to be highest in the inner ciliary epithelium (ice) (C). During late embryonic and early postnatal development *Bmp4* is expressed in the retinal pigment epithelium (rpe) and optic nerve (G). These patterns of expression are maintained in the adult eye (E and G, insert of whole optic nerve). In the adult, *Tgfβ1i4* expression in the inner ciliary epithelium and lens epithelium (le) is maintained (B). *Tgfβ1i4* expression in the retinal ganglion cells (rgc) and inner nuclear layer (inl) of the neural retina during late embryonic and postnatal development (D) is maintained in the adult retina (F). Expression of *Tgfβ1i4* was also observed around the optic nerve during embryonic and postnatal development (H). No expression data for the adult were obtained. cp – ciliary processes, L – lens, oce outer ciliary epithelium. Scale bar = 100 μm in D; 50 μm in A – C and E – H.

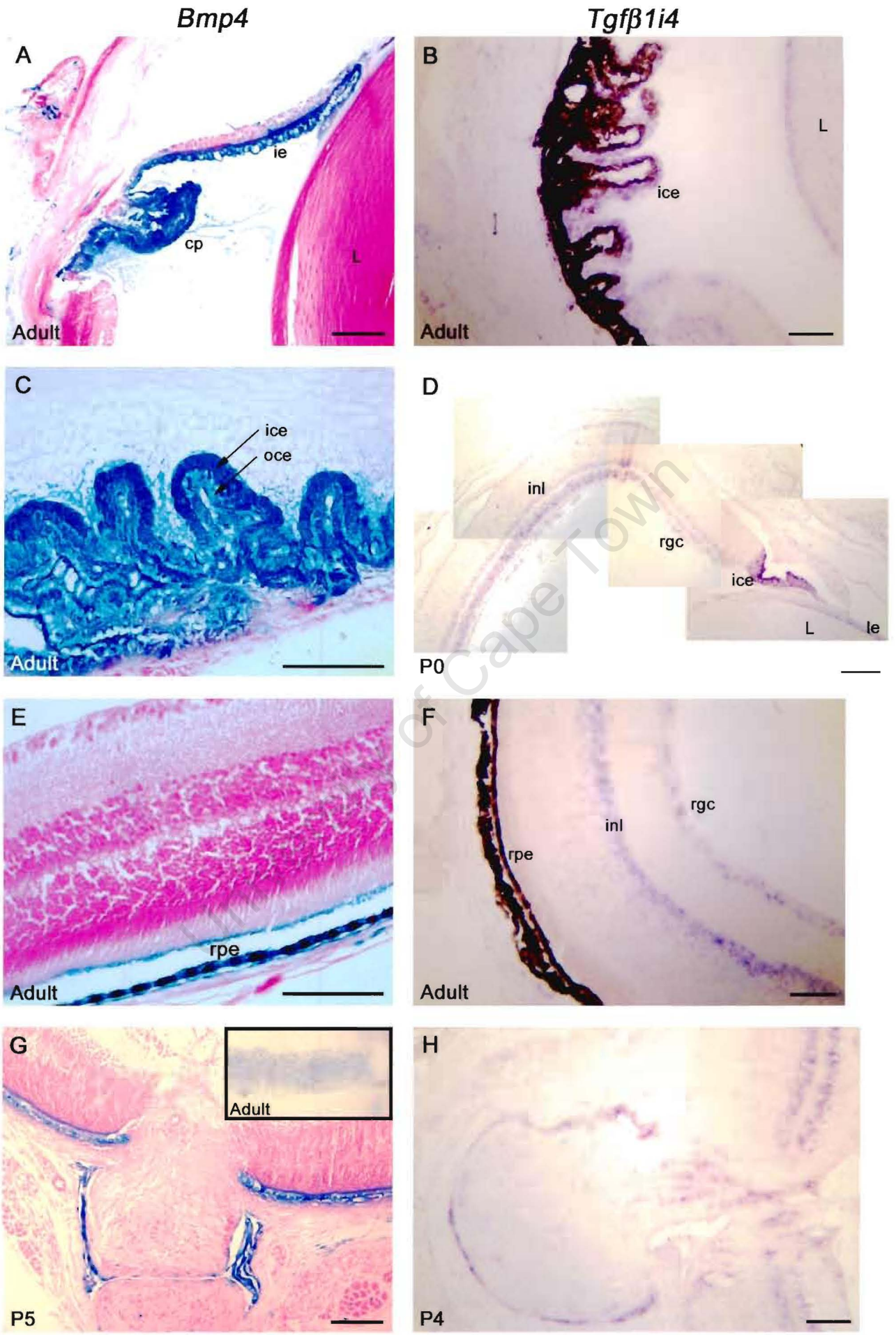

Figure 3-6

Working in the Reh laboratory presented an opportunity to study the developing ciliary body in the chick. Wnt2b signalling (mediated by LEF1) has been implicated in retinal cell differentiation at the ciliary marginal zone (Kubo et al., 2003). Although expression analyses reveal that LEF1 is expressed in the presumptive ciliary body and iris of the chick at stage 22, no attempt has been made to relate its expression to morphogenesis of the ciliary body. Thus in the context of mapping gene expression patterns over the period of ciliary folding, expression of LEF1 was assessed in the chick from stage 23 – 30. In addition to this LEF1 expression was related to the expression of neural retina (neurofilament) and ciliary body specific (collagen IX) markers.

LEF1 is initially expressed along the entire presumptive ciliary and iris epithelia at stage 23 (Figure 3-7A). Expression is most intense in the posterior half of the ciliary epithelium. Immunostaining for neurofilament after *in situ* hybridisation (Figure 3-7B) confirmed that the LEF1 expression domain is restricted only to regions anterior to the ciliary marginal zone and not in the differentiating neural retina (Figure 3-7C). By stage 25, the domain of LEF1 expression is restricted to the posterior half of the ciliary epithelium (the future pars plana) (Figure 3-7D, arrowheads). Neurofilament expression is mutually exclusive to that of LEF1 (Figures 3-7E and 3-7F). Figure 3-7F shows that low levels of LEF1 expression occur in the ciliary marginal zone at stage 25 (arrowheads). Interestingly, just as ciliary folding initiates, at stage 30, LEF1 expression intensifies in the inner ciliary epithelium and presumptive iris (Figure 3-7G). Immunostaining for neurofilament and collagen IX after *in situ* hybridisation clearly delineated the neural retina, ciliary marginal zone and ciliary body; with the ciliary marginal zone neither expressing neurofilament nor collagen IX, (Figure 3-7H, insert, arrowheads). Strong immunostaining for collagen IX is also evident in the vitreous humour, synthesised by the ciliary epithelium. Collagen IX is expressed in the iris at stage 25 (Kubota et al., 2004), however, by stage 30 expression appears to be downregulated in the iris epithelium (Figure 3-7H, arrowhead at the ciliary body – iris margin). The merged image shows LEF1 to be expressed in both the ciliary marginal zone and ciliary epithelium (Figure 3-7I). In the future it would be of great interest to compare these expression patterns to those in the developing mouse ciliary body.

Figure 3-7: LEF1 expression in the developing chick ciliary body

At HH 23 LEF1 is expressed along the entire inner ciliary epithelium and iris epithelium (A). Neurofilament staining at HH 23 shows the differentiating neural retina (B). Overlaying these images demonstrates that LEF1 expression is anterior to the differentiating neural retina (C). At HH 25, LEF1 expression is most intense in the posterior half of the ciliary epithelium (future pars plana) (D). Again the overlay of neurofilament immunostaining delineates LEF1 expression from the differentiating neural retina (E, F). Low levels of expression are evident in the ciliary marginal zone (F, arrowheads). As ciliary folding initiates at HH 30, LEF1 expression appears to intensify in the inner ciliary epithelium and iris epithelium (G, insert). Immunostaining with both neurofilament and collagen IX demarcate the neural retina, ciliary marginal zone and inner ciliary epithelium, with the ciliary marginal zone not expressing either marker (H, arrowheads in insert). Strong immunostaining for collagen IX is clear in the vitreous humour (H). At this stage collagen IX expression does not extend to the iris epithelium (H, arrowhead at ciliary body – iris margin). The merged image shows LEF1 to be expressed in both the ciliary marginal zone and ciliary epithelium (I).

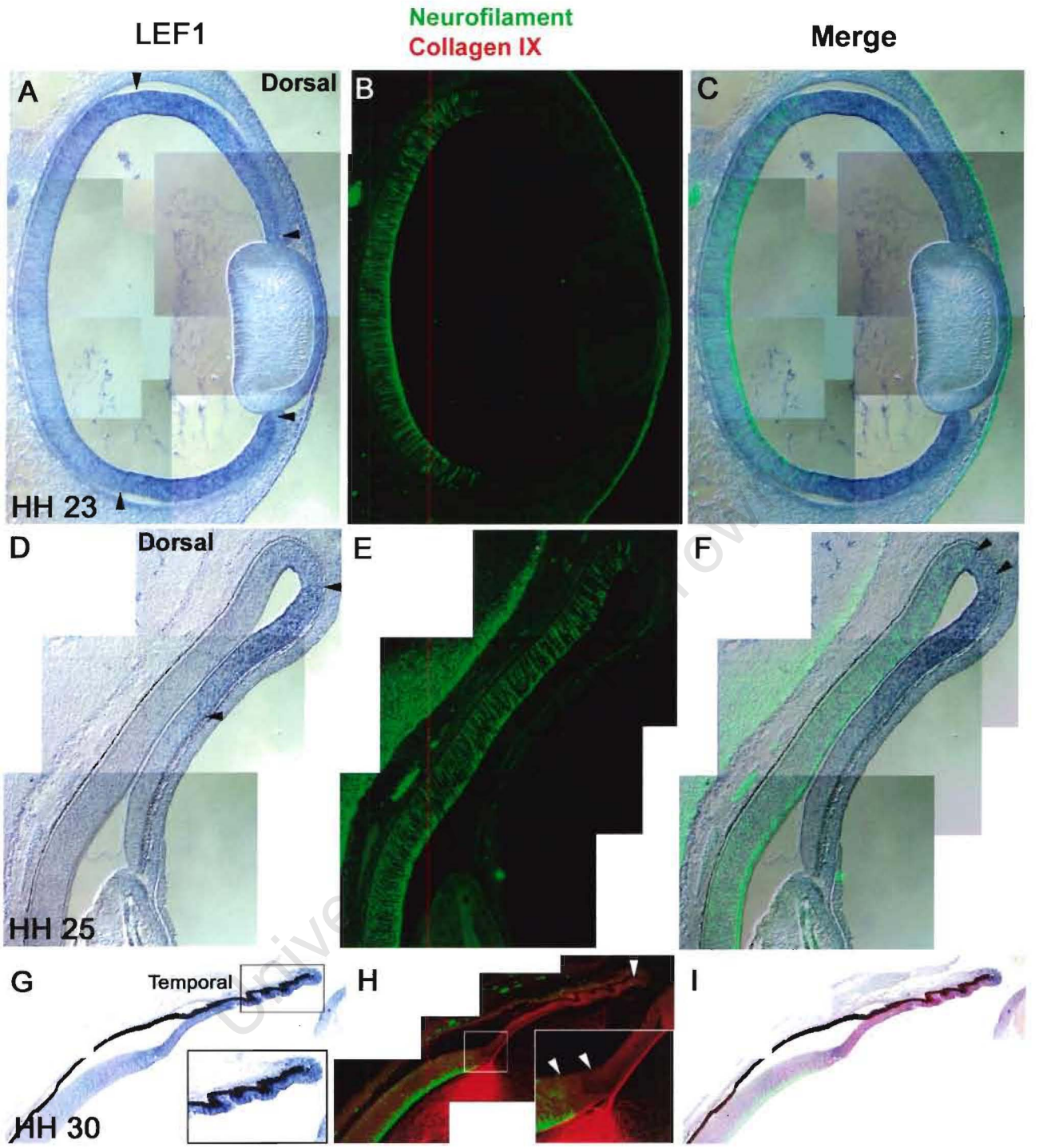

Figure 3-7: LEF1 expression in the developing chick ciliary body

3.2.4 Morphogenesis of ciliary processes

The histological and gene expression analyses described above suggest that a complex network of molecular signals direct the specification, zoning and ultimately morphogenesis of the optic cup margin. These cues are essential for differentiation of the neural retina, ciliary body and iris. The histological data reveals that the ciliary processes develop from two initially parallel epithelial sheets, which undergo dramatic shape changes to form an intricate network of ciliary folds. A detailed understanding of how this complex architecture arises is largely unknown. Importantly, it is also very difficult to relate cross sectional data to the three-dimensional changes that occur during ciliary body morphogenesis.

In order to address this, SEM of the developing ciliary body from E17.5 to P7 was performed. Unfortunately, it was not possible to separate the lens from the developing iris and ciliary body during late embryonic and early postnatal development. Figure 3-8A shows an E17.5 lens with the attached presumptive iris and ciliary body. This posterior view of the ciliary epithelia suggests that they are flat parallel sheets at this stage. Figure 3-8B provides a view of the anterior eyecup after removing the lens and attached iris and ciliary body at E18.5. At P0 the iris and ciliary body still pull off with the lens. Fortuitously, in one sample, a small portion of the partially torn ciliary epithelium has been retained (Figure 3-8C): the ciliary epithelia are separated and flapped back from the underlying uvea presenting a posterior view of the capillaries and overlying, apparently flat, ciliary epithelia. It shows that at this stage, a well-established capillary network underlying the ciliary epithelia is already formed. Capillaries were identified by the presence of a smooth endothelium and a lumen that could clearly be identified when the tissue was torn (during processing). The diameter of these vessels was approximately 10 μm, which is consistent with our histological observations, showing vessels of 10 - 15 μm (Figure 3-3E, Figure 3-4 and Figure 3-9A). In all samples analysed at P0 (n = 3) a well-established, irregularly arranged network of capillaries was evident (Figure 3-8D).

Most notable is the architecture of the capillaries at P0. Their arrangement is markedly similar to that of the adult ciliary processes (compare Figures 3-8C, 3-8D with Figure 3-2B). A distinct morphological change in the prospective ciliary zone is evident by P2 (Figure 3-8F). At this stage it was possible to successfully remove the lens without disrupting the iris or ciliary body. There is clear evidence of bulging within the ciliary zone with a primary annular bulge forming around the

Figure 3-8: Morphogenesis of the ciliary body

At E17.5 (A) it is not possible to separate the lens (l) and prospective iris and ciliary body (icb). A posterior view of the apparently flat presumptive iris and ciliary body is shown in A. Removal of the lens during dissection at E17.5 or E18.5 (B) results in the presumptive iris and ciliary body pulling away from the anterior eyecup (asterisk in B). At P0 the iris and ciliary body has pulled off with the lens, although at this stage a complicated capillary network underlying the ciliary epithelia is revealed (D - arrow). In one sample, a small portion of the partially torn ciliary epithelium was retained (C): the ciliary epithelia are separated and flapped back from the underlying uvea presenting a posterior view of the capillaries and overlying, apparently flat, ciliary epithelia. By P2 the prospective ciliary zone undergoes a marked morphological change, forming a primary annular bulge around the eye (F). Individual processes start to take shape around the circumference of this bulge. This shaping appears to occur asymmetrically. In E, there is only evidence of surface bulges in the outer ciliary epithelium, whereas in H (arrow), clefts between surface bulges are evident. Deepening of these clefts results in discrete ciliary processes (cp) forming by P7 (G, arrows). c – cornea, i – iris, nr – neural retina, p – pupil, scale bar = 50 μm.

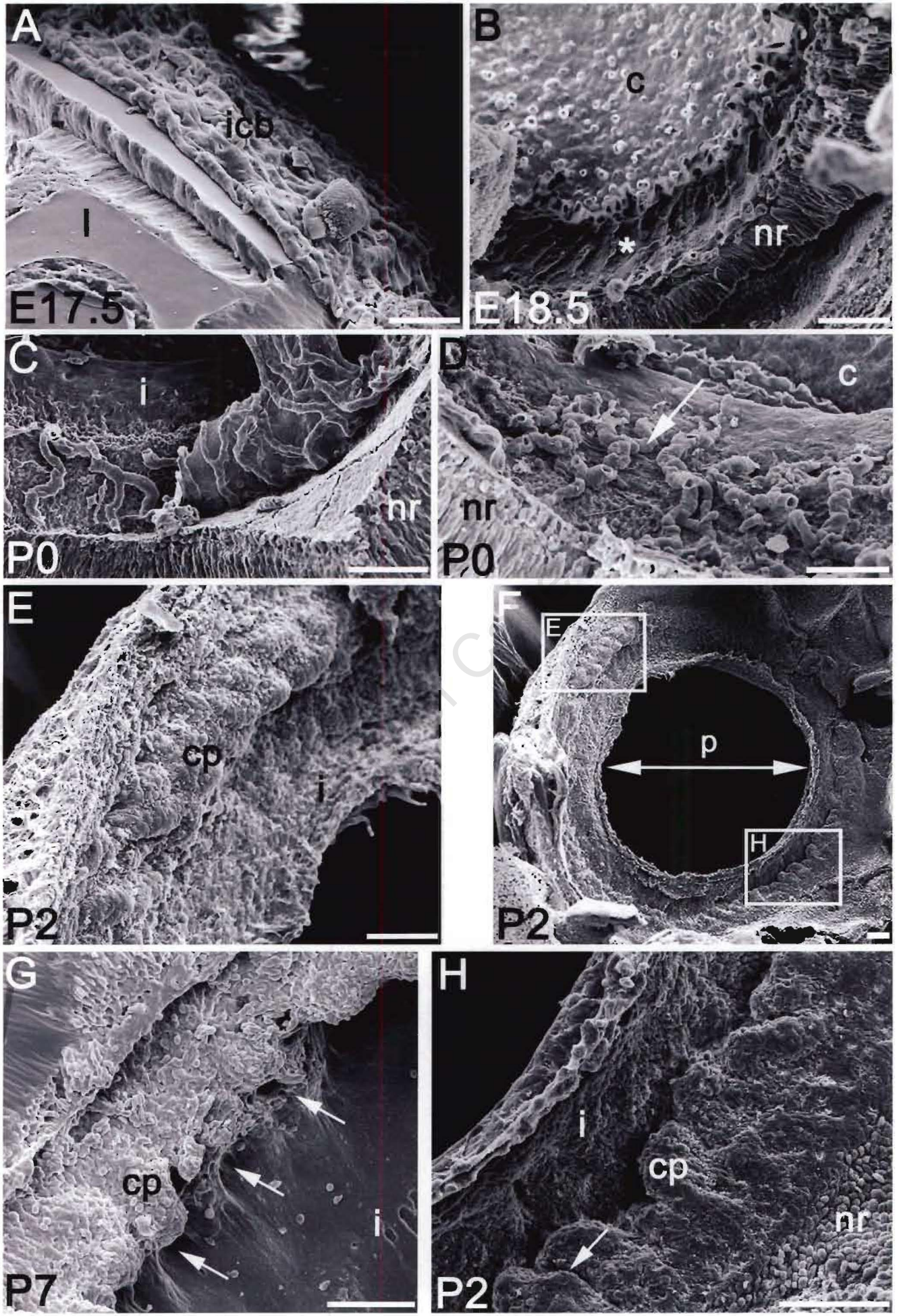
A
icb
l
E17.5
B
c
*
nr
E18.5
C
i
nr
P0
D
c
nr
P0
E
cp
i
P2
F
E
p
H
P2
G
cp
i
P7
H
i
cp
nr
P2

Figure 3-8

eye. This is then further shaped into individual processes (Figure 3-8E and 3-8H). Our observations of the full circumference of the eye suggest that the morphogenesis of ciliary processes may occur asymmetrically around the eye. For example, in Figure 3-8E, there is only evidence of surface bulges in the outer ciliary epithelium, whereas in Figure 3-8H (arrow), clefts between surface bulges are evident. Over time these clefts extend around the full circumference of the eye, are deepened and a network ciliary processes is eventually formed. By P7 the wave-like appearance of the adult ciliary processes is clearly established (Figure 3-8G). The gully between the ciliary processes and the iris is also visible at this stage (compare Figure 3-2D, 3-2E and Figure 3-8G, arrows).

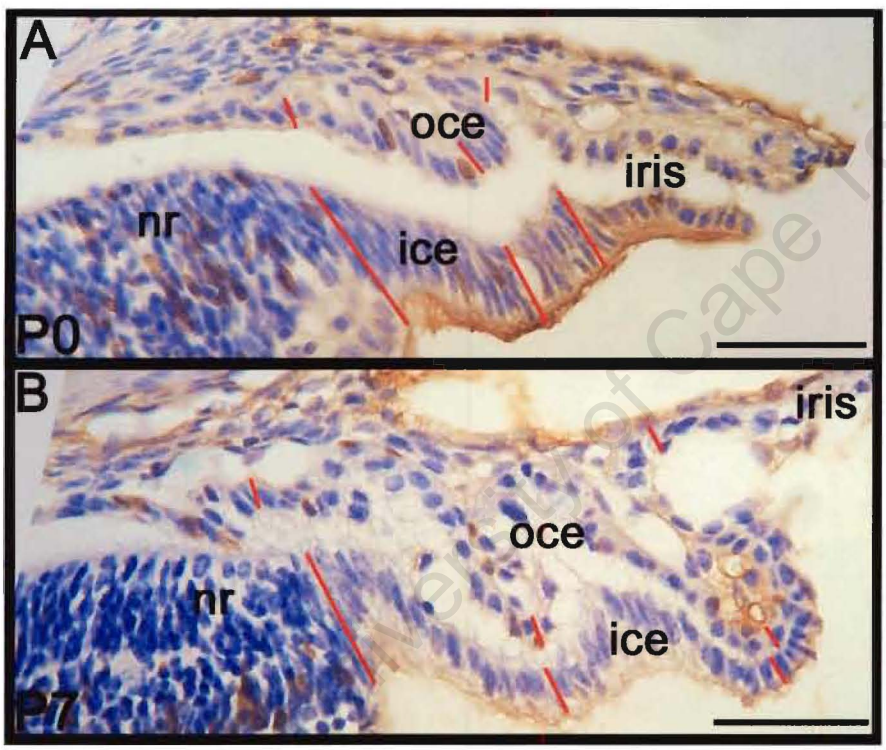

Figure 3-9: BrdU incorporation in the developing ciliary body

Proliferating cells at PO (A) and P7 (B) are stained brown, while non-dividing cells are blue. Red lines delineate boundaries between the ciliary epithelia and adjacent neural retina, retinal pigment epithelium and iris. Definition of these boundaries is based on histological observations. The neural retina is thick and has densely packed stratified layers of cells; the inner ciliary epithelium comprises pseudostratified columnar cells at P0 and low columnar cells at P7; the iris epithelium has cuboidal cells. The outer ciliary epithelial zone was assigned using the inner ciliary epithelial zone as a guide. Together with the boundary markers, the red lines at the tips of ciliary processes indicate where measurements for cell height comparisons were made. nr – neural retina, ice – inner ciliary epithelium, oce – outer ciliary epithelium, scale bar = 50 μm.

3.2.5 Cell Shape changes during morphogenesis

Both the histological and SEM data indicate that ciliary folding proceeds postnatally with clearly elaborated ciliary processes being evident by the end of the first week, P7 (Figure 3-8G and Figure 3-9B). 3-5 3-8 As the ciliary processes form (P0 – P4), it appears that the two ciliary epithelial layers change their cell heights with the outer ciliary epithelium pushing into the inner ciliary epithelium (Figure 3.5C – 3.5F). Furthermore, the clefting seen in the inner ciliary epithelium at P2 (Figure 3-8H) is likely to result from changing cell heights. In order to assess whether cell heights change during ciliary body morphogenesis, cell heights at P0 and P7 were measured and compared. Since the cell heights within each epithelial layer are not uniform along the length of the ciliary body, three different measures were made: The first at the neural retina / retinal pigment epithelium – ciliary body boundary, the second at the tips of ciliary processes and the third at the ciliary body – iris boundary (Figure 3-9).

Two types of comparison were made. Firstly at each of the regions where cell heights were measured, a comparison of relative cell heights between P0 and P7 within a given epithelial layer was made. These results are summarised in Table 3-1. For each of the three regions analysed, the mean percent change between P7 and P0 was calculated. At the neural retina – ciliary body boundary in the inner ciliary epithelium cell heights did not change significantly between P0 and P7 (Table 3-1). Cells at the tips of ciliary processes and the ciliary body – iris boundary showed at statistically significant decline in their average height between P0 and P7 (33.8% and 56.6% respectively). Similarly in the outer ciliary epithelium, cell heights declined only at the tips of ciliary processes and the iris boundary between P0 and P7 (34.2% and 25.1% respectively). These results demonstrate that the cell heights (and therefore the epithelium as a whole) decrease during the course of ciliary body development from P0 to P7.

The second set of comparisons assessed differences in cell heights within a given epithelial layer (i.e. either within the inner or outer ciliary epithelium) at either P0 or P7. In the inner ciliary epithelium cell heights decline significantly between the neural retina boundary and the tips of ciliary processes at both P0 and P7 ($p < 0.0001$). At P0 there is no significant difference in cell heights between cells at the tips of ciliary processes and cells at the iris boundary ($p = 0.2299$). However, by P7 a relative decline in cell heights at the iris boundary is evident ($p = 0.0189$). It is likely that this decline correlates with differentiation of the iris epithelium to form cuboidal cells.

There is in fact a marked reduction of cell heights at the iris boundary in the inner ciliary epithelium. At P0 the iris boundary cells are 19.4% longer than cells at the tips of ciliary processes and by P7 they are 21.7% shorter. Within the outer ciliary epithelium cells at the tips of forming processes are relatively longer (35%) than cells in the adjacent retinal pigment epithelium at P0 ($p = 0.0075$). Interestingly, by P7 when ciliary processes are well established, cell heights at the tips of ciliary processes in the outer ciliary epithelium are significantly lower (22%) than cell heights in the adjacent retinal pigment epithelium ($p = 0.0003$). No significant difference between cell heights at the tips of ciliary processes and cells at the iris boundary in the outer ciliary epithelium was found at P0 or P7 ($p = 0.0545$ and $p = 0.1250$ respectively).

Table 3-1: Comparison of cell heights between P0 and P7 in the two epithelial layers of the ciliary body

	Region of measurement	Developmental stage				Percent change	p value
		P0		P7			
		Mean cell height (μm)	n	Mean cell height (μm)	n	| P7/P0 |	
Inner ciliary epithelium	Neural retina boundary	47.17	10	43.20	10	8.4	0.078888
	Ciliary process tips	18.15	10	12.01	20	**33.8**	**0.000051**
	Iris boundary	21.67	10	9.40	10	**56.6**	**0.000184**
Outer ciliary epithelium	Retinal pigment epithelium boundary	8.28	10	9.43	10	13.9	0.109713
	Ciliary process tips	11.18	10	7.36	20	**34.2**	**0.000006**
	Iris boundary	9.00	10	6.74	10	**25.1**	**0.003744**

3.2.6 Cell proliferation and the formation of ciliary processes

The histiogenesis and cell height analyses suggest that ciliary folding in the mouse initiates with the outer ciliary epithelium pushing inwards towards the inner ciliary epithelium. This expansion and flexure could be achieved through cytoskeletal rearrangements alone, or a combination of events that includes differential growth between the two ciliary epithelia. In order to investigate this possibility BrdU labelling experiments were carried out as described in Materials and Methods, Section 2.5.2.

Of particular interest was determining whether rates of proliferation between the two ciliary epithelial layers differed. It was found that the number of dividing cells in the outer ciliary epithelium at each stage from E18.5 to P7 was significantly greater than the number of dividing cells in the inner ciliary epithelium (Table 3-2). In addition to this relative rates of proliferation within each of the ciliary epithelia were assessed over the period of morphogenesis. In the first postnatal week, both epithelial layers demonstrated a rise and fall in mitotic rates (Figure 3-10). Our data suggests that a proliferative surge in the outer ciliary epithelium occurs around P0 with significant increases in the number of dividing cells being observed between P0 and P1 ($p = 0.0001$) as well as from P1 to P2 ($p = 0.0257$). Comparing proliferative rates between E18.5 and P0 was made difficult by differences in BrdU labelling indices in these tissues. (Neonates were injected through direct subcutaneous injections whereas embryos were labelled indirectly via the placenta of the injected mother). Consequently, we are not able to state with certainty that proliferation in the outer ciliary epithelium initiates at P0 (for example it could initiate earlier). Mitotic rates in the outer ciliary epithelium start to decline at P2 with a statistically significant drop occurring between P5 and P7 ($p < 0.0001$). Mitotic rates in the inner ciliary epithelium did not differ between P0 and P1; however, a significant increase in proliferation was observed between P1 and P2 ($p = 0.0002$). Mitotic rates start to fall after reaching a peak at P2, with a significant difference being observed between P3 and P5 ($p = 0.0024$).

Table 3-2: Comparison of the number of dividing cells between the inner and outer ciliary epithelia

Developmental stage	Inner ciliary epithelium		Outer ciliary epithelium		p value
	Mean percent dividing cells	n	Mean percent dividing cells	n	
E18.5	8.18	38	10.83	38	**0.018552**
P0	4.96	31	7.26	43	**0.017778**
P1	5.22	38	12.46	38	**0.000001**
P2	9.34	34	15.99	37	**0.000004**
P3	7.97	34	14.74	35	**0.000003**
P5	5.52	37	12.50	37	**0.000000**
P7	4.16	27	8.24	29	**0.000052**

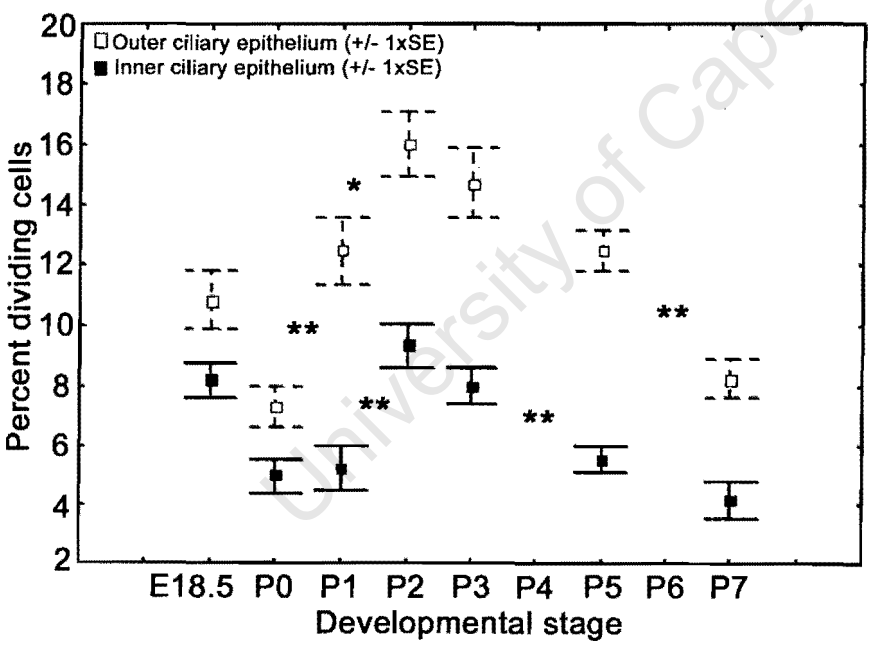

Figure 3-10: Cell division in the ciliary epithelia during postnatal development

At all stages examined from E18.5 to P7 the number of dividing cells in the outer ciliary epithelium (dashed whiskers) was significantly greater than the number of dividing cells in the inner ciliary epithelium (solid whiskers) ($p < 0.05$). Rates of proliferation in the outer ciliary epithelium increase significantly between P0 and P1 as well as from P1 to P2. After peaking at P2 mitotic rates start to decline with a significant decrease occurring between P5 and P7. In the inner ciliary epithelium rates of proliferation only show an increase between P1 and P2, again peaking at P2 and showing a significant decline between P3 and P5 (** $p < 0.01$ and * $p < 0.05$).

3.3 Establishing immortal wildtype (*Foxc1*$^{+/+}$), *Foxc1*$^{+/-}$ and *Foxc1*$^{-/-}$ cell lines of the presumptive cornea

During embryonic development migrating periocular mesenchyme cells invades the space between the corneal epithelium and lens epithelium and ultimately differentiates to form the corneal stroma and endothelium. At the cellular level, little is known of how the innermost layer of these cells differentiates to form the corneal endothelium, while the remaining cells become arranged in parallel arrays to form the stroma. It is likely that any number of signals from the rim of the optic cup, corneal epithelium and the lens epithelium play a role in patterning the undifferentiated mesenchyme cells. Obviously determining the source of these signals *in vivo* is complicated by the fact that the population of cells that migrates into the anterior region of the eye is very small and quantitating subtle changes, whether phenotypic or molecular, in these cells is very difficult. Thus the aim of this study was to establish an *in vitro* system to test and model development of the corneal endothelium.

In the mouse, periocular mesenchyme cells start to ingress between the corneal epithelium and lens epithelium from E11.5 – E12.5. Figure 3-11A shows a cross section through an E12.5 mouse eye. Cells stained in blue mark the expression of the transcription factor *Foxc1* (Kidson et al., 1999) and represent the migrating population of periocular mesenchyme cells. Explants of periocular mesenchyme from the anterior most region of E12.5 mouse eyes were microdissected and primary cultures established (Figure 3-11A, ellipse). Small wedges (±0.05 mm^3) of cells from this region were teased away using tungsten needles and placed in 24 well plates. For each embryo 4 – 5 wedges were cultured (DMEM + 20% FCS) in the same plate for 48 – 72 h (Figure 3-11B). Following this initial expansion, the primary cultures were then immortalised with a temperature sensitive mutant SV40 large T-antigen (Frederiksen *at al.*, 1988; Jat and Sharp, 1989) as described in Methods and Materials, Section 2.6.1. After infection with the oncogene, cultures were expanded in selective media containing geneticin (G418) at the permissive temperature of the oncoprotein (33°C) for 10 – 14 days. Untransformed mouse embryonic fibroblasts were used as control cultures during selection. All control cells died by the end of the first week. In total thirteen cell lines were established. Table 3-3 summarises the cell line numbers and genotyping results. Cell line 1-3 was established from a mouse on a C57BL/6

background, while all other cell lines were established from mice on a mixed C57BL/6 / 129 background.

After selection, cells were expanded, with non-clonal cell lines being established. When grown at low confluency, *Foxc1*$^{+/+}$ and *Foxc1*$^{-/-}$ cells were morphologically similar, although *Foxc1*$^{+/+}$ cells appear more dendritic than *Foxc1*$^{-/-}$ cells, which appeared more elongated (Figure 3-11C and 3-11E). When grown to confluency, *Foxc1*$^{+/+}$ cells pack very tightly and become rounder in shape (Figure 3-11D, 3-15A, 3-18A), whereas *Foxc1*$^{-/-}$ cells remain elongated and do not pack tightly (Figure 3-11F, 3-15G, 3-18B).

In order to confirm that the established cell lines stably express the SV40 T-antigen, immunocytochemistry was performed using a mouse anti-SV40 T-antigen antibody (Pab101). Figure 3-12 summarises these results, showing expression of SV40 T-antigen in almost every cell of *Foxc1*$^{+/+}$, *Foxc1*$^{+/-}$ and *Foxc1*$^{-/-}$ cell lines. All thirteen cell lines expressed the SV40 T-antigen oncoprotein.

Table 3-3: Genotyping results for cell lines

Cell line number	Genotype
1-3 55 58 62	*Foxc1*$^{+/+}$
59 60 72 75	*Foxc1*$^{+/-}$
57 70 78 80 81	*Foxc1*$^{-/-}$

Figure 3-11: Immortalising primary cultures of the presumptive cornea

A – E12.5 mouse eye, showing the periocular mesenchyme stained in blue (expression of *Foxc1*) (Kidson et al., 1999). Tungsten needles were used to dissect small wedges of tissue shown by the ellipse in A, which were then cultured for 48 – 72 h. B – Example of a mesenchyme explant, cultured for 72 h (explant delineated by dotted line). After immortalising the primary cultures with SV40 T-antigen, cell lines were expanded. At low confluency, $Foxc1^{+/+}$ and $Foxc1^{-/-}$ cells were morphologically similar, but $Foxc1^{+/+}$ cells appeared more dendritic than $Foxc1^{-/-}$ cells (C and E). When grown to confluency, $Foxc1^{+/+}$ cells pack very tightly and become rounder in shape (D), whereas $Foxc1^{-/-}$ cells remain elongated and do not pack tightly (F) ce – corneal epithelium, e – eyelid, L – lens, nr – neural retina, on – optic nerve. Scale bar = 20 μm.

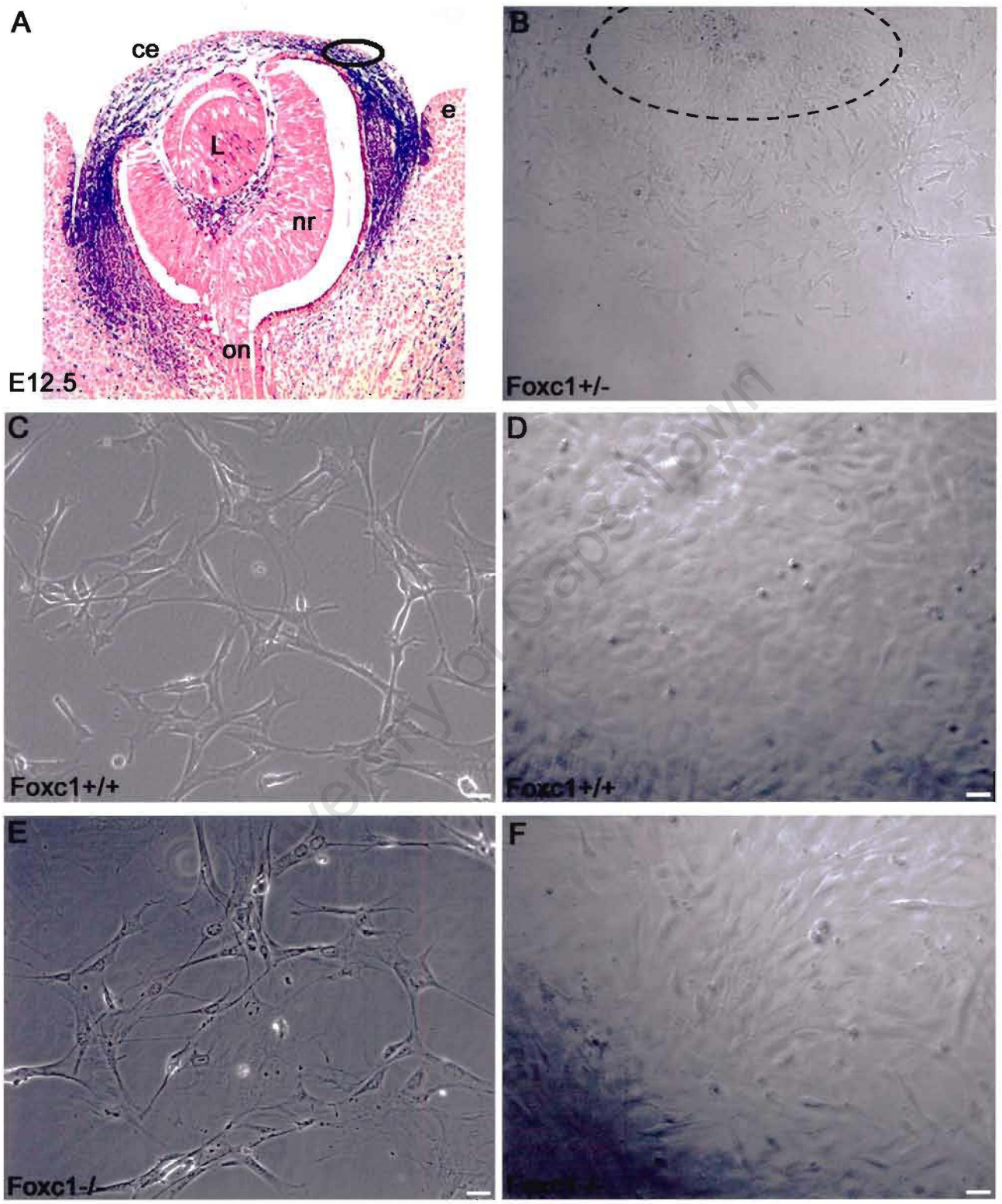

Figure 3-11: Immortalising primary cultures of the presumptive cornea

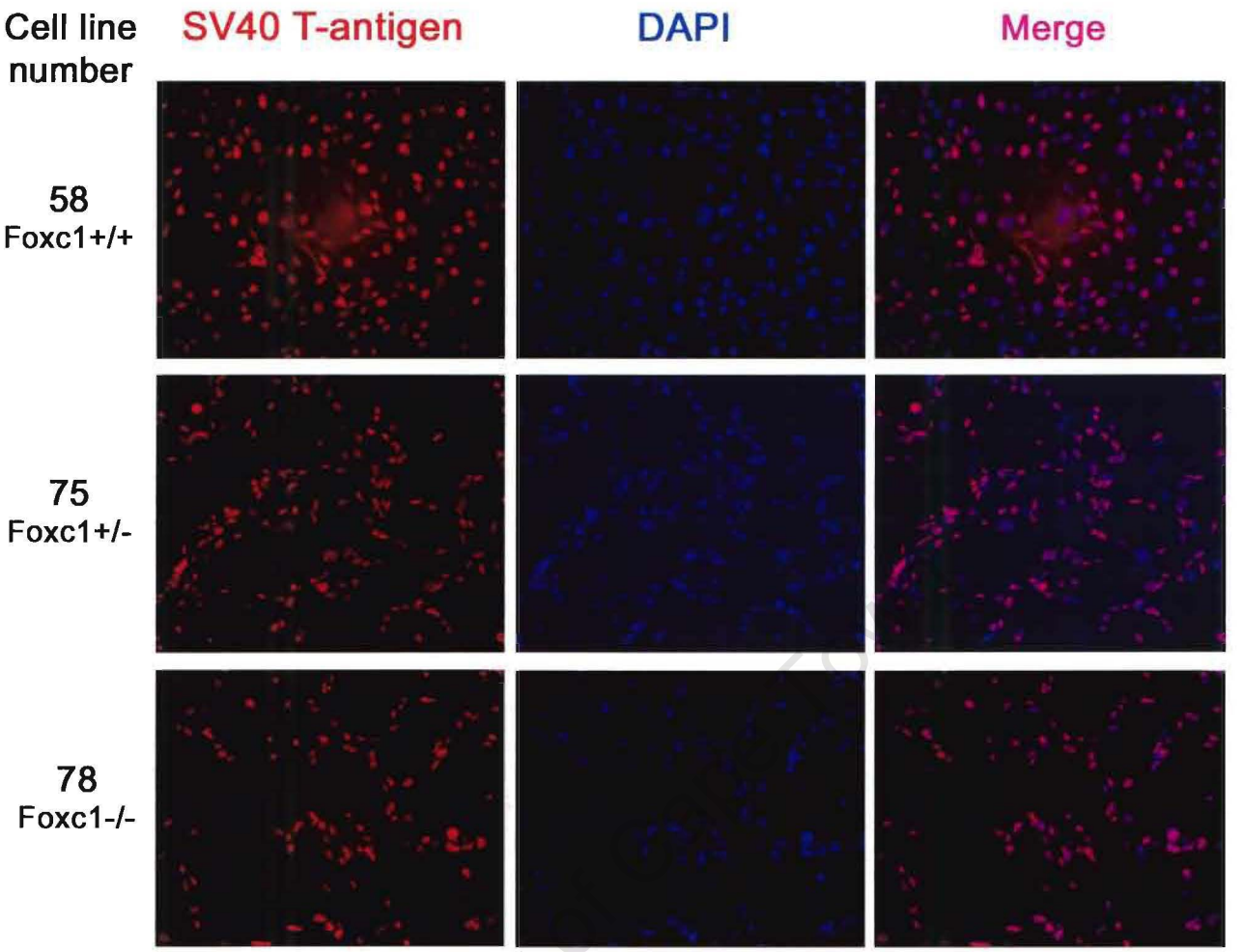

Figure 3-12: Expression of SV40 T-antigen in established cell lines

Summary of SV40 T-antigen expression in *Foxc1*$^{+/+}$, *Foxc1*$^{+/-}$ and *Foxc1*$^{-/-}$ cell lines. Clear nuclear localisation of the oncoprotein in almost every cell is evident. Each of the thirteen cell lines that were established expressed the SV40 T-antigen oncoprotein.

3.3.1 Gene expression profiles of immortal cell lines

Very few genes have been identified that are specifically expressed in the periocular mesenchyme as it migrates between the corneal epithelium and rim of the optic cup at E12.5. Of these early markers, the best characterised is *Foxc1* (Figure 3-11A). *Foxc1* is expressed from E11.5 – E12.5 in the migrating periocular mesenchyme and is only downregulated from E13.5 as the corneal endothelium starts to differentiate (Hiemisch et al. 1998 and Kidson et al. 1999). The ability of immortal wildtype cells to maintain endogenous *Foxc1* expression was thus examined.

examined. As a start to mapping the gene expression profiles of both the *Foxc1*$^{+/+}$ and *Foxc1*$^{-/-}$ cell lines, expression of Foxc2, *TGFβ1* and *Tgfβ1i4* were also examined

3.3.1.1 *Foxc1* and β-galactosidase expression

As a first step in characterising the immortal cell lines, their ability to maintain endogenous *Foxc1* expression was tested. Expression of *Foxc1* in wildtype cells was tested using Western blotting and RT-PCR, while expression of β-galactosidase in *Foxc1*$^{-/-}$ mutant cells was assayed by RT-PCR and immunocytochemistry.

Western blot analysis was performed on protein extracted from wildtype cells (passage 5 – 10) grown at the permissive (33°C) and non-permissive (37°C for 48 h) temperature of the oncoprotein. Figure 3-13A shows expression of the Foxc1 protein (85 kDa) in cells cultured at both the permissive and non-permissive temperatures. In addition RT-PCR was performed on RNA extracted from these cells. Integrity of the RNA was confirmed by performing RT-PCR using RiboS12 primers (Figure 3-13B). Multiplex PCR was then carried out with primers for both the *Foxc1* and *β-galactosidase* genes. Results demonstrated that each of the wildtype cell lines (55, 58, 62) continued to express *Foxc1* (Figure 3-13C, top panel, arrowheads). Three of the five established *Foxc1*$^{-/-}$ mutant cell lines (70, 78 and 81) maintained *β-galactosidase* expression (Figure 3-13C, bottom panel, arrowheads). As expected no *Foxc1* transcripts were detected in any of the *Foxc1*$^{-/-}$ cell lines.

To further confirm the expression patterns described above, immunocytochemistry was performed on wildtype and *Foxc1*$^{-/-}$ cells. Cells cultured at the non-permissive temperature of the oncoprotein (37°C for 48 h, or 39°C for 24 h) were immunostained using a polyclonal antibody directed against the β-galactosidase protein. Figure 3-14 summarises these findings and shows expression of β-galactosidase in *Foxc1*$^{-/-}$ cells (Figure 3-14A). Overlaying the image with DAPI stained nuclei (Figure 3-14B) shows that every cell expresses β-galactosidase (Figure 3-14C). As expected no β-galactosidase expression is detectable in wildtype cells (Figure 3-14D – 3-14F).

Table 3-4 summarises the *Foxc1* and β-galactosidase gene expression analyses. All wildtype cells continue to express *Foxc1* at both the permissive and non-permissive temperatures of the

Figure 3-13: Western blot and RT-PCR of *Foxc1* and β-galactosidase expression

Western blot analysis demonstrates that Foxc1 is expressed in wildtype cells after immortalisation at both the permissive (33˚C) and non-permissive (37˚C for 48 h) temperature of the oncoprotein (A). Protein was extracted from wildtype, adult kidney as a positive control.
RT-PCR analyses were performed on RNA extracted at the permissive temperature of the oncoprotein. All RT-PCR experiments included negative controls of RNA with no reverse transcriptase. Integrity of the RNA was confirmed first by performing RT-PCR using RiboS12 primers (B). Multiplex PCR with primers for both the *Foxc1* and β-galactosidase genes (C) showed that all wildtype cell lines (55, 58, 62) maintained endogenous *Foxc1* expression (arrowheads in top panel), while three of the five *Foxc1*$^{-/-}$ cell lines (70, 78 and 81) retained expression of β-galactosidase after immortalisation (arrowheads in bottom panel).

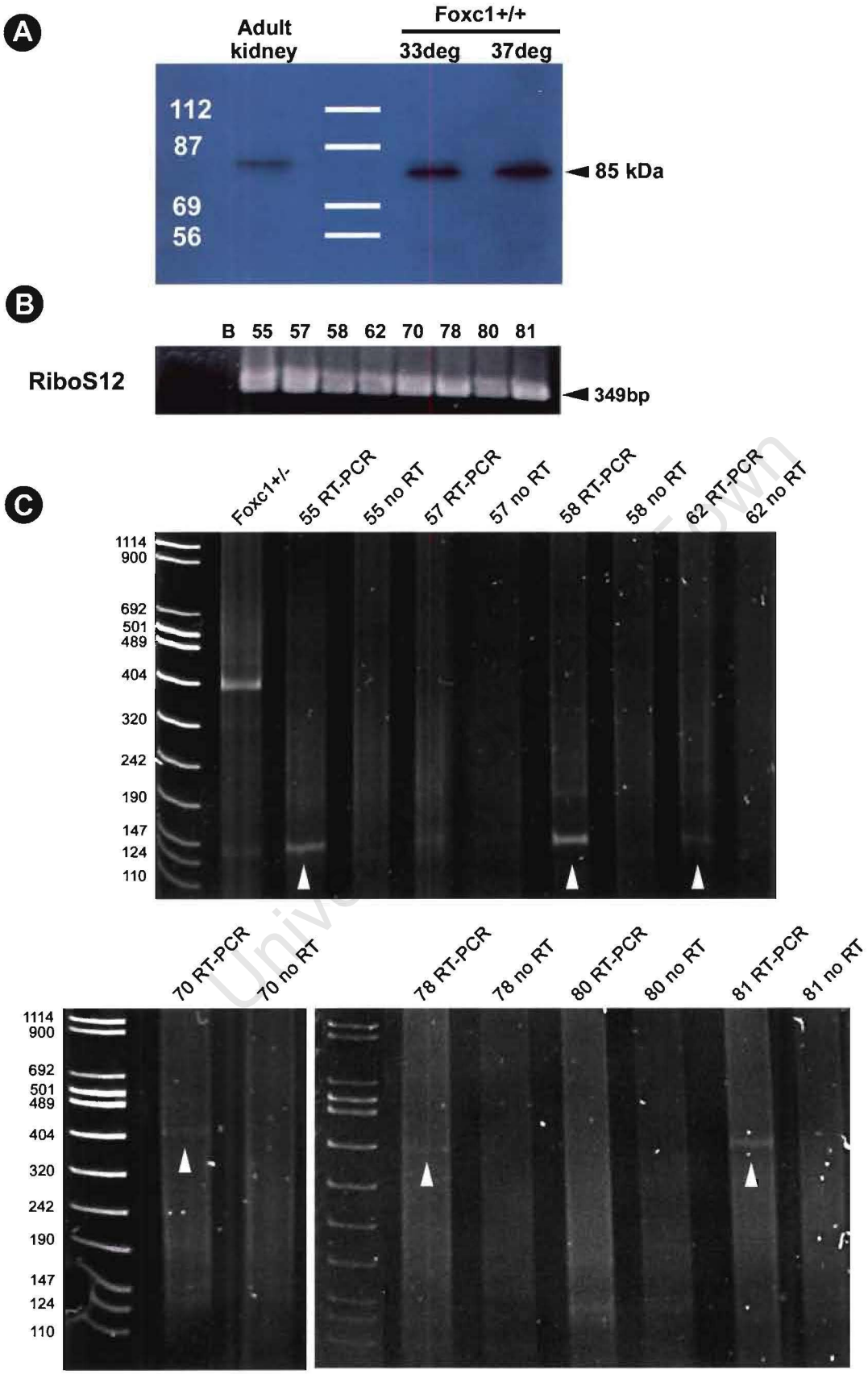

Figure 3-13: Western blot and RT-PCR of *Foxc1* and β-galactosidase expression

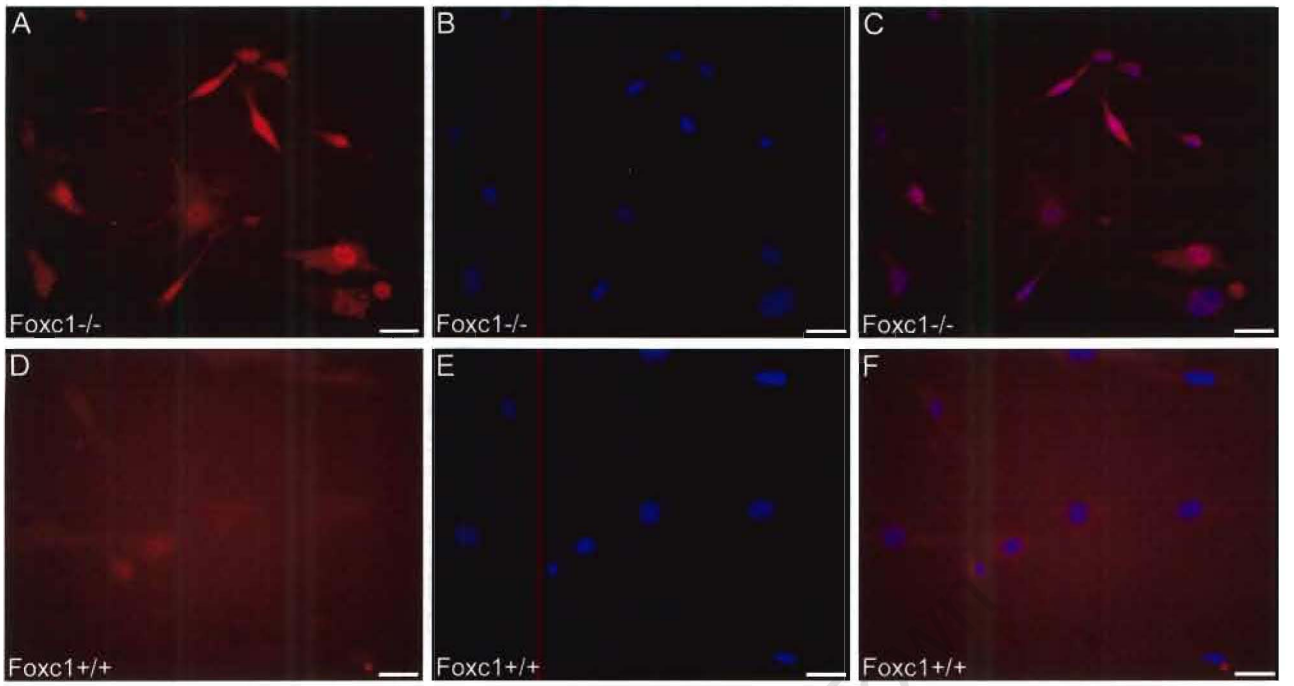

Figure 3-14: Immunocytochemistry of β-galactosidase expression

A – expression of β-galactosidase in *Foxc1*$^{-/-}$ cells cultured at the non-permissive temperature of the oncoprotein. Merging this image with nuclei stained with DAPI (B) shows every cell expresses β-galactosidase (C). As expected wildtype cells do not express β-galactosidase (D – F). Scale bar = 20 μm.

oncoprotein. Three of the five *Foxc1*$^{-/-}$ cell lines (70, 78 and 81) express β-galactosidase at both the permissive and non-permissive temperatures.

Table 3-4: Summary of *Foxc1* and β-galactosidase expression in immortal cell lines

Genotype	Cell line number	Method	Result
Foxc1$^{+/+}$	1-3	Western blot	Protein expression
	55	RT-PCR	mRNA expression
	58	RT-PCR	mRNA expression
	62	RT-PCR	mRNA expression
Foxc1$^{-/-}$	57	RT-PCR	No mRNA expression
	70	RT-PCR	mRNA expression
	78	RT-PCR	mRNA expression
	80	RT-PCR	No mRNA expression
	81	RT-PCR	mRNA expression
	81	ICC	Protein expression

3.3.1.2 Foxc2 expression

Foxc2 is a member of the winged helix / forkhead protein family of transcription factors. It is widely expressed during embryonic development, particularly in the paraxial mesoderm of the trunk and head and various mesenchymal tissues. While a detailed analysis of *Foxc2* expression in the developing eye has not been performed, this transcription factor has been implicated in regulating normal development of the anterior segment (Fang et al., 2000; Smith at al., 2000 and Traboulsi et al., 2002). In mice, defects in *Foxc2* have been shown to contribute to iris hypoplasia, irido-corneal attachments, malformations of the ciliary body, trabecular meshwork and Schlemm's canal (Smith at al., 2000). Since the periocular mesenchyme contributes to the developing cornea, iris, ciliary body and trabecular meshwork (Barrio-Asensio et al., 1999; Barrio-Asensio et al., 2002; Haustein, 1983; Kidson et al., 1999; Pei and Rhodin, 1971) it was of interest to establish whether the immortalised $Foxc1^{+/+}$ and $Foxc1^{-/-}$ cell lines expressed *Foxc2*.

Using a polyclonal antibody directed against the Foxc2 protein, immunocytochemistry was performed on $Foxc1^{+/+}$ and $Foxc1^{-/-}$ cells cultured at the non-permissive temperature of the oncoprotein (37°C for 48 h, or 39°C for 24 h). Figure 3-15 summarises these findings and shows expression of Foxc2 in both $Foxc1^{+/+}$ and $Foxc1^{-/-}$ cells (Figure 3-15A and 3-15G respectively). Clear nuclear expression of the transcription factor is demonstrated by co-localisation with the DAPI nuclear stain (Figure 3-15B, C and 3-15H, I). Negative control experiments of wildtype and mutant cells incubated without the primary antibody are shown in Figures 3-15D – F and 3-15J – L.

3.3.1.3 *TGFβ1* and *Tgfβ1i4* expression

Micro-array experiments using RNA extracted from whole heads of E13.5 wildtype and $Foxc1^{-/-}$ mice have shown an up-regulation of *Tgfβ1i4* in $Foxc1^{-/-}$ mice (Sommer et al., in preparation[1]). Since *Tgfβ1i4* expression has been reported in the developing ciliary body, further *in situ* hybridisation experiments were performed, firstly, to better map *Tgfβ1i4* expression in tissues surrounding the eye at E13.5 and secondly to compare expression in $Foxc1^{+/+}$ and $Foxc1^{-/-}$ mice.

[1] See Chapter 4, endnote

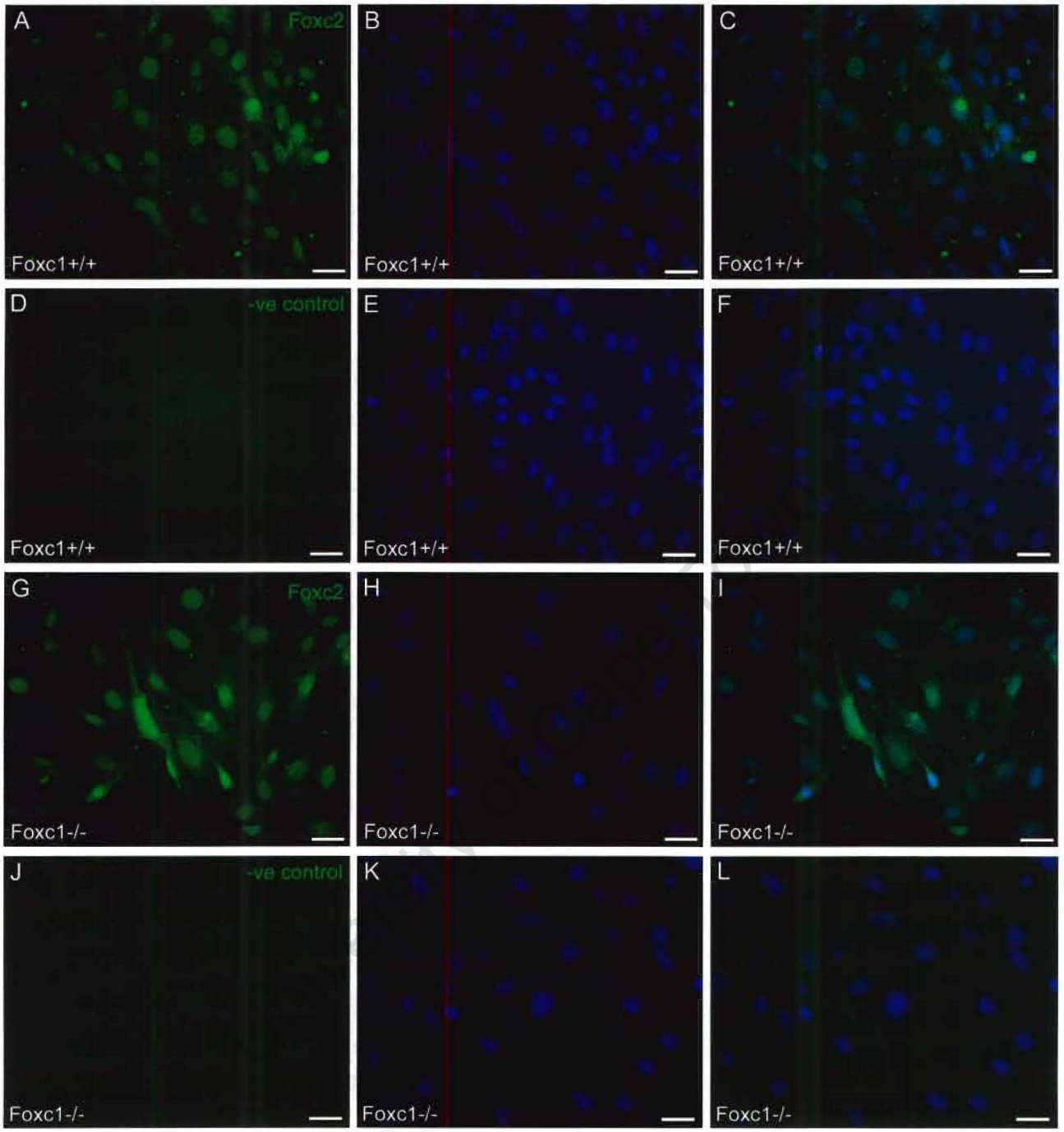

Figure 3-15: Immunocytochemistry of Foxc2 expression

Foxc2 is expressed in both *Foxc1*$^{+/+}$ and *Foxc1*$^{-/-}$ cells (A and G, respectively). Co-staining cells for DAPI (B, H) shows nuclear localisation of the Foxc2 protein (C, I). Negative control experiments of *Foxc1*$^{+/+}$ and *Foxc1*$^{-/-}$ cells incubated without the primary antibody are shown in panels D – F and J – L, respectively. Scale bar = 20 μm.

In situ hybridisation experiments showed *Tgfβ1i4* to be expressed predominantly in the inner ciliary epithelium, lens, differentiating neural retina, corneal epithelium and periocular mesenchyme at E13.5 in wildtype mice (Figure 3-16A). Faint expression around the rim of the optic cup and in the differentiating corneal mesenchyme was also evident. Expression in *Foxc1*$^{-/-}$ mice at E13.5 was far stronger; however, the domains of expression were similar, with *Tgfβ1i4* being expressed in the inner ciliary epithelium, lens, neural retina, corneal epithelium, periocular mesenchyme, optic nerve and corneal mesenchyme (Figure 3-16B). Expression in the periocular mesenchyme appears to be expanded in *Foxc1*$^{-/-}$ mice. Of note was a strong patch of expression on the nasal side of the eye, which is thought to be the mesenchyme surrounding the post-oral vibrissae (Figure 3-16B, asterisk). Expression in this region in wildtype mice was observed in other *in situ* hybridisation experiments, but expression was never as intense as in the *Foxc1*$^{-/-}$ mice.

Based on the *in situ* hybridisation results showing *Tgfβ1i4* expression in the periocular mesenchyme, expression of *Tgfβ1i4* in the immortal wildtype and *Foxc1*$^{-/-}$ cell lines was assessed using RT-PCR. Furthermore, since *TGFβ1* is thought to induce or at least stabilise *Tgfβ1i4* transcripts (Uchida et al., 2003), its expression was also analysed.

RNA was extracted from cells growing at the permissive temperature (33°C) of the oncoprotein. Initial analyses only tested for the presence or absence of gene transcripts in wildtype and mutant cell lines. Endpoint analyses showed that *TGFβ1* and *Tgfβ1i4* are expressed in all wildtype (55, 58, 62) and *Foxc1*$^{-/-}$ (70, 78, 81) cell lines (Figure 3-17).

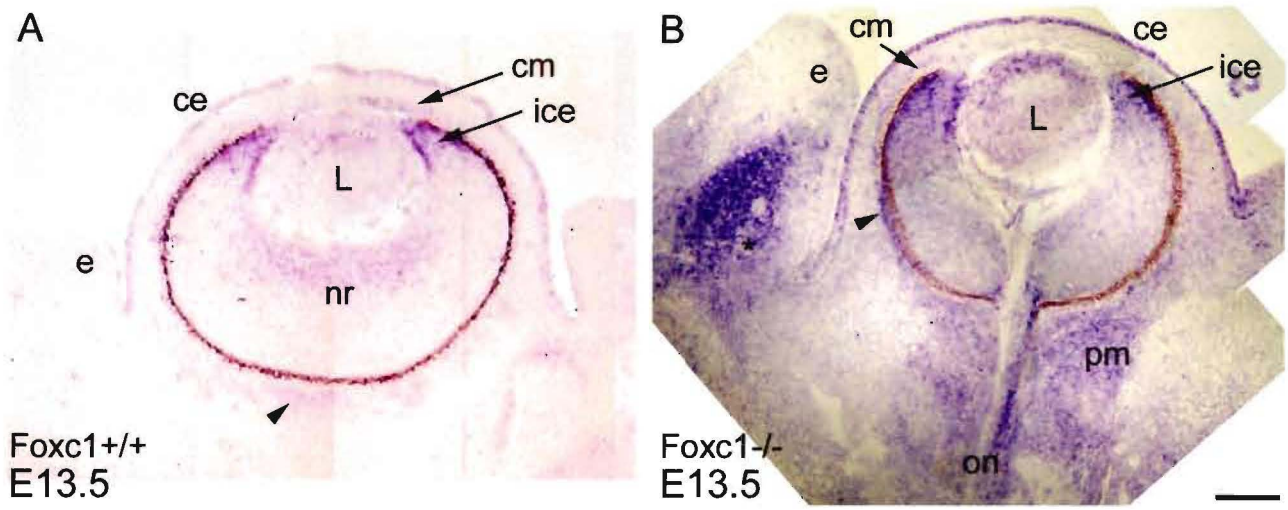

Figure 3-16: Comparison of *Tgfβ1i4* expression in *Foxc1*$^{+/+}$ and *Foxc1*$^{-/-}$ E13.5 eyes

At E13.5, in *Foxc1*$^{+/+}$ mice (A), *Tgfβ1i4* is expressed in the inner ciliary epithelium (ice), differentiating neural retina (nr), lens (L), corneal epithelium (ce), differentiating corneal mesenchyme (cm) and periocular mesenchyme (arrowhead). Expression in *Foxc1*$^{-/-}$ mice is very similar, however expression is far stronger and expression in the periocular mesenchyme is expanded. There is also clear expression in the optic nerve (on) and the mesenchyme surrounding the post-oral vibrissae (asterisk). e – eyelid, scale bar = 100 μm.

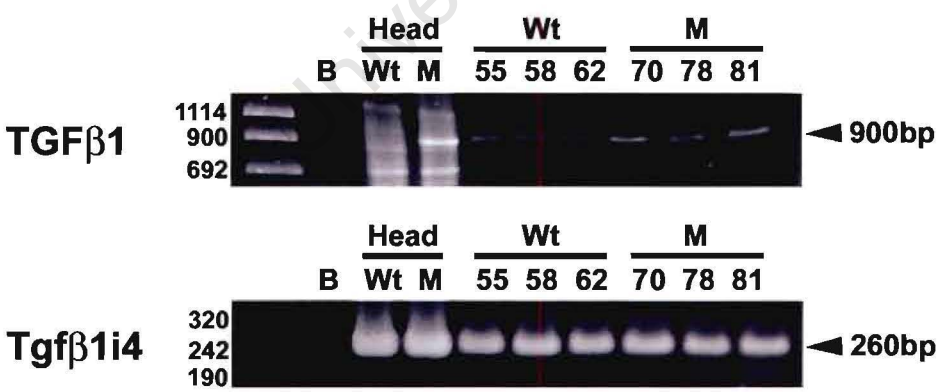

Figure 3-17: RT-PCR of *TGFβ1* and *Tgfβ1i4* in *Foxc1*$^{+/+}$ and *Foxc1*$^{-/-}$ cell lines

All *Foxc1*$^{+/+}$ (Wt) and *Foxc1*$^{-/-}$ (M) cell lines express both *TGFβ1* and *Tgfβ1i4*. RNA extracted from whole heads was used as a control.

3.3.2 Formation of cell junctions in immortal cell lines

One of the key events occurring during differentiation of the corneal endothelium is the formation of adherens and tight junctions. As well as serving a crucial physiological function in the adult, normal junction formation is thought to be an essential event that precedes formation of the anterior chamber during embryonic development. In *Foxc1*$^{-/-}$ mice tight junctions fail to form in the corneal endothelium and consequently no anterior chamber forms (Kidson et al., 1999).

Expression analyses of N-cadherin (a marker of adherens junctions) and ZO-1 (a marker of tight junctions) from E12.5 to P0 in wildtype and *Foxc1*$^{-/-}$ mutant corneas have been performed (Mgwebi, PhD thesis, 2004). The earliest observed expression of these markers in wildtype corneas was at E13.5 in discrete regions at points of cell – cell contact, with entire cell boundaries expressing these markers by E14.5 – E15.5. This study also supported previous work (Kidson et al., 1999) suggesting that *Foxc1*$^{-/-}$ mutant corneas do not form adherens or tight junctions at all.

Since the *Foxc1*$^{+/+}$ and *Foxc1*$^{-/-}$ cell lines were established with a view to studying the cell biology of corneal differentiation, characterising their ability to form cell junctions was essential. To this end immunocytochemistry using N-cadherin and Z0-1 antibodies was performed on cells cultured at the non-permissive temperature of the oncoprotein (39°C, or 37°C for 48 h). An advantage of using the non-permissive temperature is that the low proliferation rates occurring in culture parallel those of differentiating cells *in vivo*.

The ability of wildtype and mutant *Foxc1*$^{-/-}$ cells to form adherens junctions (N-cadherin expression) was compared (Figure 3-18). Under low power magnification (40x) clear junctions were seen surrounding all wildtype cells (Figure 3-18A), while no junctions were apparent in *Foxc1*$^{-/-}$ cells (Figure 3-18B). To verify these observations three independent experiments were performed and for each, four random fields of view (100x magnification) were chosen, photographed and junction formation was assessed. In each experiment all *Foxc1*$^{+/+}$ cells established adherens junctions, with the characteristic ladder like lines of connection forming between adjacent cells (Figure 3-18C, E, G). Perinuclear staining, presumably in the Golgi body was also observed (Figure 3-18C, arrowheads). In most fields of view (7/12) *Foxc1*$^{-/-}$ cells

Figure 3-18: N-cadherin expression in *Foxc1*$^{+/+}$ and *Foxc1*$^{-/-}$ cell lines

Clear adherens junctions form between cells in *Foxc1*$^{+/+}$ cell line 55 (A), while *Foxc1*$^{-/-}$ cells (cell line 81) appear not to form junctions (B). Three independent experiments confirmed that *Foxc1*$^{+/+}$ cells always form adherens junctions with adjacent cells (C, E, G). Perinuclear N-cadherin staining was also observed in wildtype cells (C, arrowheads). In most cases (7/12) *Foxc1*$^{-/-}$ cells, show no membrane-associated immunoreactivity and do not form adherens junctions (D). Perinuclear N-cadherin staining was, however, observed (D, arrowheads). In some cases (3/12) faint, diffuse immunoreactivity is observed in the cytoplasm (F, arrowheads). In 2/12 cases immunoreactivity was observed in discrete clusters in the cytoplasm (H, arrowhead). Scale bar = 20 μm.

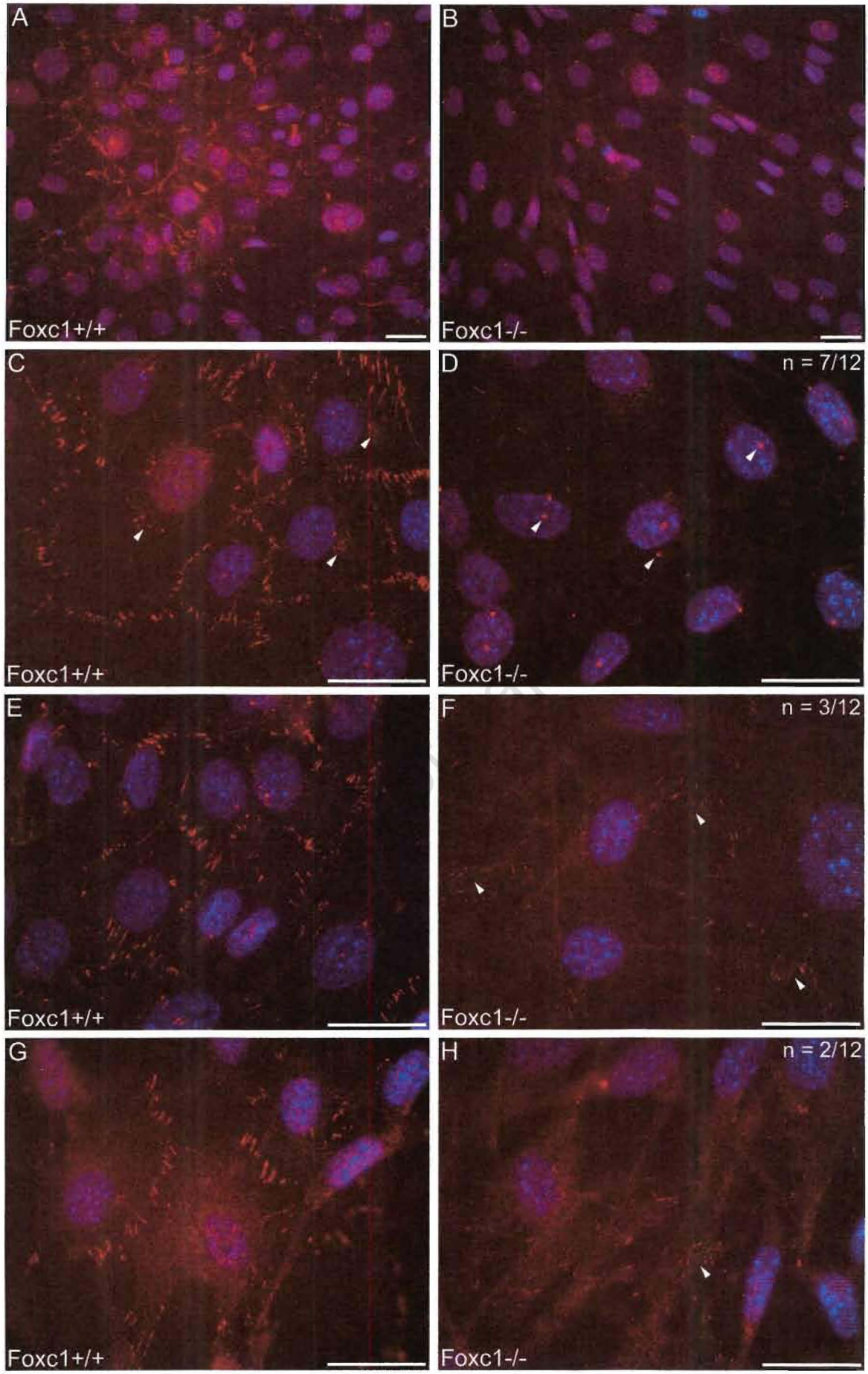
A
Foxc1+/+
B
Foxc1-/-
C
Foxc1+/+
D
n = 7/12
Foxc1-/-
E
Foxc1+/+
F
n = 3/12
Foxc1-/-
G
Foxc1+/+
H
n = 2/12
Foxc1-/-

Figure 3-18

showed no membrane-associated immunoreactivity to N-cadherin and failed to form adherens junctions (Figure 3-18D). In this field of view bright, perinuclear immunoreactivity, presumably in the Golgi body, was observed (Figure 3-18D, arrowheads). In some cases (3/12) faint, diffuse immunoreactivity was observed; however, the staining appeared randomly distributed and was not associated with cell boundaries (Figure 3-18F, arrowheads). In other cells (2/12) immunoreactivity was detected in discrete clusters within the cytoplasm (Figure 3-18H, arrowhead). Neither *Foxc1*$^{+/+}$ nor *Foxc1*$^{-/-}$ immortal cells expressed ZO-1.

The above observations suggest that a proportion of mutant cells do express N-cadherin; however, they appear unable to translocate N-cadherin to the cell membrane. Prior to translocation, the membranes of adjacent cells are temporarily stabilised by free-moving cadherin receptors in the membrane (Vasioukhin et al., 2000). The concentration of cadherin receptors determines the efficiency of subsequent junction assembly (Lambert et al., 2002). Thus in order to determine whether the lack of junction formation in *Foxc1*$^{-/-}$ cells resulted from low levels of cadherin receptors, co-cultures of *Foxc1*$^{+/+}$ and *Foxc1*$^{-/-}$ cells were established. It was hypothesised that mutant cells may be able to form stable associations with wildtype cells and so assemble junctions. In these co-cultures *Foxc1*$^{+/+}$ and *Foxc1*$^{-/-}$ cells were seeded at ratios of 3:1, 1:1 and 1:3, and cultured for 48 h at 37°C. In the co-cultures wildtype and mutant cells were distinguished using immunocytochemistry for β-galactosidase, which is only expressed in mutant cells. In each of three independent experiments five fields of view were selected, photographed and cell junctions analysed. The only criterion for field selection was that both *Foxc1*$^{+/+}$ and *Foxc1*$^{-/-}$ cells were visible. Figure 3-19 summarises the observations showing typical results for each of the three culture conditions (3-19A and B, 3:1; 3-19C and D, 1:1; 3-19E and F, 1:3 of *Foxc1*$^{+/+}$: *Foxc1*$^{-/-}$ cells). Panels 3-19A, C and E show cells immunostained for both N-cadherin and β-galactosidase. *Foxc1*$^{-/-}$ mutant cells are labelled 'm'. To interpret these results, DAPI stained nuclei were overlaid on this image and cell boundaries were extrapolated (Figures 3-19B, D, F). Irrespective of the *Foxc1*$^{+/+}$: *Foxc1*$^{-/-}$ cell ratio, in every field of view (n = 15), *Foxc1*$^{-/-}$ cells failed to form junctions between themselves or with *Foxc1*$^{+/+}$ cells. White arrowheads highlight cell boundaries of *Foxc1*$^{-/-}$ mutant cells (no junctions) and red arrowheads highlight junctions forming at the boundaries between wildtype cells. Most striking is that *Foxc1*$^{+/+}$ cells flanked by both *Foxc1*$^{+/+}$ and *Foxc1*$^{-/-}$ cells consistently form junctions with adjacent *Foxc1*$^{+/+}$ cells but do not form junctions with *Foxc1*$^{-/-}$ cells. For example, in Figure 3-19D, wildtype cell, wt1, formed strong adherens junctions with adjacent wildtype cells to the left

Figure 3-19: N-cadherin and β-galactosidase expression in *Foxc1*$^{+/+}$ and *Foxc1*$^{-/-}$ co-cultures

Co-cultures of *Foxc1*$^{+/+}$ and *Foxc1*$^{-/-}$ cells were seeded at ratios of 3:1, 1:1 and 1:3 respectively in A-B, C-D and E-F. Panels A, C and E show combined immunofluorescence for N-cadherin and β-galactosidase proteins. *Foxc1*$^{-/-}$ mutant cells (m) are readily identified by the strong nuclear immunostaining for β-galactosidase. Panels B, D and F show merged images with DAPI as a nuclear stain and cell boundaries drawn in yellow. Irrespective of cell ratios, *Foxc1*$^{-/-}$ mutant cells fail to form junctions with adjacent cells (*Foxc1*$^{+/+}$ or *Foxc1*$^{-/-}$) as shown by the white arrowheads. Panel D best highlights how *Foxc1*$^{+/+}$ cells readily form junctions with adjacent *Foxc1*$^{+/+}$ cells (red arrowheads) but do not form junctions with adjacent *Foxc1*$^{-/-}$ cells (n = 15). Scale bar = 20 μm.

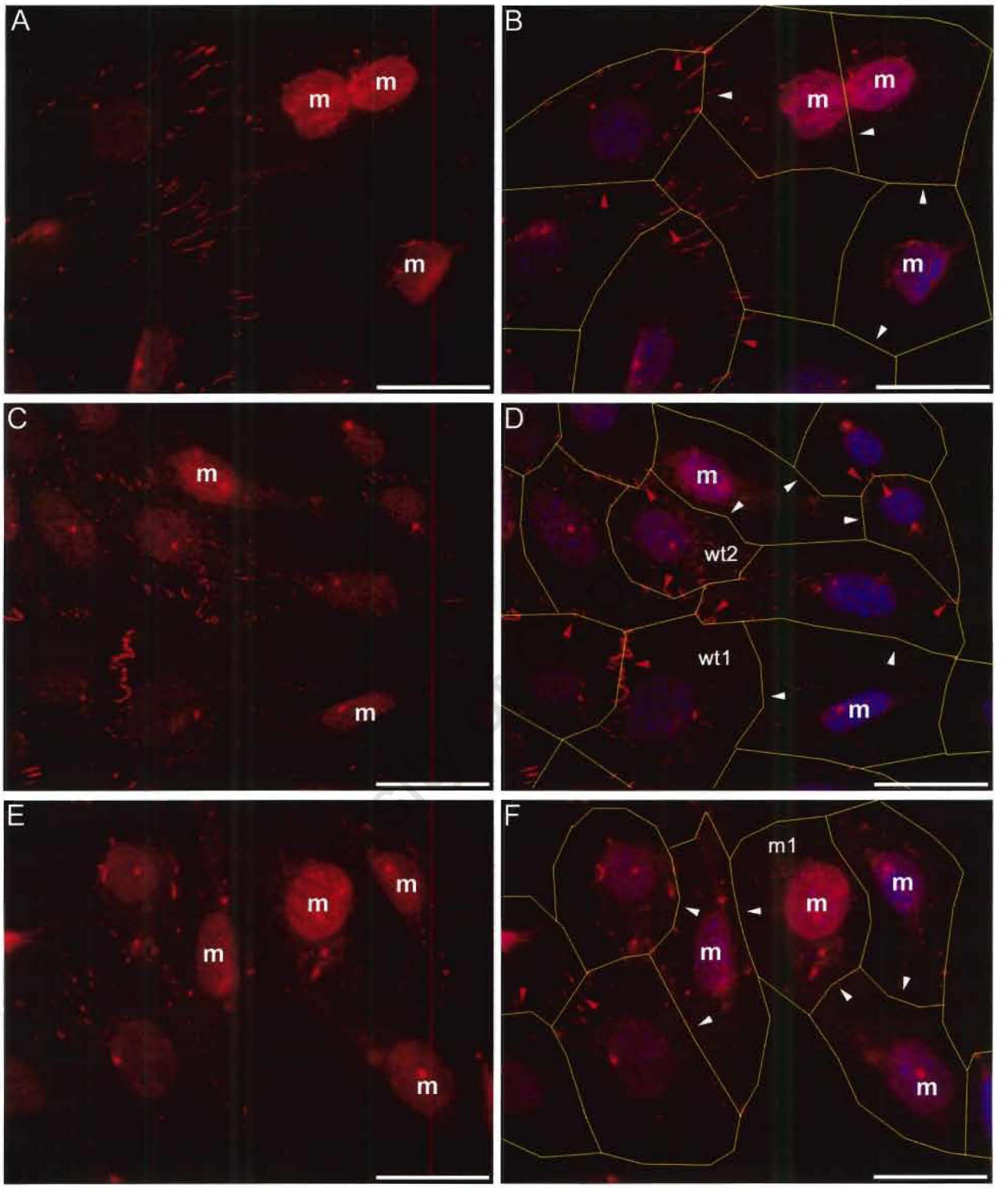

Figure 3-19: N-cadherin and β-galactosidase expression in *Foxc1*$^{+/+}$ and *Foxc1*$^{-/-}$ co-cultures

and above, but failed to form junctions with the mutant cell on its right. Similarly in the same panel, wildtype cell, wt2, formed junctions with all neighbouring wildtype cells, but failed to form adherens junctions with the mutant cell above it. Figure 3-19F, shows how adjacent mutant cells, for example, cell m1, failed to form junctions with each other as described when cultured alone.

The failure of *Foxc1*$^{-/-}$ cells to form junctions in culture might be explained by an inability to form stable associations with adjacent cells. In culture, mutant cells demonstrated a clear tendency to avoid contact (compare Figures 3-11D, 3-15A, 3-18A with Figures 3-11F, 3-15G, 3-18B). Since cell-cell contact is an integral event in establishing cadherin based junctions, a model system of hanging drop cultures, forcing cells to aggregate, was developed (Methods and Materials, Section 2.5.5.2). The resulting cell clusters were cultured for 72 h at 39°C and then processed for immunocytochemistry using an anti N-cadherin antibody.

Two independent experiments each comprising three hanging drops cultures were performed. Using confocal microscopy, the formation of cell junctions on the surface of the cell aggregates was assessed. Figures 3-20A, 3-20B and 3-20C each shows a different confocal series through different hanging drop cultures of wildtype cells. Figure 3-20A shows a typical field of view under low power magnification where some cells form adherens junctions along their boundaries (Figure 3-20A3, arrowheads), whereas other cells show strong immunostaining to N-cadherin; however, its distribution is restricted to the cell cytoplasm. Figures 3-20B and 3-20C provide optical sections through regions in wildtype hanging drops where cell junctions were present. Arrowheads in panels 3-20B7, 3-20B10 and 3-20C3 highlight cell boundaries. Asterisks in adjacent confocal sections are used to indicate the respective cells (panels 3-20B6, 3-20B9 and 3-20C2).

Figure 3-21A – D summarises junction formation in wildtype cells, with an example of a wildtype cell cluster that did not form junctions shown in Figure 3-21D. In contrast to the findings for wildtype cells, none of the cells in *Foxc1*$^{-/-}$ mutant hanging drops (n = 5) formed adherens junctions. In all cases immunoreactivity for N-cadherin was strictly observed in the cytoplasm (Figure 3-21E). Thus culturing mutant cells such that they were forced to aggregate did not promote cell junction assembly. Together with the mixed co-culture experiments, these findings suggest that *Foxc1*$^{-/-}$ mutant cells lack an ability to perceive or respond to points of cell-cell contact.

Figure 3-20: N-cadherin expression in *Foxc1*$^{+/+}$ hanging drop cultures

Confocal series through three wildtype hanging drop cultures (A, B, C) shows cell boundaries immunostained for N-cadherin (A3, B7, B10 and C3, arrowheads). Individual cells in adjacent confocal sections are indicated using an asterisk (B6, B9 and C2), highlighting the complex cell clusters that are formed in three dimensions. Scale bars: Panel A = 20 μm; Panels B and C = 8 μm.

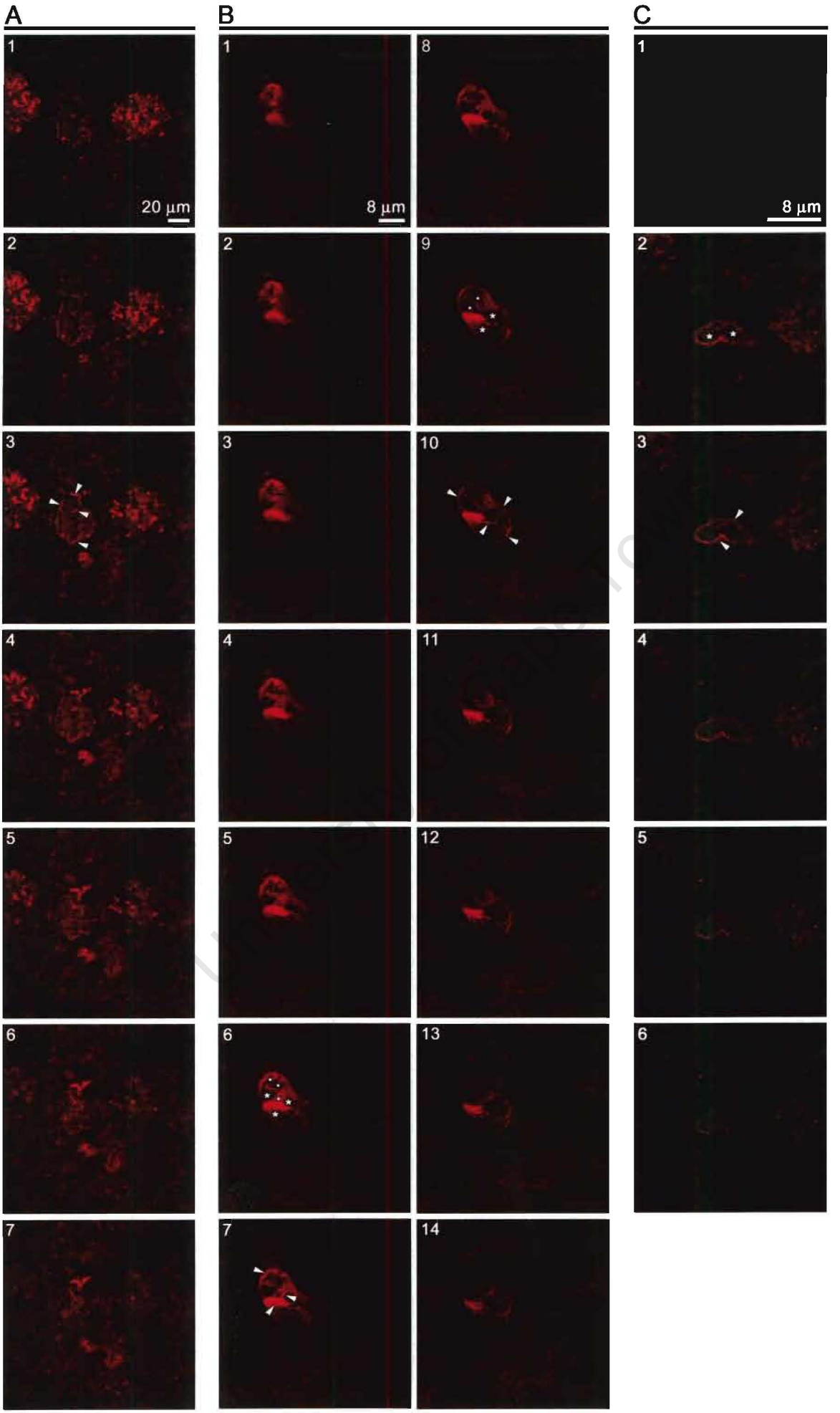

Figure 3-20

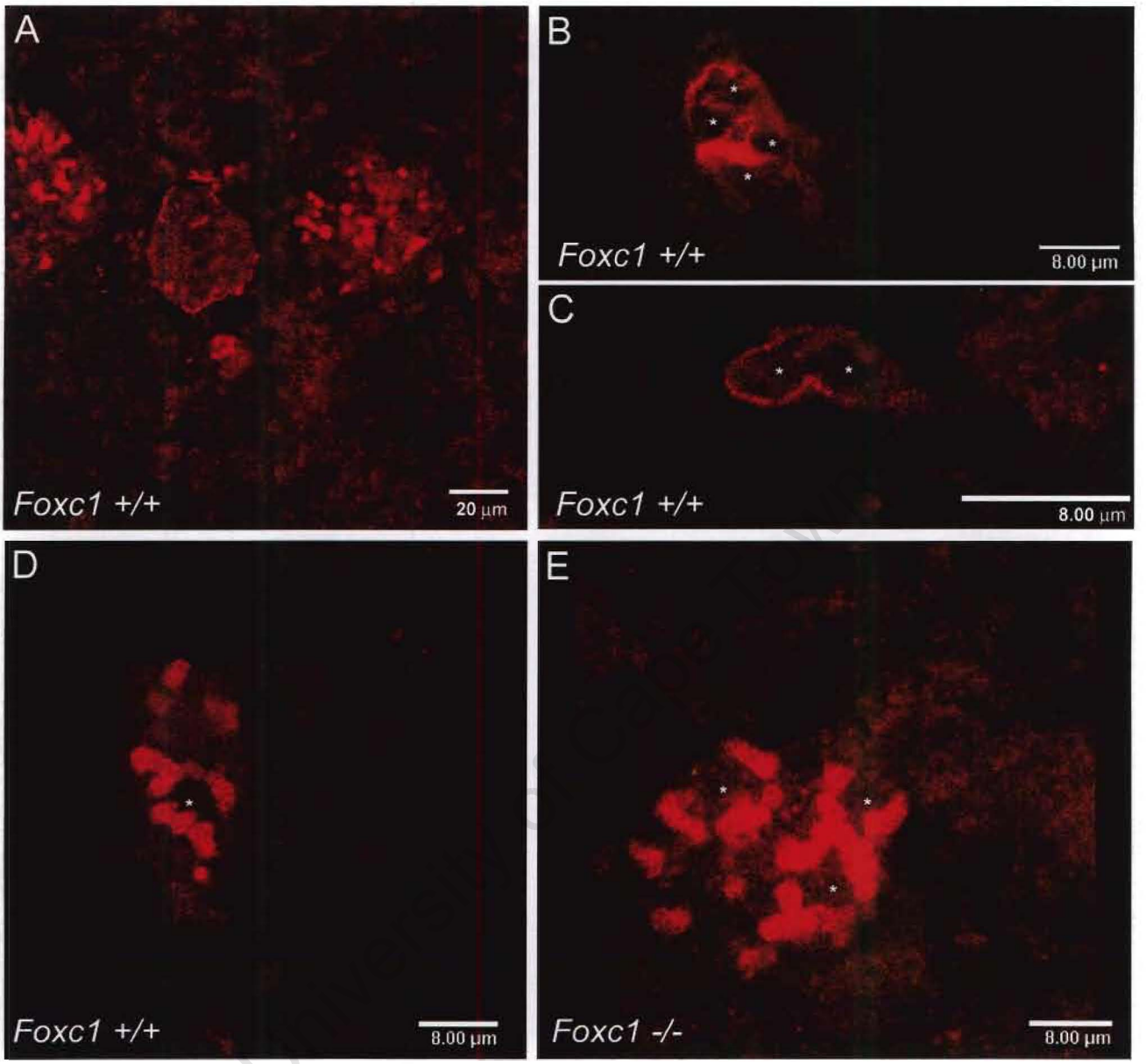

Figure 3-21: Summary of N-cadherin expression in *Foxc1*$^{+/+}$ and *Foxc1*$^{-/-}$ hanging drop cultures

Representative confocal sections of wildtype cells forming junctions in hanging drop cultures are shown in A, B and C. Cell boundaries show strong immunostaining for N-cadherin. Some clusters of wildtype cells did not form adherens junctions. Cells within these clusters showed strong cytoplasmic immunostaining for N-cadherin (D). In all cases (n = 5) *Foxc1*$^{-/-}$ cells failed to form adherens junctions in hanging drop cultures. Strong immunoreactivity was restricted to the cytoplasm (E). Asterisks indicate individual cells.

Chapter 4: Discussion

Development of the vertebrate eye is a complex multi-step process requiring communication between cells and self-organisation of tissues so that discrete structures with highly specialised functions are formed. Structural refinement of these tissues is effected and coordinated by a host of molecular cues. Depending on the stage of development and cellular context, disruptions to these signals can result in dramatic disruptions to normal eye development. More commonly, molecular disruptions cause subtle perturbations affecting specific parts of the eye. This is partly due to gene redundancies and the large number of genes involved in directing a given cellular event.

Development of the anterior segment of the eye is no exception, with many gene defects having been identified and implicated in anterior segment dysgenesis (reviewed in Gould and John, 2002; Gould et al., 2004). Even in established model systems such as the mouse, the translation of genotype into phenotype is somewhat enigmatic. Accumulating evidence suggests that stochastic events during development or allelic differences in modifier genes play an important role in the expressivity of genetic traits (Anderson et al., 2001; Chang et al., 1999; Libby et al., 2003; Savinova et al., 2001).

Although morphogenesis of the eye during early development is well characterised, little is known about the late embryonic and early postnatal stages of mouse eye development. Importantly, it is at these stages that several structures within the anterior segment develop. One of the primary objectives of this research was thus to provide a cellular and anatomical foundational study of ciliary body development. Secondly in an attempt to model the cellular and genetic events that direct normal corneal differentiation, immortal cell lines of the presumptive corneal mesenchyme in *Foxc1*$^{+/+}$ and *Foxc1*$^{-/-}$ mice were established and their ability to form cell junctions was characterised.

4.1 Ciliary body morphogenesis

Studies on ciliary body structure in humans, primates, rabbits, guinea pig and avians have revealed that ciliary processes in these species form a regular radial network of parallel folds (Kessel and Kardon, 1979; Bard and Ross, 1982b; Bard and Ross, 1982a; Ritch et al., 1996). It has been

asserted that the undulating folds of the ciliary body are responsible for providing a large surface area for the secretion of aqueous humour as well as serving as a site of attachment for zonular fibres. Although the mouse has been used extensively to model anterior segment dysgenesis, no structural description of the adult ciliary body has been presented. In this study it was shown that in mice the adult ciliary processes do not form a regular parallel array of folds as observed in other mammals. The processes intersect, cross over and interweave rather than lying parallel to one another. A complex network of zonular fibres is evident in the valleys between ciliary processes. A narrow pars plana was observed and along the iris – ciliary body margin, the iris cells formed a smooth band into which the ciliary processes merge.

The significance of these structural differences is unclear. One possibility is that in the relatively small mouse eye, the intersecting ciliary processes further increase the surface area for secretion of aqueous humour. However, certain animals such as the zebrafish (Soules and Link, 2005) and naked mole rat (Nikitina et al., 2004) also have small eyes, but have a structurally flat ciliary epithelium. In the zebrafish, ultrastructural studies have shown that the ciliary epithelium retains characteristics of a secretory epithelium (Soules and Link, 2005). These observations suggest that folding of the ciliary epithelium may impart additional functional characteristics over and above increasing the surface area for secretion of aqueous humour.

It is possible that the expansive ciliary folds observed in mammals provide a large surface area for the attachment of zonular fibres, which would presumably facilitate rapid accommodation. In cephalopods and teleosts, lens accommodation has been reported to occur via the forward and reverse movement of the lens as opposed to the lens shape changes that occur in mammals (Schaeffel et al., 1999). In teleosts this forward and reverse movement is mediated by the lens retractor muscle and requires a less elaborate arrangement of zonular fibres. Thus the absence of ciliary folds in the zebrafish eye could relate to accommodation mechanics rather than secretory functions.

Since little is known about the underlying morphogenetic mechanisms responsible for the formation of the ciliary body, a detailed analysis of its morphogenesis was undertaken. Two main questions were addressed in this work. Firstly, how do ciliary folds develop from the flat presumptive ciliary epithelia and secondly how is the irregular folding pattern established in the mouse.

Histological analyses demonstrated that the ciliary body and iris begin to differentiate morphologically from the adjacent neural retina around E15.5 and that morphogenetic folding of ciliary processes only occurs postnatally. It is likely that molecular differentiation occurs before morphological differentiation. For example, Kubota et al. (2004) and Thut et al. (2001) have demonstrated that a number of genes are selectively expressed in the inner ciliary epithelium prior to morphological differentiation in developing chick and mice eyes, respectively. Combining cross sectional information with SEM data revealed that the ciliary epithelia initially bulge inwards towards the lens as a uniform sheet. At about P2, clefts begin to form in this annular bulge and individual ciliary processes start to take shape. Interestingly this clefting appears to occur asymmetrically around the eye. It would be of interest to determine whether this asymmetric development correlates with the known asymmetric expression of early ciliary body markers such as *Msx1* and *Otx1* (Monaghan et al., 1991; Martinez-Morales et al., 2001). Between P2 and P7 these clefts extend around the entire circumference of the eye, deepen and ultimately form discrete ciliary processes by P7.

The findings of this study suggest that the ciliary capillaries play an important role in the morphogenesis of ciliary processes. A network of capillaries starts to form perinatally (E18.5) and is well established prior to ciliary folding. Of particular relevance is that, in the mouse, the architecture of these capillaries at P0 reflects that of the adult ciliary processes. This suggests that the capillaries could serve as "nucleating" centres around which the ciliary processes form. Bard and Ross (1982a) have suggested an identical mechanism in the developing chick. They demonstrated that a radial, parallel network of capillaries forms prior to ciliary folding, with the ciliary processes apparently forming around the capillaries. However, this has not been directly tested. Once spatial signals involved during vasculogenesis are better characterised, it may be possible to establish whether there is a definitive link between capillary architecture and the final arrangement of ciliary folds in the adult.

In order to better characterise the underlying cellular dynamics that occur during ciliary folding, cell heights of the inner and outer ciliary epithelium were compared. Over the period of morphogenesis (P0 – P7) a significant decline in cell heights in both epithelial layers was observed. Most notable was the relative elongation of cells in the outer ciliary epithelium at the tips of ciliary processes at P0. These cells seem to "push" into the inner ciliary epithelium, which responds by reducing cell heights to accommodate the bulging ciliary processes. Subsequently within the inner ciliary

epithelium, cells not at the apices of forming processes also reduce their heights such that discrete processes form. Analysis of cell heights in the developing chick ciliary body demonstrated a similar increase in cell heights in the outer ciliary epithelium prior to ciliary folding (stage 29); however, as ciliary folds start to form at stage 30 cells in the inner ciliary epithelium also increased in length (Reichman and Beebe, 1992).

These differences in cell height changes between the mouse and chick suggest that the underlying mechanisms that direct ciliary folding may differ. In order to address this question, a detailed analysis of cell proliferation within the developing ciliary body was performed. BrdU incorporation analyses from E18.5 – P7 demonstrated that mitotic rates in the outer ciliary epithelium were significantly higher than those in the inner ciliary epithelium at all stages examined. In addition to this, both epithelial layers demonstrated a significant increase and subsequent decline in rates of proliferation within the timeframe from P0 – P7. One criticism of the labelling approach used in the present study was that E18.5 and P0 mice were labelled for different time periods (2 and 2.5 hours respectively) while mice from P1 – P7 were labelled for 24 hours. Thus it is not strictly accurate to compare labelling indices of these early developmental stages with the later time series (P1 – P7) since labelling indices are probably under estimated at E18.5 and P0. Nevertheless a strong correlation between mitotic surges in the ciliary epithelia and the formation of ciliary processes was observed. Most striking was the observed surge in proliferation in the outer ciliary epithelium. Even if labelling indices are underestimated at P0, a significant increase in mitotic rates in the outer ciliary epithelium was observed between P1 and P2. During this time frame SEM and histological observations demonstrate dramatic structural changes within the ciliary epithelia. Proliferation in the inner ciliary epithelium appears to initiate a day later than in the outer ciliary epithelium and is not sustained for as long. It is possible that proliferation in the inner ciliary epithelium serves in shaping individual processes, with the primary driving force being the initial growth and extension of the outer ciliary epithelium. These hypotheses could be strengthened by analyses, which carefully map and compare the distribution of proliferative and postmitotic cells within the ciliary epithelia. However, preliminary analyses do not point to the presence of localised foci of proliferative cells, for example at the tips of forming processes.

In the chick, cell proliferation has also been implicated in the developing ciliary body. Global analyses of proliferation within the eyecup suggest that proliferation levels in the ciliary zone decline relative to those in the globe of the eye during differentiation (Kubota et al., 2004).

However, within the ciliary zone mitotic rates have been shown to differ between the ciliary epithelia. As ciliary processes form, rates of proliferation gradually decline in the outer ciliary epithelium with a sharp increase in mitotic rates occurring in the inner ciliary epithelium at stage 31 (Reichman and Beebe, 1992). This contrasts with observations in the mouse, suggesting that proliferative changes during ciliary body development may play different roles in the mouse and chick. The present study and those of Reichman and Beebe (1992) have only shown a temporal correlation between proliferative changes and morphogenesis. Ideally the role that cell proliferation plays in ciliary body morphogenesis should be tested directly. Inhibiting cell proliferation over the period of ciliary folding, for example by injecting cytochalasin D into the developing eye, could provide more direct evidence. However, it is likely that such approaches will cause numerous secondary effects in the developing eye and accurate interpretation of the observations would be very difficult.

Based on the results of the present study the following working model of ciliary body development in the mouse is proposed (Figure 4-1). Just before birth (E18.5), a complicated network of capillaries forms beneath the ciliary epithelia, which possibly serve as a template around which the ciliary processes start to form. On the other hand, it is also possible that the structural parallels between the capillaries and ciliary processes merely reflect their ultimate physiological relationship and not a developmental relationship. Neither Bard and Ross (1982a) nor this study has demonstrated a direct morphogenetic relationship. Directly proving that the capillaries serve as a patterning template around which the ciliary processes form is difficult. One possible approach would be to overexpress VEGF, which is a secreted angiogenic factor (reviewed in Brown et al., 1997), in the ciliary epithelia just prior to ciliary body morphogenesis (using the promoter of a ciliary body specific gene). This should lead to an expansion and disruption of the normal vasculature. If the capillaries are involved in determining the architecture of ciliary processes, a more elaborate network of ciliary processes should form in this system. Another classical approach would be to find a means (genetic, chemical or physical) to ablate the developing vasculature and monitor subsequent ciliary body development.

Returning to the model, at P0, cells in the outer ciliary epithelium, adjacent to the capillaries, first elongate and extend inwards towards the inner ciliary epithelium. Concomitantly, rates of proliferation within the outer ciliary epithelium increase (Figure 4-1, dark blue shading) and together with the increasing cell heights cause the inner ciliary epithelium to bulge inwards towards

the lens. This step of the model is supported by SEM and histological observations at P2, which clearly show bulging of the outer ciliary epithelium, with the inner ciliary epithelium just starting to reduce cell heights to accommodate the ciliary processes (Figure 4-1B). Cells in the outer ciliary epithelium continue to proliferate until P5, while cells in the inner ciliary epithelium proliferate briefly between P1 and P2 (Figure 4-1, light blue shading). The sustained proliferation in the outer ciliary epithelium probably contributes to the lengthening of each individual process. This lengthening together with continued cell height reductions in the inner ciliary epithelium results in discrete ciliary processes being shaped by P7 (Figure 4-1D).

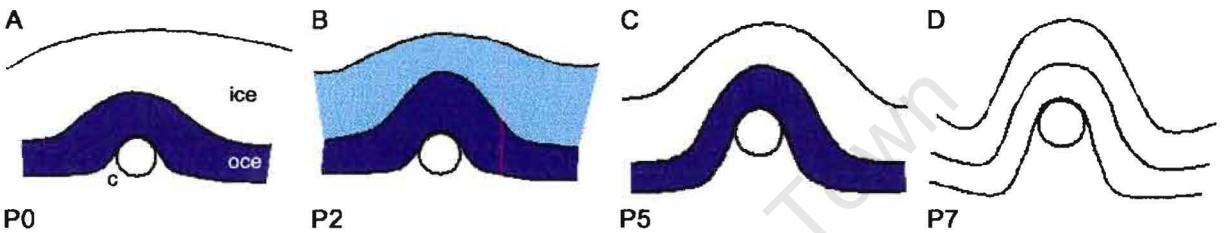

Figure 4-1: Relationship between proliferation and the formation of ciliary processes

Between E18.5 and P0 a complicated network of capillaries (c) forms beneath the outer ciliary epithelium (oce). These capillaries serve as nucleating centres around which the ciliary processes form (A). Initially cells in the outer ciliary epithelium elongate and "push" into the inner ciliary epithelium (ice). These increased cell heights, together with elevated rates of proliferation (dark blue) in the outer ciliary epithelium cause the inner ciliary epithelium to bulge inwards towards the lens. This bulging results from a brief mitotic surge in the inner ciliary epithelium between P1 and P2 (light blue). At the same time cells in the inner ciliary epithelium reduce cell heights at the apices of ciliary processes to accommodate the bulging outer ciliary epithelium (B). Secondary to this is the reduction of cell heights in-between ciliary processes in the inner ciliary epithelium. Sustained proliferation in the outer ciliary epithelium (C) results in a lengthening of each individual process. This lengthening together with continued cell height reductions in the inner ciliary epithelium results in discrete ciliary processes being shaped by P7 (D).

Identifying and characterising molecular factors that drive vasculogenesis and cell proliferation during ciliary body morphogenesis is essential to test this model. Current gene expression data is often limited to early embryonic stages of development, with postnatal expression patterns poorly described. In the developing mouse eye, members of the TGFβ superfamily of secreted signalling molecules play essential roles in tissue differentiation. In the developing ciliary body, *Bmp4*

expression impinges on the development of adjacent tissues such as the lens (Belecky-Adams et al., 2002; Faber et al., 2002) as well as playing a role in its own morphogenesis (Zhao et al., 2002). Exogenous expression of the Bmp inhibitor noggin, under the control of a αA-crystallin promoter, results in mice lacking a ciliary body. Zhao et al. (2002) provide strong evidence showing that Bmp4 plays a crucial role in the initial specification of the ciliary zone, with *Msx1* and *Otx1* expression greatly diminished in the presumptive ciliary zone of these transgenic mice. However, these experiments do not address the potential role that Bmp4 plays in the later morphogenesis of ciliary processes. In the present study, gene expression analyses from E17.5 – P7 reveal a dynamic expression pattern. *Bmp4* expression is initially restricted to the inner ciliary epithelium and iris epithelium during early postnatal development (E17.5 – P3). Whether expression in the inner ciliary epithelium contributes to the differential rates of cell proliferation between the ciliary epithelia, has not been tested. During the latter stages of ciliary body morphogenesis (P4 – P5) cells in the outer ciliary epithelium continue to proliferate and start to express *Bmp4*, with expression appearing first at the tips of ciliary processes. Again whether this upregulation contributes to the final elongation of individual ciliary processes or merely reflects a function property of the ciliary body (since Bmp4 is expressed in both ciliary epithelia in the adult) is unknown.

The transcription factor *Tgfβ1i4* (TSC-22) was initially identified as a TGFβ responsive gene (Shibanuma et al., 1992); however, recent studies show that many other growth factors and stimuli such as inflammatory cytokines also have the potential to induce its expression. Current research points to the fact that in some cases, such as effects mediated by TGFβ1, mRNA stabilisation rather than direct transcriptional activation accounts for increased levels of expression (Uchida et al., 2003). Expression analyses in the mouse have shown prominent expression of *Tgfβ1i4* at sites of epithelial to mesenchyme transition (Dohrmann et al., 1999; Kester et al., 2000). In the developing eye, expression is first detected in the presumptive ciliary body and iris zone at E12.5 (Thut et al., 2001). No detailed description of its postnatal expression, relative to ciliary body morphogenesis was provided. Furthermore, since *Tgfβ1i4* expression is negatively regulated by Bmp4 in the developing chick feather tract (Dohrmann et al., 2002), comparing *Bmp4* and *Tgfβ1i4* expression during ciliary body morphogenesis was of interest.

Since *Tgfβ1i4* expression did not change within the forming ciliary body from E18.5 – P6, with its expression restricted to the inner ciliary epithelium, it is possible that it does not play a direct role in the formation of ciliary processes. Interestingly, this expression domain overlaps with that of *Bmp4*,

suggesting that these factors may not have opposing roles in the developing ciliary body, as suggested in the developing chick feather tract (Dohrmann et al., 2002). The domain of *Tgfβ1i4* expression also serves to mark the boundary between the differentiating ciliary and iris epithelia. As soon as the iris and ciliary zones become morphologically distinct, around E18.5, no *Tgfβ1i4* expression is detectable in the iris epithelium. Only once the ciliary body and iris are more fully differentiated, does *Tgfβ1i4* expression start to extend from the inner ciliary epithelium along the iris epithelium (P4 – P6).

Within the developing chick eye, dynamic gene expression patterns also occur during ciliary body specification and morphogenesis. For example, recent studies have shown genes such as *Slc7a8* and *Cystatin* are expressed asymmetrically in the differentiating ciliary zone (Kubota et al., 2004). However, no correlation between these expression patterns and morphogenetic events was made. Other research in the developing chick has shown that canonical Wnt signalling mediated by the transcription factor LEF1 plays an important role in maintaining the proliferative potential and undifferentiated state of cells in the ciliary marginal zone (Kubo et al., 2003). However, the potential role that Wnt-2b signals play in the morphogenesis of the ciliary body were not addressed. Analysis of LEF1 expression from stages 23 – 30 revealed an initial broad domain of expression around the anterior region of the optic cup at stage 23, which recedes to the posterior half of the ciliary epithelium (the future pars plana) by stage 25. At this stage the ciliary marginal zone is bounded by neurofilament expression posteriorly, but still shows low levels of LEF1 expression. As ciliary folds form (stage 30) LEF1 expression is upregulated in the inner ciliary epithelium and iris. Faint LEF1 expression is still evident in the ciliary marginal zone, however its domain is clearly delineated by neurofilament expression posteriorly and collagen IX expression anteriorly. These expression patterns suggest that Wnt signalling mediated by LEF1 plays several roles in the anterior half of the eyecup, both in patterning and differentiation of the ciliary body and processes as well as maintaining the ciliary marginal zone.

It can thus be concluded that ciliary body morphogenesis is a tightly regulated process in both the mouse and chick. Structural complexity is achieved through the interaction of multiple genes that effect precise cellular changes. In the mouse differential rates of proliferation between the ciliary epithelia together with cell height changes play a role in the morphogenesis of ciliary processes. Whether these changes serve as the primary drivers of ciliary body folding has as yet not been determined. Further studies into the developmental relationship between the ciliary epithelia and the

underlying vasculature are also crucial for a complete understanding of the mechanics that direct ciliary body morphogenesis. Careful mapping of gene expression patterns during ciliary body morphogenesis are essential aids in bridging the gap between morphological descriptions and molecular models.

4.2 Immortal cell lines of the presumptive cornea

The cornea is a highly specialised structure, serving as both a physical barrier to the environment as well as forming a major part of the optical pathway. These functional requirements necessitate certain structural characteristics, such as transparency, lack of vasculature, immunological privilege and obviously a degree of strength. Fortuitously, these features make the cornea an ideal candidate for tissue engineering and transplantation.

Although corneal transplants have a high success rate, a major factor that limits their success is donor age (reviewed in Joyce, 2003), with a clear inverse correlation between age and the number of corneal endothelial cells having been shown (Laing et al., 1976; Murphy et al., 1984). Furthermore, since cells of the corneal endothelium are arrested at the G1-phase of the cell cycle (Joyce et al., 1996), transplanted corneas have a limited capacity to expand this cell population. Thus, characterising the molecular signals that drive differentiation of these cells has major implications in improving the efficacy of corneal transplants.

Numerous immortal cell lines of adult corneal cells (epithelial, stromal and endothelial) have been established and even successfully recombined on tissue matrix scaffolds to form corneal equivalents *in vitro* (Griffith et al., 1999). These *in vitro* systems have proven to be invaluable models of normal corneal physiology and serve as excellent substitutes for animals in chemical and drug tests (Griffith et al., 1999). Despite these advances, little is known of the underlying molecular signals that direct early development and differentiation of corneal cells.

Gene expression analyses have shown that *Foxc1* (Kidson et al., 1999), *Pitx2* (Kitamura et al., 1999), *Lmx1b* (Pressman et al., 2000), *Six3* (Hsieh et al., 2002), EGFR (Reneker et al., 1995) and *Pdgfra* (Schatteman et al., 1992) are expressed in the periocular mesenchyme and a role for each of these genes in normal corneal differentiation has been suggested. However, modelling differentiation events and gene expression hierarchies in this small population of cells *in vivo* is

difficult. Furthermore current gene expression data has only shown a temporal continuation of *Foxc1* expression in *Lmx1b* null mutants (Pressman et al., 2000), with no gene expression differences between wildtype and *Foxc1*$^{-/-}$ mice for *Pitx2*, *Lmx1b*, *Pdgfa* or *Pdgfra* transcripts being reported (Kidson et al., 1999; Smith et al., 2000). Thus, characterising hierarchies of gene expression patterns within this population of cells remains an important avenue of research. Microarray experiments have identified candidate downstream gene targets of *Foxc1* by subtracting the transcriptomes of *Foxc1*$^{+/+}$ and *Foxc1*$^{-/-}$ mice using RNA derived from the whole head at E13.5 (Sommer et al., in preparation[i]). With a view to testing these microarray candidates as well as developing an *in vitro* model of the developing corneal endothelium, immortal cell lines from the periocular mesenchyme of E12.5 *Foxc1*$^{+/+}$, *Foxc1*$^{+/-}$ and *Foxc1*$^{-/-}$ mice were established.

In order for the cell lines to serve as a suitable tool to model and interpret the microarray data, it was essential to first demonstrate that the immortal *Foxc1*$^{+/+}$ cell lines maintained endogenous *Foxc1* expression. RT-PCR analyses confirmed the continued expression of the *Foxc1* gene and Western blot analysis confirmed its translation into Foxc1 protein. Null mutants for *Foxc1* were established and the coding region replaced with the β-galactosidase gene (Kume et al., 1998). Thus β-galactosidase expression and translation was mapped in cell lines derived from *Foxc1*$^{-/-}$ mice. Three of the five *Foxc1*$^{-/-}$ cell lines continued to express β-galactosidase. Maintenance of this expression in these cell lines suggests that regulatory factors of normal *Foxc1* expression are present and act independently of the Foxc1 protein. However, the lack of β-galactosidase expression in two of the five cell lines suggests that indirect autoregulatory controls may contribute in the maintenance of *Foxc1* expression. It is possible that the observed expression in the three cell lines reflects illegitimate transcripts.

Foxc1 and Foxc2 are very closely related (97 % homology in the winged helix domain (Kume et al., 1998)) forkhead proteins and show overlapping expression domains in many tissues (Hiemisch et al., 1998; Sasaki and Hogan, 1993). Within the developing anterior segment of the eye *Foxc1* and *Foxc2* have been shown to act cooperatively (Smith et al., 2000). Stable expression of Foxc2 in both the *Foxc1*$^{+/+}$ and *Foxc1*$^{-/-}$ cell lines supports previous findings (Winnier et al., 1999) suggesting that that *Foxc1* and *Foxc2* are expressed independently of one another. Furthermore it points to a potential role of Foxc2 in normal corneal differentiation.

One of the array candidates, *Tgfβ1i4*, showed a 1.5 fold upregulation in *Foxc1*$^{-/-}$ mice when compared with expression levels in *Foxc1*$^{+/+}$ mice (Sommer et al., in preparation[i]). These results were confirmed using northern blotting and quantitative (Q)PCR (Sommer et al., in preparation[i]). *In situ* hybridisation analyses performed in this study show that in the developing eye, the domains of *Tgfβ1i4* expression are similar in *Foxc1*$^{+/+}$ and *Foxc1*$^{-/-}$ eyes. However, the hybridisation signal was consistently stronger in *Foxc1*$^{-/-}$ tissues and appeared slightly expanded in the periocular mesenchyme. Conventional RT-PCR analyses demonstrated that both *Foxc1*$^{+/+}$ and *Foxc1*$^{-/-}$ cell lines express *Tgfβ1i4* as well as *TGFβ1*, which is known to induce or at least stabilise *Tgfβ1i4* transcripts. Furthermore, QPCR results have shown *Foxc1*$^{-/-}$ cell lines have 3 times as many *Tgfβ1i4* transcripts as *Foxc1*$^{+/+}$ cell lines (Sommer et al., in preparation[i]). Importantly, these results suggest that the immortal cell lines have retained the molecular characteristics of the tissues from which they were derived.

4.2.1 Formation of cell junctions

During embryonic development the assembly and disassembly of cell junctions underlies the ability of cells to form complex tissues. As neural crest cells delaminate from the neural tube, they lose their phenotype of a polarised epithelium and form a migrating population of mesenchyme cells. The ability of these cells to later reassemble and form complex three-dimensional tissues is crucial for normal development (reviewed in Hay, 2005; Pilot and Lecuit, 2005).

The assembly of adherens junctions is a complex multi-step process. Initially, cells competent to form junctions extend filopodia, seeking points of contact. In primary cultures of keratinocytes, dimers of E-cadherin receptors are preferentially located at filopodial tips (Vasioukhin et al., 2000). Junction formation is triggered when filopodia of adjacent cells extend and interdigitate into one another (Vasioukhin et al., 2000). This contact results in rapid homotypic binding of cadherin receptors on adjacent cells (Lambert et al., 2002) and after a few hours ladder-like adhesion zippers form along adjacent cell borders (Vasioukhin et al., 2000). Formation of these adhesion zippers requires shuttling of vesicular stores of cadherin receptors to the focal contact points (Mary et al., 2002). Appropriate translocation of cadherin receptors to the cell membrane in response to cell contact requires the microtubule-associated motor kinesin as well as an intact F-actin cytoskeleton (Mary et al., 2002). Maturation and stabilisation of adherens junctions occurs through the recruitment and assembly of other junction-associated proteins such as vinculin, zyxin, VASP, and

Mena (Vasioukhin et al., 2000). While, these rearrangements occur, the intermediary adhesion zippers are stabilised by desmosomes, which form in-between the filopodia (Vasioukhin et al., 2000). Culture of α-catenin null keratinocytes alone or in combination with wildtype keratinocytes has shown that α-catenin is not necessary for the initial binding and contact between cadherin receptors; however, it is essential for the recruitment of junction associated proteins and for reorganisation of the actin cytoskeleton at points of cell contact (Vasioukhin et al., 2000).

Rho, Rac and Cdc42 are all members of the RHO family of small guanosine triphosphatases (GTPases) that are involved in many different cellular processes, including cytoskeletal remodelling (reviewed in Braga, 2000; Yap and Kovacs 2003). Rho and Rac play crucial roles in stabilising and maintaining cell junctions by assembling actin at points of cell contact (Braga et al., 1999; Lambert et al., 2002) and trafficking cadherin containing vesicles to the cell membrane (Akhtar and Hotchin, 2001). Importantly in the context of junction assembly, the initial homotypic binding of cadherin receptors occurs independently of RHO family members. Actin remodelling mediated by Rac1 is a secondary event and is necessary to anchor cadherin receptors to the cytoskeleton (Lambert et al., 2002). Independent activation of Rac or Rho is insufficient for junction assembly (Braga et al., 1999).

In the developing mouse eye a wave of neural crest derived periocular mesenchyme cells invades the anterior portion of the eyecup from E11.5 – E12.5 (Kidson et al., 1999). These cells rapidly acquire positional information, presumably from lens and ectoderm derived signals. Cells most closely apposed to the lens start to flatten, form cell-cell contacts and by E13.5 the first cell junctions, as marked by N-cadherin and ZO-1 expression, start to form (Mgwebi, PhD thesis, 2004). Prior to and during junction formation, intracellular pools of cytoplasmic N-cadherin are evident. The presence of these cytoplasmic stores is well characterised and potentiates rapid junction assembly in response to cell contact (Mary et al., 2002). Although Rac1 and Rho are known to play an essential role in shuttling these vesicles to focal points of contact (Braga et al., 1999; Lambert et al., 2002), the molecular triggers remain unclear. Furthermore the precise details of how cadherin receptors in these trafficking vesicles are released and distributed at points of contact are unknown.

Interestingly N-cadherin expression in cells of the presumptive cornea, in *Foxc1*$^{-/-}$ mice, is punctate and remains restricted to intracellular vesicles (at all stages examined from E12.5 – P0; Mgwebi, PhD thesis, 2004). It thus appears that these cells are unable to either perceive points of contact with

adjacent cells or are unable to traffic N-cadherin stores to the membrane. Further observations indicate that the N-cadherin containing vesicles are often distributed around the cell periphery. This suggests that Foxc1 may indirectly play a role in the successful unpacking of cadherin receptors from these vesicles during normal junction assembly.

Thus, with a view to improving the current understanding of cell junction formation and better characterise the role that Foxc1 plays in this process, a preliminary study of cell junction formation in *Foxc1*$^{+/+}$ and *Foxc1*$^{-/-}$ immortal cell lines was performed. In culture all wildtype (*Foxc1*$^{+/+}$) cells formed adherens junctions. Interestingly the observed junctions formed in a ladder-like manner, very similar to the intermediary adhesion zipper described by Vasioukhin et al. (2000). It is therefore possible that, in culture, wildtype cells do not form a complete belt of adherens junctions. In accordance with *in vivo* observations, cultured *Foxc1*$^{-/-}$ cells never formed adherens junctions. Nevertheless, low levels of N-cadherin expression were detected perinucularly and in some cases more extensive immunostaining was detected within the cytoplasm. Recent studies have shown that the density of N-cadherin encountered at points of cell contact correlates directly with the efficiency with which cadherin receptors are anchored to the cytoskeleton (Lambert et al., 2002). Thus the lack of junction assembly in *Foxc1*$^{-/-}$ cells may occur because of insufficient N-cadherin expression in the cell membranes. Assessing junction formation in *Foxc1*$^{-/-}$ cells overexpressing N-cadherin would help in determining whether these cells lack an ability to perceive points of cell contact or just produce insufficient levels N-cadherin to form junctions.

In *Foxc1*$^{-/-}$ cells it is possible that primary cell contacts occur, but are transitory and preclude the formation of permanent adherens junctions. In order to test this directly, co-cultures of *Foxc1*$^{+/+}$ and *Foxc1*$^{-/-}$ cells were established. It was hypothesised that wildtype cells would serve as an abundant source of N-cadherin, and may form more stable primary contacts with mutant cells, so facilitating adherens junction assembly. Irrespective of wildtype to mutant cell ratios, neighbouring *Foxc1*$^{+/+}$ and *Foxc1*$^{-/-}$ cells never formed junctions. Mutant cells surrounded by wildtype cells often demonstrated strong peripheral localisation of N-cadherin containing vesicles. This suggests that these cells might perceive points of cell contact and respond by shuttling vesicular stores of N-cadherin to the cell surface, but fail to assemble and localise N-cadherin at these points of contact.

Furthermore, in culture *Foxc1*$^{-/-}$ cells avoid contact, forming long bipolar cells as opposed to the rounder, densely packed cells observed in *Foxc1*$^{+/+}$ cultures. In order to further test whether *Foxc1*$^{-/-}$

cells fail to traffic N-cadherin to the membrane despite stable cell contact, hanging drop cultures were established. These cultures provided a stable three-dimensional culture system and forced cell aggregation. Although *Foxc1*$^{+/+}$ cells readily formed adherens junctions in this culture system, *Foxc1*$^{-/-}$ cells failed to form junctions.

These results indicate that *Foxc1* expression in the presumptive corneal mesenchyme plays a pivotal role in determining their ability to form adherens junctions. Of great interest is determining the downstream gene targets of this transcription factor, which mediate this process. For example, *Msx1* is expressed in the periocular mesenchyme from E9.5 – E11.5 and is downregulated at E12.5, precisely when adherens junctions start to form (Monaghan et al., 1991). This downregulation is probably pivotal in junction assembly, since it has been shown that expression of *Msx1* or *Msx2 in vitro* decreases cadherin-mediated cell adhesion (Lincecum et al., 1998). Furthermore, Foxc1 is thought to regulate *Msx2* expression in calvarial mesenchyme (Rice et al., 2003). It is thus possible that adherens junctions fail to form in the corneal mesenchyme of *Foxc1*$^{-/-}$ mice, through inappropriate regulation of *Msx1*. In order to explore this hypothesis, gene expression analyses of *Msx1* in *Foxc1*$^{-/-}$ mice from E11.5 – E14.5 could be performed. Additionally the expression profile of *Msx1* in *Foxc1*$^{+/+}$ and *Foxc1*$^{-/-}$ cell lines could be compared.

Gene expression analyses in the developing hair have shown that endogenous *Foxn1* expression in the cuticle and cortex (Lee et al., 1999) positively regulates Dsc2 (a desmosome associated cadherin protein) expression in adjacent medulla cells (Johns et al., 2005; Schlake and Boehm, 2001). These findings suggest that Foxn1 regulates the expression of a secreted regulatory factor. Interestingly conditioned medium harvested from *Foxc1*$^{+/+}$ cells has been shown to negatively regulate *Tgfβ1i4* expression in *Foxc1*$^{-/-}$ cells (Sommer et al., in preparation[i]). This suggests that corneal mesenchyme cells produce secreted factors, which specifically direct their differentiation. This autoregulation is likely to play a crucial role in specifying corneal cell fates, by determining which lens derived signals are perceived. For example, *in vivo*, lens derived signals are known to induce *Tgfβ1i4* expression in the ciliary zone (Thut et al., 2001), but the differentiating corneal stroma and endothelium do not express *Tgfβ1i4*, despite their proximity to the lens.

The co-culture experiments with mixed *Foxc1*$^{+/+}$ and *Foxc1*$^{-/-}$ cells suggest that N-cadherin expression in periocular mesenchyme cells is not regulated by signals derived from the cells themselves. Irrespective the predominance (for example, in cultures with 3 wildtype : 1 mutant cell)

and proximity to wildtype cells and their secreted factors, no change in cadherin immunoreactivity or junction assembly was observed. This supports the long-standing theory suggesting that additional, independent signals contribute to normal corneal differentiation. Numerous experiments in the developing chick have shown that lens-derived signals are essential for normal corneal differentiation (Coulombre and Coulombre, 1964; Genis-Galvez, 1966; Genis-Galvez et al., 1967) and are necessary for the establishment of N-cadherin based adherens junctions in the corneal endothelium (Beebe and Coats, 2001). It is thus likely that *Foxc1* expression in migrating periocular mesenchyme cells may serve as a necessary competence factor for these cells to perceive and interpret signals derived from the lens and or corneal epithelia. However, this role is restricted to early specification of the cornea, since *Foxc1* expression is downregulated at E13.0 (Kidson et al., 1999). Following this corneal differentiation proceeds independently of Foxc1.

Foxc1$^{+/+}$ immortal cells continue to express *Foxc1* and demonstrate the potential to form adherens junctions in the absence of lens-derived signals. Since *Foxc1*$^{-/-}$ cells do not display this potential, it seems that Foxc1 is essential for the initial establishment of cell junctions in the corneal endothelium. During embryonic development tight junctions start to form in the corneal endothelium at E13.5 just as adherens junctions are forming. Thus the ability of *Foxc1*$^{+/+}$ immortal cells to form tight junctions in culture was assessed to address two questions: Firstly, whether tight junctions could form in cultured *Foxc1*$^{+/+}$ immortal cells despite the continued expression of *Foxc1* and secondly to determine if tight junctions could form independently of lens derived signals.

The establishment of tight junctions has been well characterised in epithelial tissues. Appropriate localisation of E-cadherin to the cell membrane is essential in establishing cell polarity and also serves as a primary site of association for ZO-1 (Itoh et al., 1993; Tunggal et al., 2005). The association of ZO-1 with these points of contact is stable and has even been associated with adherens junctions in non-epithelial tissues (Itoh et al., 1999). In polarised epithelia, tight junction assembly requires a loss of association between ZO-1 and E-cadherin proteins, with ZO-1 transferring its association to occludin proteins (Ando-Akatsuka et al., 1999; Itoh et al., 1993). Importantly the signals directing this shift in association are poorly characterised. Furthermore, it has been shown that ZO-1 is not an essential element for tight junction assembly, with related proteins such as ZO-2 able to compensate for a loss of ZO-1 (Umeda et al., 2004).

In culture, neither *Foxc1*$^{+/+}$ nor *Foxc1*$^{-/-}$ immortal cells formed tight junctions, as marked by the expression of ZO-1. The lack of ZO-1 expression in *Foxc1*$^{+/+}$ cells is surprising since normal N-cadherin based adherens junctions are present and form an appropriate scaffold for tight junction assembly. However, during normal embryonic development, tight junctions only form in the corneal endothelium at E13.5, immediately after *Foxc1* expression is downregulated in these cells (Kidson et al., 1999). It is thus possible that the maintenance of *Foxc1* expression in the immortal cell lines prevents further differentiation such as the formation of tight junctions.

This hypothesis could be tested *in vitro* using RNA interference experiments, knocking down Foxc1 expression in cultured wildtype cells and mapping tight junction formation. As part of this experiment, the potential role that lens derived signals play in corneal differentiation such as their role in regulating Foxc1 expression could be tested.

In summary, *Foxc1* expression in the migrating periocular mesenchyme from E11.5 – E12.5 (Figure 4-2A, B; blue cells) is essential for early specification of corneal cell fates. Its expression has been shown to negatively regulate expression of *Tgfβ1i4* (Sommer et al., in preparation[i]), which is normally induced by lens-derived signals in the ciliary zone (Thut et al., 2001). Furthermore, evidence from *in vitro* culture experiments and comparative studies *in vivo* between *Foxc1*$^{+/+}$ and *Foxc1*$^{-/-}$ mice have shown that *Foxc1* is a necessary factor in establishing adherens junctions in the presumptive corneal endothelium. This effect is possibly mediated by the downregulation of Msx1. Subsequent formation of tight junctions in the corneal endothelium correlates temporally with the downregulation of *Foxc1* expression in these cells (Figure 4-2C; grey cells). The lack of tight junction assembly in wildtype immortal cells is possibly explained by the continued expression of *Foxc1* and/or a lack of lens derived signals (Figure 4-2C; red arrows).

The close correlation between *in vivo* differentiation events and those observed in the immortal cell lines supports the use of this system as a model for early corneal differentiation. In particular the immortal cell lines have proved to be a useful and original system in characterising junction assembly. Comparative gene expression analyses between *Foxc1*$^{+/+}$ and *Foxc1*$^{-/-}$ cells should prove invaluable in characterising gene networks and determining hierarchies of regulation.

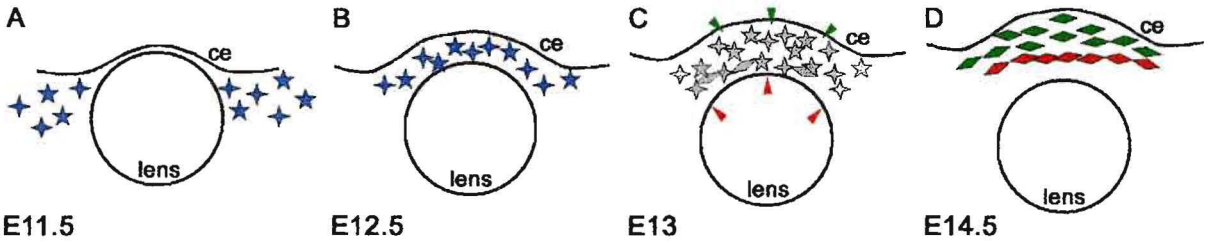

Figure 4-2: Relationship between *Foxc1* expression and corneal differentiation

As periocular cell migrate between the lens and corneal epithelium (ce) from E11.5 – E12.5, they express *Foxc1* (A and B, blue cells). Between E12.5 and E13.5, Foxc1 expression is downregulated (C, grey cells) and cells closest to the lens start to form adherens junctions. It is likely that lens-derived signals (red arrows) direct tight junction assembly in the forming corneal endothelium. Differentiation of the corneal stroma is probably influenced by corneal epithelial signals (green arrows). By E14.5 (D) the corneal endothelium has differentiated such that the anterior chamber forms.

[i] Sommer P., Napier HRL., Hogan BLM. and Kidson SH. 2005. Identification of *Tgfβ1i4* as a downstream target of *Foxc1*. In preparation.

Appendix

Table A-1: Genotyping primer sequences and PCR reaction mixes

	Primer sequence	Master mix (25 µl)	Cycling conditions
Bmp4: lacZ	**F:** 5' acccaacttaatcgccttgc 3' **R:** 5' aacaaacggcggattgacc 3'	1 µl DNA 2.5 µl 10x NH_4 buffer (Bioline) 1.25 µl $MgCl_2$ (50 mM stock, Bioline) 0.5 µl lacZ F primer (20 µM stock) 0.5 µl lacZ R primer (20 µM stock) 2 µl dNTPs (5mM stocks) 16.95 µl dH_2O 0.3 µl Bioline Taq	94 °C: 5 min **30 cycles:** 94 °C: 30 s 55 °C: 45 s 72 °C: 55 s 72 °C: 7 min 4 °C: Hold
Bmp4: flanking	**F:** 5' agaagccacgctgagatcat 3' **R:** 5' gttttcccagtcacgacgtt 3'	1 µl DNA 2.5 µl 10x NH_4 buffer (Bioline) 1 µl $MgCl_2$ (50 mM stock, Bioline) 0.5 µl Bmp4 F primer (20 µM stock) 0.5 µl Bmp4 R primer (20 µM stock) 2 µl dNTPs (5mM stocks) 17.2 µl dH_2O 0.3 µl Bioline Taq	94 °C: 5 min **30 cycles:** 94 °C: 30 s 58 °C: 60 s 72 °C: 60 s 72 °C: 5 min 4 °C: Hold
Foxc1	**F:** 5' gccctacagctacatcgctcttatc 3' **R:** 5' ccctgcttattgtcccgatagaa 3' **R_m:** 5' accgtgcatctgccagtttgag 3'	2 µl DNA 2.5 µl 10x KCl buffer (with 15mM $MgCl_2$) (Bioline) 0.5 µl Foxc1 F primer (25 µM stock) 0.5 µl Foxc1 R primer (25 µM stock) 0.5 µl Foxc1 R_m primer (25 µM stock) 1 µl dNTPs (5mM stocks) 17.7 µl dH_2O 0.3 µl Bioline Taq	94 °C: 90 s **35 cycles:** 94 °C: 30 s 62 °C: 30 s 72 °C: 90 s 72 °C: 10 min 4 °C: Hold

Table A-2: Xgal staining solution

Xgal staining solution
5 mM $K_4Fe(CN)_6 \cdot 3H_2O$
5 mM $K_3Fe(CN)_6$
2 mM $MgCl_2$
0.01% Sodium deoxycholate
0.02% Nonidet P-40
1 mg/ml Xgal
20 mM Tris·HCl (pH 7.3)
Make up in 1 x PBS

Table A-3: *In situ* hybridisation solutions

***In situ* hybridisation solutions**		
Hybridisation Buffer	**MABT**	**NTMT**
50% deionised formamide 1 x Denhardt's solution (Invitrogen) 10% dextran sulphate 1 µg/ml yeast tRNA (Invitrogen) 200 mM NaCl 8.9 mM Tris·HCl 1.1 mM Tris base 5 mM $NaH_2PO_4 \cdot H_2O$ 1 mM Na_2HPO_4 5 mM EDTA	0.1 M Maleic acid disodium (Sigma) 150 mM NaCl 0.1% Tween-20	5 mM NaCl 1 M Tris (pH 9.5) 1 M $MgCl_2$ 0.1% Tween-20

Table A-4: Western blot solutions

Western blot solutions		
Complete extraction buffer	**Sample buffer (5x)**	**TBS-T**
0.1 M Tris·HCl (pH 7.2) 0.01% Nonidet P-40 0.01% SDS 1 µg/ml Aprotinin 0.1 mM PMSF (phenyl methyl sulfonic fluoride)	4% SDS 20% glycerol 10% β-mercaptoethanol 0.125 M Tris·HCl (pH 76.8)	0.1 M Tris·HCl (pH 7.4) 0.15 M NaCl 0.01% Tween-20

Table A-5: RT-PCR primer sequences and PCR reaction mixes

	Primer sequence	Master mix	Cycling conditions
RiboS12	**F:** 5'ggaaggcatagctgctggaggtgt 3' **R:** 5' ctcaggccaaggatgtcatcg 3'	1 µl cDNA 1 µl 10x NH_4 buffer (Bioline) 0.3 µl $MgCl_2$ (50 mM stock, Bioline) 1 µl RiboS12 F primer (20 µM stock) 1 µl RiboS12 R primer (20 µM stock) 0.4 µl dNTPs (5mM stocks) 5.2 µl dH_2O 0.1 µl Bioline Taq	94°C: 90s **30 cycles:** 94°C: 30 s 60°C: 30 s 72°C: 90 s 72°C: 10 min 4°C: Hold
TGFβ1	**F:** 5' cctgtccaaactaaggc 3' **R:** 5' cacgtagtagacgatggg 3'	1 µl cDNA 2.5 µl 10x NH_4 buffer (Bioline) 0.75 µl $MgCl_2$ (50 mM stock, Bioline) 1 µl TGFβ1 F primer (20 µM stock) 1 µl TGFβ1 R primer (20 µM stock) 1 µl dNTPs (5mM stocks) 18.45 µl dH_2O 0.3 µl Bioline Taq	94°C: 90s **30 cycles:** 94°C: 30 s 59°C: 30 s 72°C: 90 s 72°C: 10 min 4°C: Hold
Tgfβ1i4	**F:** 5' gtagaccagtggcgatggat 3' **R:** 5' tccagctgggagtttttctc 3'	1 µl cDNA 2.5 µl 10x NH_4 buffer (Bioline) 1.6 µl $MgCl_2$ (50 mM stock, Bioline) 0.5 µl Tgfβ1i4 F primer (20 µM stock) 0.5 µl Tgfβ1i4 R primer (20 µM stock) 2 µl dNTPs (5mM stocks) 18.6 µl dH_2O 0.3 µl Bioline Taq	94°C: 90s **30 cycles:** 94°C: 30 s 60°C: 30 s 72°C: 90 s 72°C: 10 min 4°C: Hold
Foxc1 and β-galactosidase	**F:** 5' gccctacagctacatcgctcttatc 3' **R:** 5' ccctgcttattgtcccgatagaa 3' **R_m:** 5'accgtgcatctgccagtttgag 3'	1 µl cDNA 2.5 µl 10x KCl buffer (with 15mM $MgCl_2$) (Bioline) 0.5 µl Foxc1 F primer (25 µM stock) 0.5 µl Foxc1 R primer (25 µM stock) 0.5 µl Foxc1 R_m primer (25 µM stock) 1 µl dNTPs (5mM stocks) 18.7 µl dH_2O 0.3 µl Bioline Taq	94 °C: 90 s **35 cycles:** 94 °C: 30 s 62 °C: 30 s 72 °C: 90 s 72 °C: 10 min 4 °C: Hold

References

Aboalchamat B., Engelmann K., Bohnke M., Eggli P. and Bednarz J. 1999. Morphological and functional analysis of immortalized human corneal endothelial cells after transplantation. Exp. Eye Res. 69:547-553.

Acampora D., Mazan S., Avantaggiato V., Barone P., Tuorto F., Lallemand Y., Brulet P. and Simeone A. 1996. Epilepsy and brain abnormalities in mice lacking the Otx1 gene. Nat. Genet. 14:218-222.

Akhtar N. and Hotchin NA. 2001. RAC1 regulates adherens junctions through endocytosis of E-cadherin. Mol. Biol. Cell. 12:847–862.

Alberts B., Bray D., Lewis J., Raff M., Roberts K. and Watson JD. 1994. Molecular biology of the cell. Third Edition. New York: Garland Publishing.

Adler R. and Belecky-Adams TL. 2002. The role of bone morphogenetic proteins in the differentiation of the ventral optic cup. Development 129:3161-3171.

Ali SH. and DeCaprio JA. 2001. Cellular transformation by SV40 large T antigen: interaction with host proteins. Seminars in Cancer Biology 11:15-22.

Anderson MG., Smith RS., Savinova OV., Hawes NL., Chang B., Zabaleta A., Wilpan R., Heckenlively JR., Davisson M. and John SWM. 2001. Genetic modification of glaucoma associated phenotypes between AKXD-28/Ty and DBA/2J mice. BMC Genetics 2:1.

Ando-Akatsuka Y., Yonemura S., Itoh M., Furuse M, Tsukita S. 1999. Differential behavior of E-cadherin and occludin in their colocalization with ZO-1 during the establishment of epithelial cell polarity. J. Cell. Physiol. 179:115-125.

Bach A., Lallemand Y., Nicola M., Ramos C., Mathis L., Maufras M. and Robert B. 2003. *Msx1* is required for dorsal diencephalons patterning. Development 130:4025-4036.

Balda MS. and Matter K. 2000. Transmembrane proteins of tight junctions. Seminars in Cell and Developmental Biology 11:281-289.

Balemans W. and Van Hul W. 2002. Extracellular regulation of BMP signaling in vertebrates: A cocktail of modulators. Dev. Biol. 250:231-250.

Bao Z. and Cepko CL. 1997. The expression and function of notch pathway genes in the developing rat eye. J. Neurosci. 17:1425–1434.

Bard JB. and Abbott AS. 1979. Matrices containing glycosaminoglycans in the developing anterior chambers of chick and Xenopus embryonic eyes. Dev. Biol. 68:472-86.

Bard JBL. and Ross ASA. 1982a. The morphogenesis of the ciliary body of the avian eye I. Lateral cell detachment facilitates epithelial folding. Dev. Biol. 92:73-86.

Bard JBL. and Ross ASA. 1982b. The morphogenesis of the ciliary body of the avian eye II. Differential enlargement causes an epithelium to form radial folds. Dev. Biol. 92:87-96.

Barrio-Asensio C., Murillo-Gonzalez J., Pena-Meliann A. and Puerta-Fonolla J. 1999. Immunocytochemical study on the triple origin of the sphincter iris in the chick embryo. Dev. Genes. Evol. 209:620-624.

Barrio-Asensio C., Pena-Melian A., Puerta-Fonolla J., Vazquez-Osorio T. and Murillo-Gonzalez J. 2002. Ciliary muscle in avian is derived from mesenchymal and epithelial cells. Vision Res. 42:1695-1699.

Baulmann DC., Ohlmann A., Flügel-Koch C., Goswami S., Cvekl A. and Tamm ER. 2002. Pax6 heterozygous eyes show defects in chamber angle differentiation that are associated with a wide spectrum of other anterior eye segment abnormalities. Mech. Dev. 118:3–17.

Beebe DC., Latker CH., Jebens HAH., Johnson MC., Feagans DE. and Feinberg RN. 1986. Transport and steady-state concentration of plasma proteins in the vitreous humor of the chicken embryo: Implications for the mechanism of eye growth during early development. Dev. Biol. 114:361-368.

Beebe DC. 1986. Development of the ciliary body: A brief review. Trans. Opthalmol. Soc. U.K. 105:123-130.

Beebe DC. and Coats JM. 2000. The lens organises the anterior segment: Specification of neural crest cell differentiation in the avian eye. Dev. Biol. 220:424-431.

Bejjani BA., Xu L., Armstrong D., Lupski JR. and Reneker LW. 2002. Expression patterns of cytochrome P4501B1 (*Cyp1b1*) in FVB/N mouse eyes. Exp. Eye Res. 75:249-257.

Belecky-Adams TL. and Adler R. 2001. Developmental expression patterns of bone morphogenic proteins, receptors, and binding proteins in the chick retina. J. Comp. Neurol. 430:562-572

Belecky-Adams TL., Adler R. and Beebe DC. 2002. Bone morphogenetic protein signaling and the initiation of lens fiber cell differentiation. Development 129:3795-3802.

Bishop PN., Takanosu M., le Goff M. and Mayne R. 2002. The role of the posterior ciliary body in the biosynthesis of vitreous humour. Eye 16:454-460.

Braga VMM., Maschio AD., Machesky L. and Dejana E. 1999. Regulation of cadherin function by Rho and Rac: Modulation by junction maturation and cellular context. Mol. Biol. Cell. 10:9-22.

Braga V. 2000. Epithelial cell shape: Cadherins and small GTPases. Exp. Cell Res. 83-90.

Braga VMM. 2002. Cell-cell adhesion and signalling. Current Opinion in Cell Biology 14:546-556.

Braissant O. and Wahli W. 1998. A simplified *in situ* hybridization protocol using non-radioactively labeled probes to detect abundant and rare mRNAs on tissue sections. Biochemica 1:10–16.

Brown LF., Detmar M., Claffey K., Nagy JA., Feng D., Dvorak AM. and Dvorak HF. 1997. Vascular permeability factor/vascular endothelial growth factor: a multifunctional angiogenic cytokine. EXS. 79:233-269.

Carl M., Loosli F. and Wittbrodt J. 2002. *Six3* inactivation reveals its essential role for the formation and patterning of the vertebrate eye. Development 129:4057-4063.

Carlsson P. and Mahlapuu M. 2002. Forkhead transcription factors: Key players in development and metabolism. Dev. Biol. 250:1-23.

Chaloin-Dufau C., Pavitt I., Delorme P. and Dhouailly D. 1993. Identification of keratins 3 and 12 in corneal epithelium of vertebrates. Epithelial Cell Biol. 2:120-125.

Chang B., Smith RS., Hawes NL., Anderson MG., Zabaleta A., Savinova O., Roderick TH., Heckenlively JR., Davisson MT. and John SWM: Interacting loci cause severe iris atrophy and glaucoma in DBA/2J mice. Nat. Genet. 21:405-409.

Chang B., Smith RS., Peters M., Savinova OV., Hawes NL., Zabaleta A., Nusinowitz S., Martin JE., Davisson ML., Cepko CL., Hogan BL., John SW. 2001. Haploinsufficient Bmp4 ocular phenotypes include anterior segment dysgenesis with elevated intraocular pressure. BMC Genet 2:18.

Chappuis-Flament S., Wong E., Hicks LD., Kay CM. and Gumbiner BM. 2001. Multiple cadherin extracellular repeats mediate homophilic binding and adhesion. The Journal of Cell Biology 154:231-243.

Chow RL. and Lang RA. 2001. Early eye development in vertebrates. Annu. Rev. Cell Dev. Biol. 17:255-296.

Clark KL., Halay ED., Lai E. and Burley SK. 1993. Cocrystal structure of the HNF-3/fork head DNA-recognition motif resembles histone H5. Nature 364:412-420.

Coca-Prados M., Escribano J. and Ortego J. 1999. Differential gene expression in the human ciliary epithelium. Progress in Retinal and Eye Research 18:403-429.

Collinson JM., Hill RE. and West JD. 2000. Different roles for *Pax6* in the optic vesicle and facial epithelium mediate early morphogenesis of the murine eye. Development 127:945–956.

Collinson J.M., Quinn J.C., Buchanan M.A., Kaufman M.H., Wedden S.E., West J.D. and Hill R.E. 2001. Primary defects in the lens underlie complex anterior segment abnormalities of the Pax6 heterozygous eye. Proc. Natl. Acad. Sci. USA 98:9688–9693.

Collinson JM., Quinn JC., Hill RE. and West JD. 2003. The roles of *Pax6* in the cornea, retina, and olfactory epithelium of the developing mouse embryo. Dev. Biol. 255:303-312.

Coulombre AJ. and Coulombre JL. 1957. The role of intraocular pressure in the development of the chick eye: III. Ciliary body. Am. J. Ophthalmol. 44:85-93.

Coulombre AJ. and Coulombre JL. 1964. Development. Role of the lens in eye growth. J. Exp. Zool. 156:39-48.

Davson H. 1990. Davson's physiology of the eye. Fifth Edition. London: Macmillan Press Ltd.

Davis-Silberman N., Kalich T., Oron-Karni V., Marquardt T., Kroeber M., Tamm ER. and Ashery-Padan R. 2005. Genetic dissection of Pax6 dosage requirements in the developing mouse eye. Hum. Mol. Genet. 14:2265-2276.

De Baere E., Van Roy N., Speleman F., Fukushima Y., De Paepe A. and Messiaen L. 1999. Closing in on the BPES gene on 3q23: mapping of a de Novo reciprocal translocation t(3;4)(q23;p15.2) breakpoint within a 45-kb cosmid and mapping of three candidate genes, RBP1, RBP2, and beta'-COP, distal to the breakpoint. Genomics. 57:70-78.

Dhawan RR. and Beebe DC. 1994. Differential localisation of collagen type IX isoform messenger RNAs during early ocular development. Invest. Ophthalmol. Vis. Sci. 35:470-478.

Dohrmann CE., Belaoussoff M. and Raftery LA. 1999. Dynamic expression of TSC-22 at sites of epithelial-mesenchymal interactions during mouse development. Mech. Dev. 84:147-151.

Dohrmann CE., Normaly S., Raftery LA. and Morgan BA. 2002. Opposing effects on TSC-22 expression by BMP and receptor tyrosine kinase signals in the developing feather tract. Dev. Dyn. 223:85-95.

Dünker N. and Krieglstein K. 2000. Targeted mutations of transforming growth factor-β genes reveal important roles in mouse development and homeostasis. Eur. J. Biochem. 267:6982-6988.

Faber SC., Roninson ML., Makarenkova HP. and Lang RP. 2002. Bmp signaling is required for development of primary lens fiber cells. Development 129:3727-3737.

Fang J., Dagenais SL., Erickson RP., Arlt MF., Glynn MW., Gorski JL., Seaver LH. and Glover TW. 2000. Mutations in FOXC2 (MFH-1), a forkhead family transcription factor, are responsible for the hereditary lymphedema–distichiasis syndrome. Am. J. Hum. Genet. 67:1382–1388.

Foerst-Potts L. and Sadler TW. 1997. Disruption of *Msx-1* and *Msx-2* reveals roles for these genes in craniofacial, eye, and axial development. Dev. Dyn. 209:70-84.

Fujiwara T., Dunn NR. and Hogan BLM. 2001. Bone morphogenetic protein 4 in the extraembryonic mesoderm is required for allantois development and the localization and survival of primordial germ cells in the mouse. PNAS 98:13739-13744.

Furuta Y. and Hogan BLM. 1998. BMP4 is essential for lens induction in the mouse embryo. Genes Dev. 12:3764-3775.

Gage PJ., Suh H. and Camper SA. 1999. Dosage requirement of Pitx2 for development of multiple organs. Development 126:4643-4651.

Genis-Galvez JM. 1966. Role of the lens in the morphogenesis of the iris and cornea. Nature 210:209-210.

Genis-Galvez JM., Santos-Gutierrez L. and Rios-Gonzalez A. 1967. Causal factors in corneal development: An experimental analysis in the chick embryo. Exptl. Eye Res. 6:48-56.

Goodenough DA. 1999. Plugging the leaks. PNAS 96:319-321.

Gordon-Thomson C., de Iongh RU., Hales AM., Chamberlain CG. and McAvoy JW. 1998. Differential cataractogenic potency of TGF-β_1, -β_2, and β_3 and their expression in the postnatal rat eye. Invest. Ophthalmol. Vis. Sci. 39:1399-1409.

Gould DB. and John SWM. 2002. Anterior segment dysgenesis and the developmental glaucomas are complex traits. Hum. Mol. Genet. 11:1185-1193.

Gould DB., Smith RS. and John SW. 2004. Anterior segment development relevant to glaucoma. Int. J. Dev. Biol. 48:1015-1029.

Graw J. 1996. Genetic aspects of embryonic eye development in vertebrates. Developmental Genetics 18:181-197.

Griffith M., Osborne R., Munger R., Xiong X., Doillon CJ., Laycock NLC., Hakim M., Song Y. and Watsky MA. 1999. Functional human corneal equivalents constructed from cell lines. Science 286:2169-2172.

Grindley JC., Davidson DR. and Hill RE. 1995. The role of Pax-6 in eye and nasal development Development 121:1433-1442.

Gruneberg H. 1943. Congenital hydrocephalus in the mouse, a case of spurious pleiotropism. J. Genet. 45:1–21.

Haegel H., Larue L., Ohsugi M., Fedorov L., Herrenknecht K. and Kemler R. 1995. Lack of beta-catenin affects mouse development at gastrulation. Development 121:3529-37.

Hanna C., Bicknell D.S., O'Brien J. 1961. Cell turnover in the adult human eye. Arch. Ophthalmol. 65:695-698.

Hanssen E., Franc S. and Garrone R. 2001. Synthesis and structural organization of zonular fibers during development and aging. Matrix Biology 20:77-85.

Harrington L., Klintworth G.K., Secor T.E. and Breitman M.L. 1991. Developmental analysis of ocular morphogenesis in αA-Crystallin/Diptheria toxin transgenic mice undergoing ablation of the lens. Dev. Biol. 148:508-516.

Haustein, J. 1983. On the ultrastructure of the developing and adult mouse corneal stroma. Anat. Embryol. 168:291–305.

Hay ED. 1979. Development of the vertebrate cornea. Int. Rev. Cytol. 63:263–322.

Hay ED. 2005. The mesenchymal cell, its role in the embryo, and the remarkable signaling mechanisms that create it. Dev. Dyn. 233:706–720.

Hide T., Hatakeyama J., Kimura-Yoshida C., Tian E., Takeda N., Ushio Y., Shiroishi T., Aizawa S. and Matsuo I. 2002. Genetic modifiers of otocephalic phenotypes in Otx2 heterozygous mutant mice. Development 129:4347-4357.

Hiemisch, H., Monaghan AP., Schütz, G., and Kaestner, KH. 1998. Expression of the mouse Fkh1/Mf1 and Mfh1 genes in late gestation embryos is restricted to mesoderm derivatives. Mech. Dev. 73:129–132

Hill RE., Favor J., Hogan BL., Ton CC., Saunders GF., Hanson IM., Prosser J., Jordan T., Hastie ND. and van Heyningen V. 1991. Mouse small eye results from mutations in a paired-like homeobox-containing gene. Nature 354:522–525.

Hirsch M., Renard G., Faure JP., Pouliquen Y. 1977. Study of the ultrastructure of the rabbit corneal endothelium by the freezefracture technique: apical and lateral junctions. Exp. Eye Res. 25:277–288.

Hogan BLM. 1996. Bone morphogenetic proteins: multifunctional regulators of vertebrate development. Genes Dev. 10:1580-1594.

Holmberg A. 1959. Ultrastructure of the ciliary epithelium. Arch. Ophthalmol. 62:935-948.

Holmberg AKE. 1959b. The ultrastructure of the capillaries in the ciliary body. Arch. Ophthalmol. 62:949-951.

Hong H., Lass JH. and Chakravarti A. 1999. Pleiotropic skeletal and ocular phenotypes of the mouse mutation congenital hydrocephalus (*ch/Mf1*) arise from the winged helix/forkhead transcription factor gene. Hum. Mol. Genet. 8:625-637.

Honkanen RA., Nishimura DY., Swiderski RE., Bennett SR., Hong S., Kwon YH., Stone EM., Sheffield VC. and Alward WL. 2003. A family with Axenfeld-Rieger syndrome and Peters' Anomaly caused by a point mutation (Phe112Ser) in the FOXC1 gene. Am. J. Ophthalmol. 135:368-375.

Houzelstein D. Cohen A., Buckingham ME. and Robert B. 1997. Insertional mutation of the mouse Msx1 homeobox gene by an nlacZ reporter gene. Mech. Dev. 65:123-133.

Hsieh Y., Zhang X., Lin E., Oliver G. and Yang X. 2002. The homeobox gene Six3 is a potential regulator of anterior segment formation in the chick eye. Dev. Biol. 248:265–280.

Hussein SM., Duff EK. and Sirard C. 2003. Smad4 and β-Catenin Co-activators functionally interact with lymphoid-enhancing factor to regulate graded expression of Msx2. J Biol. Chem. 278:48805-48814.

Hyldahl L. 1985. Factor VIII expression in the human embryonic eye. Differences between endothelial cells of different origin. Ophthalmologica 191:184-187.

Ickes R., Harris D.L., Joyce N.C. 2002. "Classical" cadherin expression in corneal endothelium" [abstract]. 2002 Annual Meeting Abstract and Program Planner accessed at www.arvo.org. Association for Research in Vision and Ophthalmology, Abstract #3190.

Iida K., Koseki H., Kakinuma H., Kato N., Mizutani-Koseki Y., Ohuchi H., Yoshioka H., Noji S., Kawamura K., Kataoka Y., Ueno F., Taniguchi M., Yoshida N., Sugiyama T. and Miura N. 1997. Essential roles of the winged helix transcription factor MFH-1 in aortic patterning and skeletogenesis. Development 124:4627–4638.

Itoh M., Nagafuchi A., Yonemura S., Kitani-Yasuda T., Tsukita S. and Tsukita S. 1993. The 220-kD protein colocalizing with cadherins in non-epithelial cells is identical to ZO-1, a tight junction-associated protein in epithelial cells: cDNA cloning and immunoelectron microscopy. The Journal of Cell Biology 121:491-502.

Itoh M., Morita K. and Tsukita S. 1999. Characterization of ZO-2 as a MAGUK family member associated with tight as well as adherens junctions with a binding affinity to occludin and αCatenin. J Biol. Chem. 274:5981-5986.

Iwamoto T., Smelser G.K. 1965. Electron microscopy of the human corneal endothelium with reference to transport mechanisms. Invest. Ophthalmol. 4:270–279.

Jamora C. and Fuchs E. 2002. Intercellular adhesion, signalling and the cytoskeleton. Nature Cell Biology 4:101-108.

Johns SA., Soullier S., Rashbass P. and Cunliffe VT. 2005. Foxn1 is required for tissue assembly and desmosomal cadherin expression in the hair shaft. Dev. Dyn. 232:1062-1068.

Johnston MC, Noden DM, Hazelton RD, Coulombre JL, Coulombre AJ. 1979. Origins of avian ocular and periocular tissues. Exp. Eye Res. 29:27-43.

Joo C., Pepose JS. and Fleming TP. 1994. In vitro propogation of primary and extended life span murine corneal endothelial cells. Invest. Ophthalmol. Vis. Sci. 35:3952-3957.

Joyce NC., Navon SE., Roy S. and Zieske JD. 1996. Expression of cell cycle-associated proteins in human and rabbit endothelium in situ. Invest. Ophthalmol. Vis. Sci. 37:1566-1575.

Joyce NC. and Zieske JD. 1997. Transforming growth factor-β receptor expression in human cornea. Invest. Ophthalmol. Vis. Sci. 38:1922-1928.

Joyce NC., Harris DL. and Mello DM. 2002. Mechanisms of mitotic inhibition in corneal endothelium: Contact inhibition and TGF-β2. Invest. Ophthalmol. Vis. Sci. 43:2152-2159.

Joyce NC. 2003. Proliferative capacity of the corneal endothelium. Progress in Retinal and Eye Research 22:359-389.

Kaartinen V., Voncken JW., Shuler C., Warburton D., Bu D., Heisterkamp N. and Groffen, J. 1995. Abnormal lung development and cleft palate in mice lacking TGF-beta 3 indicates defects of epithelial-mesenchymal interaction. Nat. Genet. 11:415-421.

Kaufman PL. and Alm A. 2003. Adler's physiology of the eye. Clinical application. Tenth edition. Missouri, St. Louis: Mosby.

Kaufmann E. and Knöchel W. 1996. Five years on the wings of the fork head. Mech. Dev. 57:3-20.

Kessel RG. and Kardon RH. 1979. Tissues and Organs: A text-atlas of scanning electron microscopy. San Francisco: W.H. Freeman and company. p 98.

Kester HA., Ward-van Oostwaard THMJ., Goumans MJ. Van Rooijen MA., van der Saag PT., van der Burg B. and Mummery CL. 2000. Expression of TGF-β stimulated clone-22 (TSC-22) in mouse development and TGF-β signalling. Dev. Dyn. 218:563-572.

Key B., Liu L., Potter SS., Kaur S. and Akeson R. 1992. Lens structures exist transiently in development of transgenic mice carrying an alpha-crystallin-diphtheria toxin hybrid gene. Exp. Eye Res. 55:357-367.

Kidson SH., Kume T., Deng K., Winfrey V. and Hogan BLM. 1999. The forkhead/winged helix gene, Mfl, is necessary for the normal development of the cornea and formation of the anterior chamber in the mouse eye. Dev. Biol. 211:306-322.

Kitamura K., Miura H., Miyagawa-Tomita S., Yanazawa M., Katoh-Fukui Y., Suzuki R., Ohuchi H., Suehiro A., Motegi Y., Nakahara Y., Kondo S. and Yokoyama M. 1999. Mouse Pitx2 deficiency leads to anomalies of the ventral body wall, heart, extra- and periocular mesoderm and right pulmonary isomerism. Development 126:5749-5758.

Klein KL., Klintworth GK., Bernstein A. and Breitman ML. 1992. Embryology and morphology of microphthalmia in transgenic mice expressing a gamma F-crystallin/diphtheria toxin A hybrid gene. Lab Invest. 67:31-41.

Koroma B., Yang JM. and Sundin O. 1997. The Pax6 Homeobox gene is expressed throughout the corneal and conjunctival epithelial. Invest. Olphthamol. Vis. Sci. 38:108–120.

Kreutziger GO. 1976. Lateral membrane morphology and gap junction structure in rabbit corneal endothelium. Exp. Eye Res. 23:285–293.

Kubo F, Takeichi M, Nakagawa S. 2003. Wnt2b controls retinal cell differentiation at the ciliary marginal zone. Development 130:587-598.

Kubota R., McGuire C., Dierks B. and Reh TA. 2004. Identification of ciliary epithelial-specific genes using subtractive libraries and cDNA arrays in the avian eye. Dev. Dyn. 229:529-540.

Kulkarni AB., Huh C., Becker D., Geiser A., Lyght M., Flanders KC., Roberts AB., Sporn MB., Ward JM. and Karlsson S.1993. Transforming growth factor β1 null mutation in mice causes excessive inflamitory response and early death. PNAS 90:770-774.

Kume T., Deng K., Winfrey V., Gould DB., Walter MA. and Hogan BLM. 1998. The forkhead/winged helix gene *Mfl* is disrupted in the pleiotropic mouse mutation *congenital hydrocephalus*. Cell 93:985-996.

Kume T., Deng K. and Hogan BLM. 2000. Murine forkhead/winged helix genes Foxc1 (Mfl) and Foxc2 (Mfh1) are required for the early organogenesis of the kidney and urinary tract. Development 127:1387-1395.

Kume T., Jiang H., Topczewska JM. and Hogan BLM. 2001. The murine winged helix transcription factors, Foxc1 and Foxc2, are both required for cardiovascular development and somitogenesis. Genes Dev. 15:2470-2482.

Kurihara T., Kitamura K., Takaoka K. and Nakazato H. 1993. Murine bone morphogenetic protein-4 gene: existence of multiple promoters and exons for the 5'-untranslated region. Biochem Biophys Res Commun. 192:1049-1056.

Kurita R., Sagara H., Aoki Y., Link BA., Arai K. and Watanabe S. 2003. Suppression of lens growth by alphaA-crystallin promoter-driven expression of diphtheria toxin results in disruption of retinal cell organization in zebrafish. Dev. Biol. 255:113-27.

Laing R.A., Sandstrom M.A., Berrospi A.R. and Leibowitz H.M. 1976. Changes in the corneal endothelium as a function of age. Exp. Eye Res. 22:587-594.

Lambert M., Choquet D. and Mège R. 2002. Dynamics of ligand-induced, Rac1-dependent anchoring of cadherins to the actin cytoskeleton. Journal of Cell Biology 157:469-479.

Larue L., Ohsugi M., Hirchenhain J. and Kemler R. 1994. E-cadherin null mutant embryos fail to form a trophectoderm epithelium. PNAS 91:8263-8267.

Lawson KA., Dunn NR., Roelen BA., Zeinstra LM., Davis AM., Wright CV., Korving JP. and Hogan BL. 1999. Bmp4 is required for the generation of primordial germ cells in the mouse embryo. Genes Dev. 13:424-436.

Lee D., Prowse DM. and Brissette JL. 1999. Association between mouse nude gene expression and the initiation of epithelial terminal differentiation. Dev. Biol. 208:362–374.

Lehmann O.J., Ebenezer ND., Jordan T., Fox M., Ocaka L., Payne A., Leroy BP., Clark BJ., Hitchings RA., Povey S. Khaw PT. and Bhattacharya SS. 2000. Chromosomal duplication involving the forkhead transcription factor gene FOXC1 causes iris hypoplasia and glaucoma. Am. J. Hum. Genet. 67:1129-1135.

Lehmann OJ., Sowden JC., Carlsson P., Jordan T. and Bhattacharya SS. 2003. Fox's in development and disease. Trends in Genetics 19:339-344.

Leuenberger, PM. 1973. Lanthanum hydroxide tracer studies on rat corneal endothelium. Exp. Eye Res. 15:85–91.

Li DQ., Lee SB. and Tseng SC. 1999. Differential expression and regulation of TGF-beta1, TGF-beta2, TGF-beta3, TGF-betaRI, TGF-betaRII and TGF-betaRIII in cultured human corneal, limbal, and conjunctival fibroblasts. Curr. Eye Res. 19:154-61.

Libby RT., Smith RS., Savinova OV., Zabaleta A., Martin JE., Gonzales FJ. and John SWM. 2003. Modification of ocular defects in mouse developmental glaucoma models by tyrosinase. Science 299:1578-1581.

Lin CR., Kioussi C., O'Connell S., Briata P., Szeto D. Liu F., Izpisúa-Belmonte JC. and Rosenfeld MG. 1999. Pitx2 regulates lung asymmetry, cardiac positioning and pituitary and tooth morphogenesis. Nature 401:279-282.

Lincecum JM., Fannon A., Song K., Wang Y. and Sassoon DA. 1998. Msh homeobox genes regulate cadherin-mediated cell adhesion and cell-cell sorting. J Cell Biochem. 70:22-28.

Link BA. and Nishi R. 1998. Development of the avian iris and ciliary body: Mechanisms of cellular differentiation during the smooth-to-striated muscle transition. Dev. Biol. 203:163-176.

Linsenmayer TF., Fitch JM., Gordon MK., Cai C., Igoe F., Marchant JK. and Birk DE. 1998. Development and roles of collagenous matrices in the embryonic avian cornea. Progress in Retinal and Eye Research 17:231-265.

Lu MF., Pressman C., Dyer R., Johnson RL. and Martin JF. 1999. Function of Rieger syndrome gene in left–right asymmetry and craniofacial development. Nature 401:276–278.

Luetteke NC., Qiu TH., Peiffer RL., Oliver P., Smithies O. and Lee DC. 1993. TGF alpha deficiency results in hair follicle and eye abnormalities in targeted and waved-1 mice. Cell 73:263-278.

Luetteke NC., Phillips HK., Qiu TH., Copeland NG., Earp HS., Jenkins NA. and Lee DC. 1994. The mouse waved-2 phenotype results from a point mutation in the EGF receptor tyrosine kinase. Genes Dev. 8:399-413.

Macdonald R. and Wilson SW. 1996. Pax proteins and eye development Curr. Opin. Neurobiol. 6:49-56.

Mann GB, Fowler KJ, Gabriel A, Nice EC, Williams RL, Dunn AR. 1993. Mice with a null mutation of the TGF alpha gene have abnormal skin architecture, wavy hair, and curly whiskers and often develop corneal inflammation. Cell 73:249-261.

Martinez-Morales JR, Signore M, Acampora D, Simeone A and Bovolenta P. 2001. Otx genes are required for tissue specification in the developing eye. Development 128:2019-2030.

Mary S., Charrasse S., Meriane M., Comunale F., Travo P., Blangy A. and Gauthier-Rouvière C. 2002. Biogenesis of N-cadherin-dependent cell-cell contacts in living fibroblasts is a microtubule-dependent kinesin-driven mechanism. Mol. Biol. Cell. 13:285–301.

Masos T., Dan J. and Miskin R. 2000. Plasminogen activator inhibitor-1 mRNA is localised in the ciliary epithelium of the rodent eye. Invest. Ophthalmol. Vis. Sci. 41:1006-1011.

Masterson E., Edelhauser HF. and Van Horn DL. 1975. Development of corneal transparency in embryonic chick: influence of exogenous thyroxine and thiouracil on structure, water and electrolyte content. Dev. Biol. 43:233-239.

Matter K. and Balda MS. 2003. Signalling to and from tight junctions. Nat. Rev. Mol. Cell Biol. 4:225-236.

McAvoy JW. 1980. Cytoplasmic processes interconnect lens placode and optic vesicle during eye morphogenesis. Exp. Eye Res. 31:527-534.

McComb RD., Jones TR., Pizzo SV. and Bigner DD. 1982. Specificity and sensitivity of immunohistochemical detection of factor VIII/von Willebrand factor antigen in formalin-fixed paraffin-embedded tissue. J. Histochem. Cytochem. 30:371-377.

McLaughlin BJ., Caldwell RB., Sasaki Y. and Wood TO. 1985. Freeze-fracture quantitative comparison of rabbit corneal epithelial and endothelial membranes. Curr. Eye Res. 4:951-961

Mears AJ., Jordan T, Mirzayans F., Dubois S., Kume T., Parlee M., Ritch R., Koop B., Kuo WL., Collins C., Marshal J., Gould DB., Pearce W., Carlsson P., Enerback S., Morissettte J., Bhattacharya S., Hogan B., Raymond V. and Walter M.A. 1998. Mutations of the forkhead/winged helix gene, FKHL7, in patients with Axenfeld-Rieger anomaly. Am. J. Hum. Genet. 63:1316-1328.

Mgwebi T. 2004. Morphological investigations into the development of the mammalian corneal endothelium using the mouse model. PhD thesis, University of Cape Town.

Mirzayans F., Gould DB., Heon E., Billingsley GD., Cheung JC., Mears AJ. and Walter MA. 2000. Axenfeld-Rieger syndrome resulting from mutations of the FKHL7 gene on chromosome 6p25. Eur. J. Hum. Genet. 8:71-74.

Monaghan AP., Davidson DR., Sime C., Graham E., Baldock R., Bhattacharya SS. and Hill RE. 1991. The Msh-like homeobox genes define domains in the developing vertebrate eye. Development 112:1053-1061.

Morrison-Graham K., Schatteman GC., Bork T., Bowen-Pope DF. and Weston JA. 1992. A PDGF receptor mutation in the mouse (*Patch*) perturbs the development of a non-neuronal subset of neural crest-derived cells. Development 115:133-142.

Montcourrier P. and Hirsch M. 1985. Intercellular junctions in the developing rat corneal endothelium. Ophthalmic Res. 17:207–215.

Murphy C., Alvarado J., Juster R. and Maglio M.1984. Prenatal and postnatal cellularity of the human corneal endothelium. Invest. Ophthalmol. Vis. Sci. 25:312-322.

Newsome DA., Gross J. and Hassell JR. 1982. Human corneal stroma contains three distinct collagens. Invest. Ophthalmol. Vis. Sci. 22:376-381.

Nikitina NV., Maughn-Brown B., O'Rian MJ. and Kidson SH. 2004. Postnatal development of the eye in the naked mole rat (*Heterocephalus glaber*). Anat. Rec. Part A 277A:317-337.

Nishimura DY., Swiderski RE., Alward WL., Searby CC., Patil SR., Bennet SR., Kanis AB., Gastier JM., Stone EM. and Sheffield VC. 1998. The forkhead transcription factor gene FKHL7 is responsible for glaucoma phenotypes which map to 6p25. Nat. Genet. 19:140-147.

Nishimura DY., Searby CC., Alward WL., Walton D., Craig JE., Mackey DA., Kawase K., Kanis AB., Patil SR., Stone EM. and Sheffield VC. 2001. A spectrum of FOXC1 mutations suggests gene

dosage as a mechanism for developmental defects of the anterior chamber of the eye. Am. J. Hum. Genet. 68:364-372.

Noden DM. 1975. An analysis of the migratory behaviour of avian cephalic neural crest cells. Dev. Biol. 42:106-130.

Ober M. and Rohen JW. 1979. Regional differences in the fine structure of the ciliary epithelium related to accommodation. Invest. Ophthalmol. Vis. Sci. 18:655-664.

O'Rahilly R. 1975. The prenatal development of the human eye. Exp. Eye Res. 21:93-112.

Ormestad M., Blixt A., Churchill A., Martinsson T., Enerbäck S. and Carlsson P. 2002. *Foxe3* haploinsufficiency in mice causes anterior segment malformations similar to Peters' anomaly. Invest. Ophthalmol. Vis. Sci. 43:1350-1357.

Ortego J., Escribano J., Becerra SP. and Coca-Prados M. 1996. Gene expression of the neurotrophic pigment epithelium-derived factor in the human ciliary epithelium. Invest. Ophthalmol. Vis. Sci. 37:2759-2767.

Osumi-Yamashita N., Ninomiya Y. Doi H. and Eto K. 1994. The contribution of both forebrain and midbrain crest cells to the mesenchyme in the frontonasal mass of mouse embryos. Dev. Biol. 164:409-419.

Panicker SG., Sampath S., Mandal AK., Reddy ABM., Ahmed N. and Hasnain SE. 2002. Novel mutation in FOXC1 wing region causing Axenfeld-Rieger anomaly. Invest. Ophthalmol. Vis. Sci. 43:3613-3616.

Pappas GD., Smelser GK. and Brandt PW. 1959. Studies on the ciliary epithelium and the zonule. II. Electron and fluorescence microscope observations on the function of membrane elaborations. Arch. Ophthalmol. 62:959-965.

Pei YF. and Rhodin JA. 1970. The prenatal development of the mouse eye. Anat. Rec. 168:105-125.

Pei YF. and Rhodin JA. 1971. Electron microscopic study of the development of the mouse corneal endothelium. Invest. Opthalmol. 10:811–825.

Pelton RW., Saxena B., Jones M., Moses HL., and Gold LI. 1991. Immunohistochemical localization of TGF beta 1, TGF beta 2, and TGF beta 3 in the mouse embryo: Expression patterns suggest multiple roles during embryonic development. J. Cell Biol. 115:1091–1105.

Petroll WM., Hsu JK., Bean J., Cavanagh HD. and Jester JV. 1999. The spatial organization of apical junctional complex associated proteins in feline and human corneal endothelium. Curr. Eye Res. 18:10–19.

Pilot F. and Lecuit T. 2005. Compartmentalized morphogenesis in epithelia: From cell to tissue shape. Dev. Dyn. 232:685-694.

Pipas JM. and Levine AJ. 2001. Role of T antigen interactions with p53 in tumorigenesis. Seminars in Cancer Biology 11:23-30.

Porte A., Stoeckel ME., Brini A. and Metais P. 1968. Structure et differentiation du corps ciliare et du feuillet pigmente de la retine chez le poulet. Arch. Ophthalmol. 28:259-282.

Pressman CL., Chen H. and Johnson RL. 2000. Lmx1b, a LIM homeodomain class transcription factor, is necessary for normal development of multiple tissues in the anterior segment of the murine eye. Genesis 26:15-25.

Proetzel G., Pawlowski SA., Wiles MV., Yin M., Boivin GP., Howles PN., Ding J., Ferguson MW. and Doetschman T. 1995. Transforming growth factor-beta 3 is required for secondary palate fusion. Nat. Genet. 11:409–414.

Radice GL., Celeste Ferreira-Cornwell M., Robinson SD., Rayburn H., Chodish LA., Takeichi M. and Hynes RO. 1997a. Precocious mammary gland development in P-cadherin-deficient mice. J. Cell Biol. 139:1025-1032.

Radice GL., Rayburn H., Matsunami H., Knudsen KA., Takeichi M. and Hynes RO. 1997b. Developmental defects in mouse embryos lacking N-cadherin. Dev. Biol. 181:64-78.

Raviola G. 1971. The fine structure of the ciliary zonule and ciliary epithelium. With special regard to the organization and insertion of the zonular fibrils. Invest. Ophthalmol. 10:851-869.

Raviola G. 1977. The structural basis of the blood-ocular barriers. Exp. Eye Res. 25 Suppl:27-63.

Raviola G. and Raviola E. 1978. Intercellular junctions in the ciliary epithelium. Invest. Ophthalmol. Vis. Sci. 17:958-981.

Reichman EF. and Beebe DC. 1992. Changes in cellular dynamics during the development of the ciliary epithelium. Dev. Dyn. 193:125-135.

Reneker LW., Silversides DW., Patel K. and Overbeek PA. 1995. TGF alpha can act as a chemoattractant to perioptic mesenchymal cells in developing mouse eyes. Development 121:1669–1680.

Reneker LW., and Overbeek PA. 1996. Lens-specific expression of PDGF-A alters lens growth and development. Dev. Biol. 180:554–565.

Reneker LW., Silversides DW., Xu L. and Overbeek, PA. 2000. Formation of corneal endothelium is essential for anterior segment development–a transgenic mouse model of anterior segment dysgenesis. Development 127:533–542.

Rice R., Rice DP., Olsen BR. and Thesleff I. 2003. Progression of calvarial bone development requires Foxc1 regulation of Msx2 and Alx4. Dev. Biol. 262:75–87.

Rice R., Rice DP. and Thesleff I. 2005. Foxc1 integrates Fgf and Bmp signalling independently of twist or noggin during calvarial bone development. Dev. Dyn. 233:847–852.

Ritch R., Shields MB. and Krupin T. 1996. The Glaucomas. Basic Sciences Second Edition, Volume 1. Missouri, St. Louis: Mosby.

Riethmacher D., Brinkmann V. and Birchmeier C. 1995. A targeted mutation in the mouse E-cadherin gene results in defective preimplantation development. PNAS 92:855-859.

Robinson ML. and Overbeek PA. 1996. Differentail expression of A- and B-crystallin during murine ocular development. Invest. Ophthalmol. Vis. Sci. 37:2276-2284.

Saika S., Saika S., Liu C., Azhar M., Sanford LP., Doetschman T., Gendron RL., Kao CW-C. and Kao WW-Y. 2001. TGFb2 in Corneal morphogenesis during mouse embryonic development. Dev. Biol. 240:419–432.

Sakuta H., Suzuki R., Takahashi H., Kato A., Shintani T., lemura S., Yamamoto TS., Ueno N. and Noda M. 2001. Ventroptin: A BMP-4 antagonist expressed in a double-gradient pattern in the retina. Science 293:111-115.

Sambrook J., Fritsch EF. And Maniatis T. 1989. Molecular Cloning: A laboratory manual. Second Edition. Cold Spring Harbor Laboratory Press, USA.

Sanford LP., Ormsby I., Gittenberger-de Groot AC., Sariola H., Friedman R., Boivin GP., Cardell EL. and Doetschman T. 1997. TGFbeta2 knockout mice have multiple developmental defects that are non-overlapping with other TGFbeta knockout phenotypes. Development 124:2659–2670.

Sasaki H. and Hogan BLM. 1993. Differential expression of multiple fork head related genes genes during gastrulation and axial pattern formation in the mouse embryo. Development 118:47-59.

Satokata I. and Maas R. 1994. Msx1 deficient mice exhibit cleft palate and abnormalities of craniofacial and tooth development. Nat. Genet. 6:348-356.

Savinova OV., Sugiyama F., Martin JE., Tomarev SI., Paigen BJ., Smith RS. and John SWM. 2001. Intraocular pressure in genetically distinct mice: an update and strain survey. BMC Genetics 2:12

Schaeffel F., Murphy CJ. and Howland HC. 1999. Accommodation in the cuttlefish (*Sepia officinalis*). J. Exp. Biol. 202(Pt 22):3127-3134.

Schatteman GC., Morrison-Graham K., Van Koppen A., Weston JA. and Bowen-Pope DF. 1992. Regulation and role of PDGF receptor a-subunit expression during embryogenesis. Development 115:123 –131.

Schedl A., Ross A., Lee M., Engelkamp D., Rashbass P., van Heyningen V. and Hastie ND. 1996. Influence of Pax6 Gene Dosage on Development: Overexpression causes severe eye abnormalities. Cell 86:71-82.

Schlake T. and Boehm T. 2001. Expression domains in the skin of genes affected by the nude mutation and identified by gene expression profiling. Mech. Dev. 109:419–422.

Semina EV., Bronwell I., Mintz-Hittner HA., Murray JC. and Jamrich M. 2001. Mutations in the human forkhead transcription factor FOXE3 associated with anterior segment ocular dysgenesis and cataracts. Hum. Mol. Genet. 10:231-236.

Shibanuma M., Kuroki T and Nose K. 1992. Isolation of a gene encoding a putative leucine zipper structure that is induced by transforming growth factor β1 and other growth factors. J Biol. Chem. 267:10219-10224.

Shull MM., Ormsby I., Kier AB., Pawlowski S., Diebold RJ., Yin M., Allen R., Sidman C., Proetzel G., Calvin D., Annunziata N. and Doetschman T. 1992. Targeted disruption of the mouse transforming growth factor-beta 1 gene results in multifocal inflammatory disease. Nature 359:693-699.

Simeone A., Acampora D., Mallamaci A., Stornaiuolo A., D'Apice MR., Nigro V. and Boncinelli E. 1993. A vertebrate gene related to orthodenticle contains a homeodomain of the bicoid class and demarcates anterior neuroectoderm in the gastrulating mouse embryo. EMBO Journal 12:2735-2747.

Simonsen AH., Sorensen KE. and Sperling S. 1981. Thymidine incorporation by human corneal endothelium during organ culture. Acta. Ophthalmol. (Copenh). 59:110-118.

Singh S., Mishra R., Arango NA., Deng JM., Behringer RR. and Saunders GF. 2002. Iris hypoplasia in mice that lack the alternatively spliced *Pax6(5a)* isoform. PNAS 99:6812-6815.

Smith RS. 1971. Ultrastructural studies of the blood aqueous barrier. I. Transport of an electron-dense tracer in the iris and ciliary body of the mouse. Am. J. Ophthalmol. 71:1066-1077.

Smith RS. and Rudt LA. 1973. Ultrastructural studies of the blood aqueous barrier. 2. The barrier to horseradish peroxidase in primates. Am. J. Ophthalmol. 76:937-947.

Smith RS., Hawes NL., Kuhlmann SD., Heckenlively JR., Chang B., Roderick TH. and Sundberg JP. 1996. Corn1: a mouse model for corneal surface disease and neovascularization. Invest. Ophthalmol. Vis. Sci. 37:397-404.

Smith RS., Zabaleta A., Kume T., Savinova OV., Kidson SH., Martin JE., Nishimura DY., Alward WLM., Hogan BLM. and John SWM. 2000. Haploinsufficiency of the transcription factors FOXC1 and FOXC2 results in aberrant ocular development. Hum. Mol. Genet. 9:1021-1032.

Soriano P. 1997. The PDGFα receptor is required for neural crest cell development and for normal patterning of the somites. Development 124:2691-2700.

Soules KA. and Link BA. 2005. Morphogenesis of the anterior segment in the zebrafish eye. BMC Dev Biol. 5:12

Stiemke MM., McCartney MC., Cantu-Crouch D. and Edelhauser HF. 1991. Maturation of the corneal endothelial tight junction. Invest. Ophthalmol. Vis. Sci. 32:2757–2765.

Stroeva OG. 1967. The correlation of the processes of proliferation and determination in the morphogenesis of iris and ciliary body in rats. J. Embryol. Exp. Morphol. 18:269-287.

Suzuki A., Ueno N. and Hemmati-Brivanlou A. 1997. *Xenopus msx1* mediates epidermal induction and neural inhibition by BMP4. Development 124:3037-3044.

Thut CJ., Rountree RB., Hwa M. and Kingsley DM. 2001. A large-scale in situ screen provides molecular evidence for the induction of eye anterior segment structures by the developing lens. Dev. Biol. 231:63-76.

Torres M., Stoykova A., Huber O., Chowdhury K., Bonaldo P., Mansouri A., Butz S., Kemler R. and Gruss P. 1997. An alpha-E-catenin gene trap mutation defines its function in preimplantation development. PNAS 94:901-906.

Traboulsi EI., Al-Khayer K., Matsumoto M., Kimak MA., Crowe S., Wilson SE., Finegold DN., Ferrell RE. and Meisler DM. 2002. Lymphedema–Distichiasis syndrome and FOXC2 gene mutation. Am. J. Ophthalmol 134:592–596.

Tunggal JA., Helfrich1 I., Schmitz A., Schwarz H., Günzel D., Fromm M., Kemler R., Krieg T. and Niessen CM. 2005. E-cadherin is essential for *in vivo* epidermal barrier function by regulating tight junctions. The EMBO Journal 24:1146-1156.

Uchida D., Omotehara F., Nakashiro K., Tateishi Y., Hino S., Begum N., Fujimori T. and Kawamata H. 2003. Posttranscriptional regulation of TSC-22 (TGF-β-stimulated clone-22) gene by TGF-β1. Biochem. Biophys. Res. Commun. 305:846-854.

Umeda K., Matsui T., Nakayama M., Furuse K., Sasaki H, Furuse M. and Tsukita S. 2004. Establishment and characterization of cultured epithelial cells lacking expression of ZO-1. J. Biol. Chem. 279:44785-44794.

Uramoto H., Hackzell A., Wetterskog D., Bellági A., Izumi H. and Funa K. 2004. pRb, Myc and p53 are critically involved in SV40 large T antigen repression of PDGF β-receptor transcription. Journal of Cell Science 117:3855-3865.

Van Leen RW. Breuer ML., Lubsen NH. and Schoenmakers JGG. 1987. Developmental expression of crystallin genes: *In situ* hybridisation reveals a differntial localisation of specific mRNAs. Dev. Biol. 123:338-345.

Vasioukhin V., Bauer C., Yin M. and Fuchs E. 2000. Directed actin polymerization is the driving force for epithelial cell–cell adhesion. Cell 100:209–219.

Walther C. and Gruss P. 1991. Pax-6, a murine paired box gene, is expressed in the developing CNS. Development 113:1435-1449.

Wang IJ., Kao CW.-C., Liu C., Saika S., Nishina PM., Sundberg JP., Smith RS. and Kao WW.-Y. 2000. Characterization of Corn1 mice: Alteration of epithelial and stromal cell gene expression. Mol. Vis. 2000:7:20-26.

Wilson SE., Lloyd SA., He Y. and McCash CS. 1993. Extended life of human corneal endothelial cells transfected with the SV40 large T antigen. Invest. Ophthalmol. Vis. Sci. 34:2112-2123.

Winnier G., Blessing M., Labosky PA. and Hogan BL. 1995. Bone morphogenetic protein-4 is required for mesoderm formation and patterning in the mouse. Genes Dev. 9:2105– 2116.

Winnier GE., Hargett LK. and Hogan BLM. 1997. The winged helix transcription factor, MFH1, is required for proliferation and patterning of the paraxial mesoderm in the mouse embryo. Genes Dev. 11:926–940.

Winnier GE., Kume T., Deng K., Rogers R., Bundy J., Raines C., Walter MA. Hogan BLM. and Conway SJ. 1999. Roles for the winged helix transcription factors MF1 and MFH1 in cardiovascular development revealed by nonallelic noncomplementation of null alleles. Dev. Biol. 213:418-431.

Wu L., Li M., Hinton DR., Guo L., Jiang S., Wang JT., Zeng A. Xie JB., Snead M., Shuler C., Maxson Jr RE. and Liu Y. 2003. Microphthalmia resulting from *Msx2*-induced apoptosis in the optic vesicle. Invest. Ophthalmol. Vis. Sci. 44:2404-2412.

Xu P., Zhang X., Heaney S., Yoon A., Michelson AM. and Maas RL. 1999. Regulation of Pax6 expression is conserved between mice and flies. Development 126:383-395.

Xu L., Overbeek PA. and Reneker LW. 2002. Systematic Analysis of E-, N-, and P-cadherin Expression in Mouse Eye Development. Exp. Eye Res. 74:753-760.

Yap AS. and Kovacs EM. 2003. Direct cadherin-activated cell signalling: a view from the plasma membrane. The Journal of Cell Biology 160:11-16.

Ylikärppä R., Eklund L., Sormunen R., Kontiola AI., Utriainen A., Määttä M., Fukai N., Olsen BR. and Pihlajaniemi T. 2003. Lack of type XVIII collagen results in anterior ocular defects. FASEB Journal. 17:2257-2259.

Zhao G. 2003. Consequences of knocking out BMP signaling in the mouse. Genesis 35:43-56.

Zhao S., Chen Q., Hung FC. and Overbeek PA. 2002. BMP signaling is required for development of the ciliary body. Development 129:4435-4442.